

**FLUID EVOLUTION OF THE MAGMATIC HYDROTHERMAL BRECCIA
OF THE GOAT HILL OREBODY, QUESTA CLIMAX-TYPE PORPHYRY
MOLYBDENUM SYSTEM,
NEW MEXICO – A FLUID INCLUSION STUDY**

By

Amanda Rowe

UNPUBLISHED THESIS

**Submitted in Partial Fulfillment
of the Requirements for the**

Master of Science in Geology

**Department of Earth and Environmental Science
New Mexico Institute of Mining & Technology**

Socorro, New Mexico

May 2005

ABSTRACT

The Goat Hill orebody of the Questa Climax-type porphyry molybdenum system is composed of a magmatic-hydrothermal breccia (MHBX) and later quartz-molybdenite stockwork veinlets. Ross (2002) defined five distinct stratified facies (A-E) within the Goat Hill MHBX based upon matrix mineralogy and clast alteration and texture. Higher temperature mineralogic and alteration assemblages occur in the facies closest to the source intrusion (facies A and B), and lower temperature mineralogic and alteration assemblages occur in the facies most distal to the source (facies D and E). It was proposed by Ross (2002) that evolution of the magmatic-hydrothermal fluid away from its source is one of the possible mechanisms for these differences in the breccia facies.

A fluid inclusion study was performed on MHBX matrix quartz in order to delineate if there was a fluid evolution that occurred within the MHBX facies. Four major fluid inclusion types are identified at Questa: liquid-vapor type I inclusions, halite-bearing type II inclusions, halite+sylvite-bearing type III inclusions, and CO₂-rich type IV inclusions. Fifty percent of halite-bearing fluid inclusions homogenized by halite dissolution at temperatures of 100-350°C greater than liquid-vapor homogenization (T_{lv}), resulting in unrealistic calculated pressures and depths of formation based upon phase equilibria constraints. It is concluded that these inclusions are a result of the trapped halite phenomenon. The fluid became saturated with respect to halite, most likely caused by boiling. Evidence of boiling and trapped halite is observed in the MHBX.

Due to the trapped halite phenomenon, data is reported in terms of Tlv rather than final temperatures of homogenization in order to avoid over-estimates of temperature and be more representative of the temperature of trapping.

The fluid inclusion analyses resulted in a very broad range of temperatures and salinities (Tlv range of 68-520°C and salinity range of 0-64 eq. wt.% NaCl+/-KCl+/-CaCl₂). No fluid evolution pattern based upon MHBX facies is evident, an ionindicator that the fluid evolution of the system was independent of the mineralogic/alteration zonation of the MHBX. However, a fluid evolution pattern and possible fluid paths within the system can be identified when the data is scrutinized on a smaller scale (individual inclusions) than facies. Nine distinct fluid inclusion populations are identified on a Tlv vs. salinity diagram. Based upon these populations, an evolution of the fluids in this system from the earliest, most pristine fluid to the latest meteoric influx can be identified and is thought to be a result of three mechanisms – boiling, cooling, and meteoric mixing. From the spatial distribution of these fluid inclusion populations, it is determined that the Goat Hill MHBX cooled and crystallized from the inside out. It is also concluded that cooling of the saline fluids along the halite saturation curve was the mechanism for high grade molybdenite mineralization and is also associated with the QSP alteration for the MHBX.

This paper is dedicated to my parents, Larry and Jeannie Rowe,
for their undying love and support.

ACKNOWLEDGEMENTS

First and foremost, I would like to thank God for all that He has given me. Thanks so much to my committee, Andy Campbell (advisor) and Dave Norman of NMT, Bruce Walker of Molycorp, Inc., and Ginger McLemore of the NMBGMR, for their faith in me and this project, their support, and their valuable contributions to this project. A special thanks to Molycorp, Inc. for granting permission to perform this study and for the many forms of financial support that I received from Molycorp, Inc. while working on this project. A special thanks to Pierre-Simon Ross for setting the fantastic and very interesting groundwork for this project, and giving me a very concentrated MHBX 101 in such a short period of time. Thanks to Bill Chavez of NMT for sharing his plethora of mining geology knowledge, and for the opportunity to visit an abundant number of mines. I would like to thank my Aunt Kathy for moving to Phoenix, Arizona, so that I could come to the Southwest, fall in love with rocks and geology, and later follow my dream and become a geologist. I would like to thank my South African friend, Nigel Blamey, for always lending a helping hand and an idea. Thanks to my invaluable undergraduate helpers, Joel Bensing and Penny Ortiz, for sample prep and running analyses. This project would still not be done if I had to perform all of those tasks without their help. Thanks to Dave Jacobs of UNOCAL for his input at the very end of this project. I would like to thank my dear friends Shane Clarkson, Rachel Salazar, Kenda Wines, Kristie and Ryan McLin, Reyna Abeyta, Shannon Seneca, and Kelly

Donahue, who have seen me through it, and are STILL my friends! Special thanks to Andy Graves and Jess Lynch for taking me to the emergency room at 4 a.m. after my accident in the stable isotopes lab...I will never forget them for all that they did for me during that time. Most of all, I would like to thank my family for their love and support. This project was funded in part by the New Mexico Bureau of Geology & Mineral Resources, the New Mexico Geological Society, the Geological Society of America, the New Mexico Tech Graduate Student Association Matuszeski Research Grant, and the Society of Economic Geologists.

TABLE OF CONTENTS

| | Page |
|-----------------------------------------------------------------|-------------|
| ACKNOWLEDGEMENTS | ii |
| TABLE OF CONTENTS | iv |
| LIST OF TABLES | vi |
| LIST OF FIGURES | vii |
| INTRODUCTION | 1 |
| BACKGROUND | 2 |
| Molybdenum | 2 |
| Climax-type vs. Qtz Monzonite-type Porphyry Molybdenum Deposits | 3 |
| Location | 3 |
| Mining History | 8 |
| Rocks and Geologic History of the Questa Area | 12 |
| Goat Hill Orebody | 15 |
| The Goat Hill Magmatic-hydrothermal Breccia (MHBX) | 17 |
| Previous Fluid Inclusion Studies | 21 |
| <i>Climax, Colorado</i> | 21 |
| <i>Henderson, Colorado</i> | 24 |
| <i>Questa, New Mexico</i> | 26 |
| METHODS | 33 |
| Petrographic Analysis | 34 |
| Fluid Inclusion Analysis | 34 |
| RESULTS | 36 |
| Petrography | 36 |
| <i>MHBX Clasts and Clast Alteration</i> | 36 |
| <i>MHBX Matrix</i> | 38 |
| <i>Other Observations</i> | 38 |
| Fluid Inclusions | 42 |
| <i>Paragenesis</i> | 45 |

| | |
|---------------------------------------------------------------------|-----|
| <i>Types</i> | 45 |
| <i>MHBX Facies Distribution</i> | 58 |
| DATA ANALYSIS AND INTERPRETATION | 64 |
| Final Th vs. Tlv – Trapped Halite | 64 |
| Temperature and Salinity Distribution – Fluid Evolution | 73 |
| Pressure Corrections | 86 |
| CONCLUSIONS | 86 |
| COMPARISON WITH PREVIOUS CLIMAX-TYPE STUDIES | 89 |
| BIBLIOGRAPHY | 94 |
| APPENDIX A – FLUID INCLUSION RAW DATA | 98 |
| APPENDIX B – PETROGRAPHIC ANALYSIS | 109 |
| APPENDIX C – SPATIAL DISTRIBUTION OF FLUID INCLUSION POPULATIONS | 126 |

LIST OF TABLES

| | | Page |
|---------|----------------------------------------------------------------------------------|-------------|
| Table 1 | Comparison of Climax-type and Quartz Monzonite-type porphyry molybdenum deposits | 5 |
| Table 2 | Magmatic-hydrothermal Breccia (MHBX) classification by Ross | 20 |
| Table 3 | Fluid inclusion types | 50 |
| Table 4 | Na and k data from sylvite and halite-bearing fluid inclusions | 59 |
| Table 5 | Pearsons correlation data between facies and type, Tlv final Th, and salinity | 76 |
| Table 6 | Facies and type occurrence for fluid inclusion populations 1-9 | 79 |
| Table 7 | Comparison of Climax-type data and interpretations | 90 |

LIST OF FIGURES

| | | Page |
|-----------|---------------------------------------------------------------------------------|-------------|
| Figure 1 | Mine location map | 6 |
| Figure 2 | Regional location map | 7 |
| Figure 3 | Geologic map of the Questa-Red River Area | 9 |
| Figure 4 | Respective cross-sections from Figure 3 | 10 |
| Figure 5 | General stratigraphic column of the Questa-Red River area | 16 |
| Figure 6 | Long-section along Line 8-9 | 18 |
| Figure 7 | Short-section along Panel 26 | 19 |
| Figure 8 | MHBX grade distribution | 22 |
| Figure 9 | Facies distribution of minerals in MHBX clasts | 37 |
| Figure 10 | MHBX clast paragenesis | 39 |
| Figure 11 | Facies distribution of minerals in MHBX matrix | 40 |
| Figure 12 | MHBX matrix paragenesis | 41 |
| Figure 13 | Tlv distribution for all fluid inclusions with a measureable Tlv | 43 |
| Figure 14 | Tlv vs. salinity diagram for all inclusion with Tlv and salinity data | 44 |
| Figure 15 | Superimposed fluid inclusion populations in A1 matrix | 46 |
| Figure 16 | Secondary fluid inclusion plan in A3 matrix | 47 |
| Figure 17 | Tlv histograms for each assigned paragenetic species | 48 |
| Figure 18 | Tlv vs. salinity diagrams for each assigned paragenetic species | 49 |
| Figure 19 | Tlv distribution for each fluid inclusion type and subtype | 54 |
| Figure 20 | Tlv vs. salinity diagram for types and subtypes | 55 |
| Figure 21 | Tlv for each inclusion and its respective phase change for final Th | 56 |
| Figure 22 | Tlv vs. salinity graph indicating which phase change was exhibited for final Th | 57 |
| Figure 23 | Tlv distribution for facies | 61 |
| Figure 24 | Comparative Tlv histogram by facies | 62 |
| Figure 25 | Tlv vs. salinity diagram by facies | 63 |

| | | |
|-----------|----------------------------------------------------------------------------------------------------|----|
| Figure 26 | Tlv vs. Tshl diagram in terms of type for inclusions containing a halite daughter | 65 |
| Figure 27 | Tlv vs. Tshl diagram in terms of facies for inclusions containing a halite daughter | 66 |
| Figure 28 | Tshl-Tlv distribution | 67 |
| Figure 29 | Photograph of solid inclusions of halite in quartz adjacent to mult-solid fluid inclusions | 69 |
| Figure 30 | Photographs of co-existing liquid-rich and vapor-rich inclusions | 71 |
| Figure 31 | Schematic P-T diagram for the water-NaCl system | 72 |
| Figure 32 | Final Th distribution | 74 |
| Figure 33 | Final Th vs. salinity diagram | 75 |
| Figure 34 | Tlv vs. salinity distributions for individual facies | 78 |
| Figure 35 | Tlv vs. salinity diagram for individual facies with identified distinct populations of 1 through 9 | 79 |
| Figure 36 | Schematic fluid flow paths for the populations that represent real fluids | 81 |
| Figure 37 | Tlv vs. salinity distribution by type with populations 1-9 | 84 |

INTRODUCTION

The genetic origin of Climax-type porphyry molybdenum deposits (i.e. Questa, NM and Climax and Henderson, CO) has been debated throughout the economic geology community. Various previous studies on Climax-types have concluded magmatic, magmatic and meteoric mixing, or evolution from magmatic to meteoric, as the origin of the molybdenum-bearing fluids and associated molybdenite mineralization. Fluid inclusion analyses yielding different types, temperatures of homogenization, and salinities, have been utilized to determine the genetic origin of Climax-type deposits. High salinity fluid inclusions with a temperature of halite dissolution much greater than the temperature of liquid-vapor homogenization have been identified and are common in this type of deposit (Hall, 1974; Kamilli, 1978; Bloom, 1981; White et al., 1981; Smith, 1983; Carten, 1987; Cline and Bodnar, 1994; Cline and Vanko, 1995; Ross, 2002; Ross et al., 2002; Seedorff and Einaudi, 2004). Several authors have used these high salinity brines as a justification for a magmatic origin for the ore fluids, in that the fluids exsolved directly from the silicic melt (Kamilli, 1978; White et al., 1981; Cline and Bodnar, 1994; Cline and Vanko, 1995). Other authors debate that this type of fluid inclusion is a result of the trapped halite phenomenon, and not representative of a real fluid at all (Eastoe, 1978; Wilson, 1978; Erwood et al., 1979; Bloom, 1981; Campbell et al., 1995; and Koderer et al., 2004).

At the Questa porphyry Mo system, the Goat Hill orebody consists of a magmatic-hydrothermal breccia (MHBX) and cross-cutting quartz-molybdenite veins. The Goat Hill MHBX is composed of five distinct stratified facies (A-E), which are defined by clast alteration and textures, and matrix mineralogy. Higher temperature

mineralogic and alteration assemblages occur at the bottom of the breccia and closest to the source intrusion (facies A), and lower temperature mineralogic and alteration assemblages occur at the top and distal edges of the MHBX (facies D and E). The facies closest to the source intrusion (A) appears to contain recognizable magmatic textures (quench), in addition to higher temperature assemblages (Ross, 2002; Ross et al., 2002).

In hopes to gain a better understanding of the origin of Climax-types, the purpose of this study was to use fluid inclusion analyses on the Questa Goat Hill MHBX matrix quartz to determine the genetic origin of the ore-fluids, the mechanism for molybdenite mineralization, and if there was a fluid evolution for the Goat Hill MHBX that coincided with the mineralogic/alteration zonation of the MHBX facies, i.e. an evolution from a magmatic A facies to perhaps a meteoric, or mixed magmatic and meteoric, D and E facies. Another purpose for this study was to better define the origin of the debated high salinity inclusions, where the temperature of halite dissolution is much greater than the temperature of liquid-vapor homogenization.

BACKGROUND

Molybdenum

Molybdenum (Mo) was discovered in 1778 by Carl Wilhelm Scheele in Sweden while performing research on an already known mineral called molybdenite (MoS_2). The word molybdenite was derived from the Greek word “*molydos*” meaning lead. Scheele discovered that molybdenite did not contain lead as suspected, but a new element that he called molybdenum after the mineral molybdenite. Molybdenum was discovered to be a transition metal with atomic number 42 on the periodic table. It is a hard, silvery white metal that has a melting temperature of 4730°F (2610 °C). Mo is not found as a free

metal in nature, but primarily as a mineral compound such as molybdenite (MoS_2), powellite (CaMoO_4), wulfenite (PbMoO_4), molybdite (MoO_3), and ferribmolybdite ($\text{Fe}_2\text{O}_3 \cdot 3\text{MoO}_3 \cdot 8\text{H}_2\text{O}$). Molybdenite (mo) is the principle molybdenum ore mineral (Ford, 1966; International Molybdenum Association, 2003).

Molybdenum is used in metallurgical applications as a valuable alloy agent (Smith, 1983). It contributes to the hardness, toughness, and corrosion resistance of steels and improves the strength of steels at high temperatures. Molybdenum is also used in other applications, such as nuclear energy, missile and aircraft/aerospace parts, as a catalyst in refining petroleum, as a pigment (orange) in paint, and as filament material in electronics. Molybdenum is also an essential trace element in plant nutrition. The mineral molybdenite is used as a lubricant, especially at high temperatures where oils can decompose (International Molybdenum Association, 2003).

Approximately half of the world's production of molybdenum comes from porphyry molybdenum deposits as the primary recovery metal. The remaining half of the world's molybdenum is produced mostly as a by-product from mining of copper porphyry deposits. Minor contributions to world production comes from lead-zinc and tungsten mining operations as a by-product (Smith, 1983). Approximately half of the world's molybdenum is mined in the United States. Other major sources of molybdenum are in Chile, Canada, and China, with minimal production from Mexico, Peru, Iran, and the Commonwealth of Independent States (ex-USSR) (International Molybdenum Association, 2003).

Climax-type vs. Quartz Monzonite-type Porphyry Molybdenum Deposits

Porphyry molybdenum deposits are the most significant source of molybdenum known. These types of deposits are genetically related to porphyritic intrusions ranging from quartz-monzonite to granite in composition. Based upon the composition of the source intrusion and their fluorine content, porphyry molybdenum deposits are divided into two subclasses, the low-fluorine quartz monzonite-type and the high-fluorine Climax-type (name originating from Climax, CO, a world-class porphyry Mo deposit with a high-silica, alkali-rich granite source intrusion). In addition to having different source intrusion whole-rock compositions and fluorine content, these two types vary in other characteristic features as well, such as grade, orebody size, Cu: Mo ratio, tectonic setting, age-range, mineralogy, geochemical signature, etc. Table 1 is a comparison chart between the two different types. Questa is classified as a Climax-type porphyry Mo deposit (White et al., 1981; Cox and Singer, 1986; Guilbert and Park, 1986; White et al., 1990; Carten et al., 1993; Donahue, 2002).

Location

The Questa mine Climax-type porphyry molybdenum system (Questa system) is located in north-central New Mexico in the Taos Range of the Sangre de Cristo Mountains (Figure 1). The Questa system is sited on the southern flank of the Tertiary Questa Caldera in the Tertiary Latir volcanic field (Figure 2). The Questa Caldera is rectilinear in shape, 10 miles on a side, and is rift-front normal faulted on its western margin into the Rio Grande Rift (Figure 3) (Leonardson et. al., 1983; Smith, 1983). Mineralization of the Questa system follows a structural trend along the southern flank of the caldera that is referred to as the Red River Trench, a Precambrian shear zone with a

| Characteristic | Climax-type | Quartz monzonite-type |
|-------------------------------------|---------------------------------------------------------------------------------------------------------------------------------------------------------------------------------------------|----------------------------------------------------------------------------------------------------------------------------------------------------------------------------------------------------------------------------------------------------------------------------------------------------------------------------------------------------------------------------------|
| Source Intrusion | Granite porphyry | Quartz monzonite porphyry |
| Geochemistry | High silica, peralkaline, F-rich (>0.1% F), Rb, Y and Nb are high, Ba, Sr and Zr are low | Calc-alkaline, low F content (<0.1% F) |
| Deposition | Multiple intrusions of granite | Composite intrusions of diorite to quartz monzonite in orogenic belts |
| Age range | Paleozoic to Tertiary, but mainly Mid-Tertiary | Archean to Tertiary, but most commonly Mesozoic and Tertiary |
| Tectonic Setting | Rift zones in areas of thick cratonic crust | Subduction zones related to arc-continent or continental collision |
| Associated ore deposit types | Ag-base-metal veins and polymetallic replacement deposits, possibly rhyolite-hosted Sn deposits and porphyry W deposits; possibly Mo, Sn, and W greisen systems | Porphyry Cu-Mo, Cu skarn, volcanic-hosted Cu-As-Sb deposits |
| Mineralogy | Molybdenite, quartz, K-feldspar, fluorite, fluorine-rich biotite and topaz, pyrite, calcite, rutile, anhydrite, sericite, clays, wolframite, cassiterite, rhodochrosite, sphalerite, galena | Molybdenite, pyrite, scheelite, chalcocopyrite, argentian tetrahedrite, quartz, K-feldspar, biotite, calcite, sericite, clays, galena |
| Alteration | Intense silicification and potassic alteration, upper zones of phyllic propylitic alteration, quartz-sericite-pyrite alteration, minor greisen below orebody | Potassic outward to propylitic, phyllic and propylitic overprint, minor peripheral argillic |
| Texture | Predominantly in veinlets and fractures; minor disseminations; breccias | Disseminated and in veinlets and fractures; breccias |
| Ore controls | Stockwork ore zone draped over small stocks; multiple stages of intrusion and mineralization | Stockwork in felsic porphyry and surrounding country rock; multiple stages of mineralization are common |
| Geochemical signature | Mo, Sn, W and Rb anomalies near ore zones; Pb, Zn, F, and U anomalies in periphery up to 2 km | Mo, Cu, W, and F anomalies near ore zones; Pb, Zn, Au and Ag anomalies in periphery up to several km |
| Average ore grade | 0.3-0.45% MoS ₂ | 0.1-0.2% MoS ₂ |
| Cu:Mo ratio | 1:100 to 1:50 | 1:30 to 1:1 |
| Examples of deposit type | Colorado: Climax, Henderson, Silver Creek, Urad, Mount Emmons, Redwell Basin; New Mexico: Questa ; Utah: Pine Grove; Greenland: Malmberg, Erzberg; Norway: Nordli | British Columbia, Canada: Endako, Boss Mountain, Kitsault, Adanac, Carmi, Bell Moly, Red Bird, Trout Lake, Storie Moly, Ajax; Yukon, Canada: Boswell River, Red Mountain; Alaska: Quartz Hill; Montana: Cannivan; Idaho: Thomson Creek, White Cloud, Cumo; Nevada: Nevada Moly, Pine Nut, Buckingham; Peru: Compaccha; Russia: East Kounrad; Mexico: Creston; China: Jinduicheng |

Table 1. Comparison of Climax-type and quartz monzonite type porphyry molybdenum deposits. Data taken from or modified from Donahue (2002), Ludington (1986), Ludington et al. (1995), Sinclair (1995a and b), Theodore (1986), and White et al. (1981).

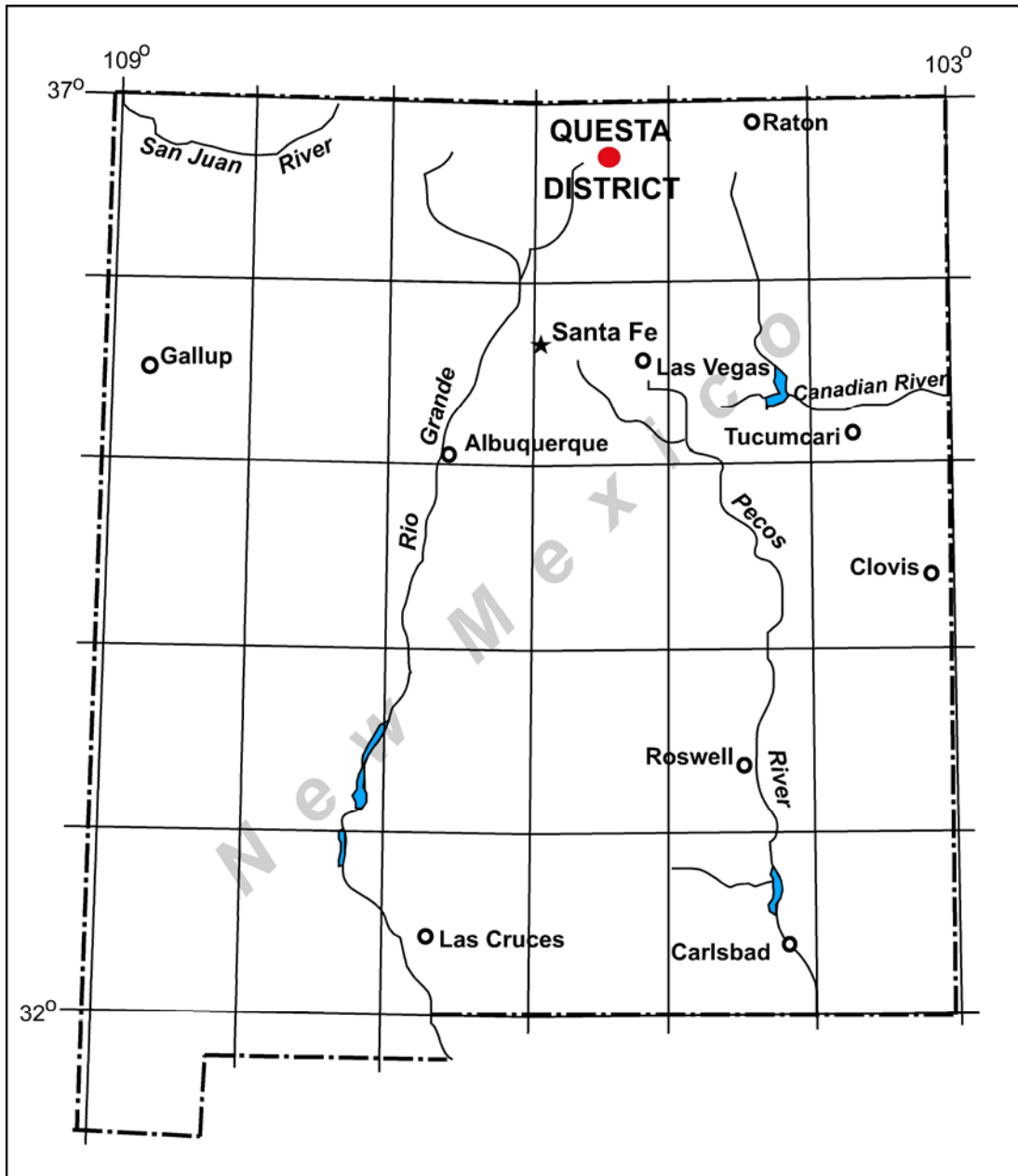


Figure 1. Mine location map. Modified from Smith, 1983.

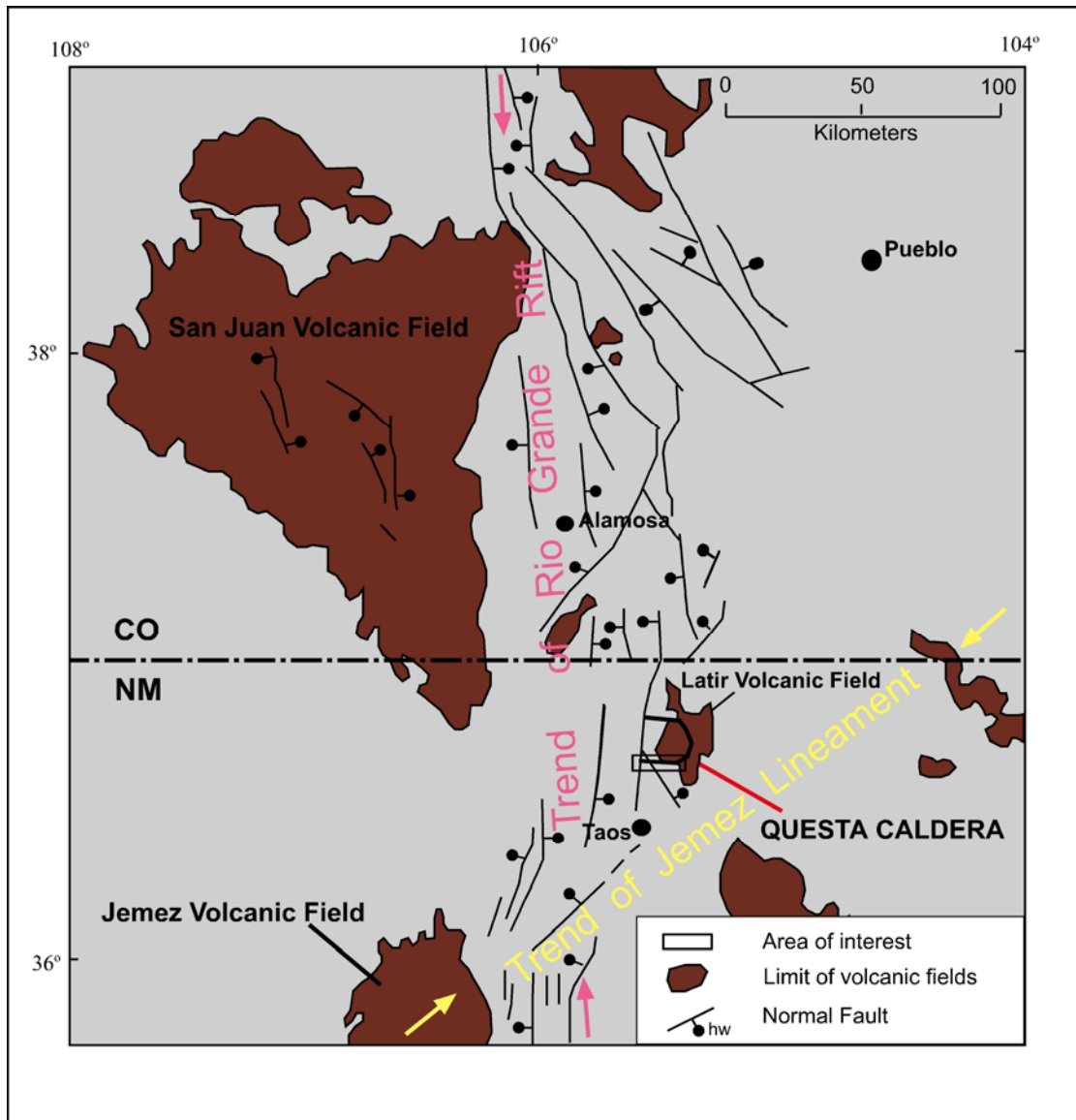


Figure 2. Regional location map. Included are the Questa Caldera, major structural trends, and volcanic fields. Modified from Meyer and Leonardson (1990) and Meyer and Foland (1991).

N70°E to N75°E orientation (Figure 3)(Lipman, 1992; Ross, 2002; Ross et al., 2002).

This mineralization occurs as three distinct Mo deposits from west to east – the Log Cabin, Central, and Spring Gulch deposits. The Central deposit is the only site of historic Mo mining in the district. It is horseshoe-shaped and consists of two distinct ore zones, the Northeast and Southwest. Several distinct orebodies exist within these ore zones and are defined by a 0.2% MoS₂ grade cutoff (Figure 4) (Ross, 2002; Ross et al., 2002).

Production figures for the Central deposit, including the Goat Hill orebody (area of study) and D-orebody (site of current mining operations), are in the following *Mining History* section of this paper.

Mining History

The Questa-Red River mining district has been historically mined for gold, silver, copper, and molybdenum since the late 1800s and early 1900s (Carpenter, 1968; Schilling, 1956; Ross, 2002). Molybdenum is the only commodity being mined in the Questa-Red River mining district at the present time (Ross, 2002; Ross et al., 2002).

Ferrimolybdite (Fe₂(MoO₄)₃nH₂O) and molybdenite were discovered along the Sulphur Gulch drainage of the Red River in 1916-1917 (Martineau et. al., 1977; Schilling, 1956). By 1921, the Sulphur Gulch claims, located five miles east of the town of Questa and six miles west of the town of Red River, were acquired by the Molybdenum Corporation of America (Carpenter, 1968; Schilling, 1956). Underground lode mining began in 1923 on the Old Underground Mine, with a production of 50 tons/day at >4% MoS₂ (Carpenter, 1968; Ross, 2002; Ross et al., 2002). Quartz-carbonate-molybdenite-fluorite veins were mined and milled until 1958 when production ceased due to exhaustion of the veins (Carpenter, 1968; Schilling, 1956; Ross, 2001). By

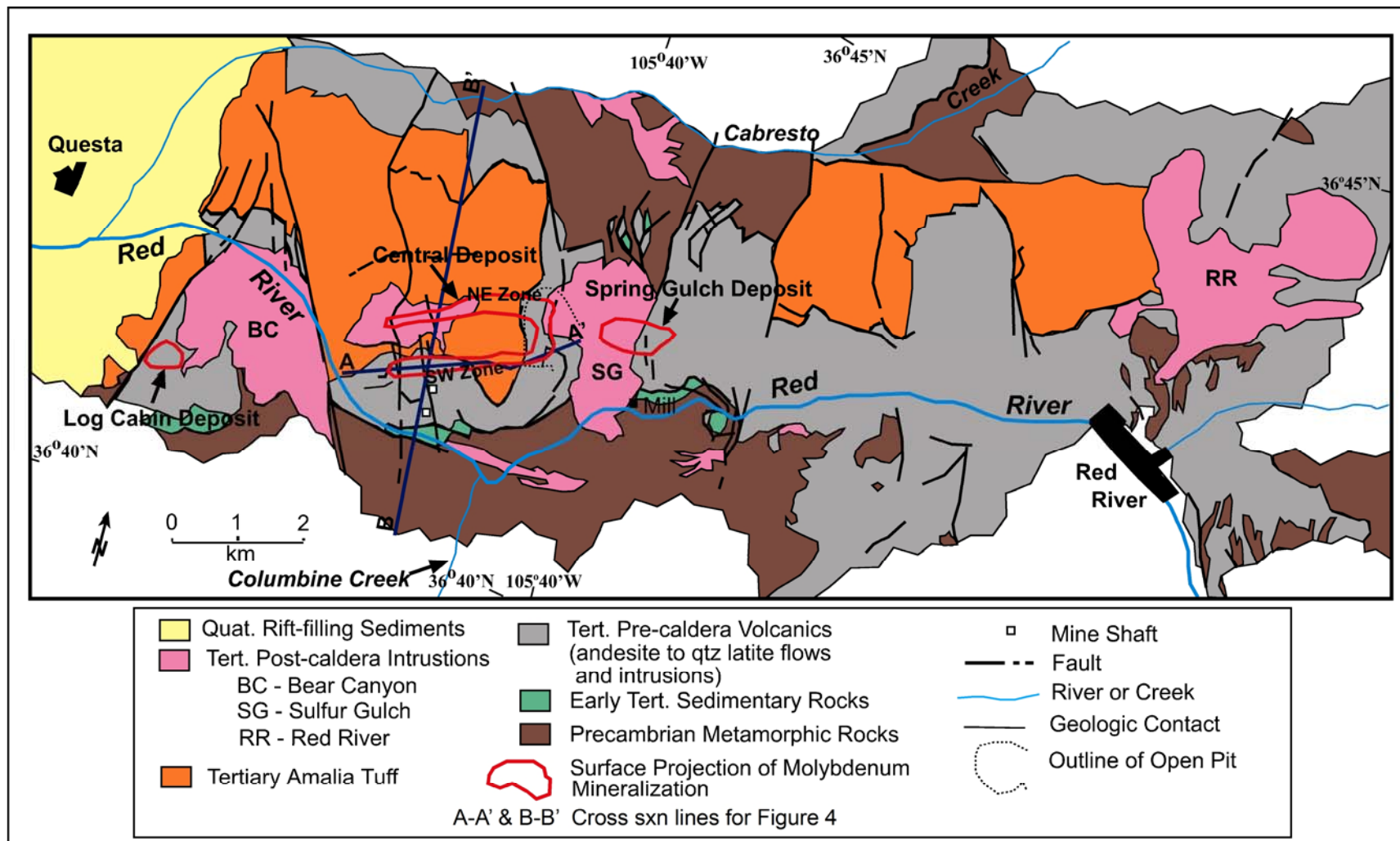


Figure 3 - Geologic map of the Questa-Red River area. Modified from Meyer and Foland (1991).

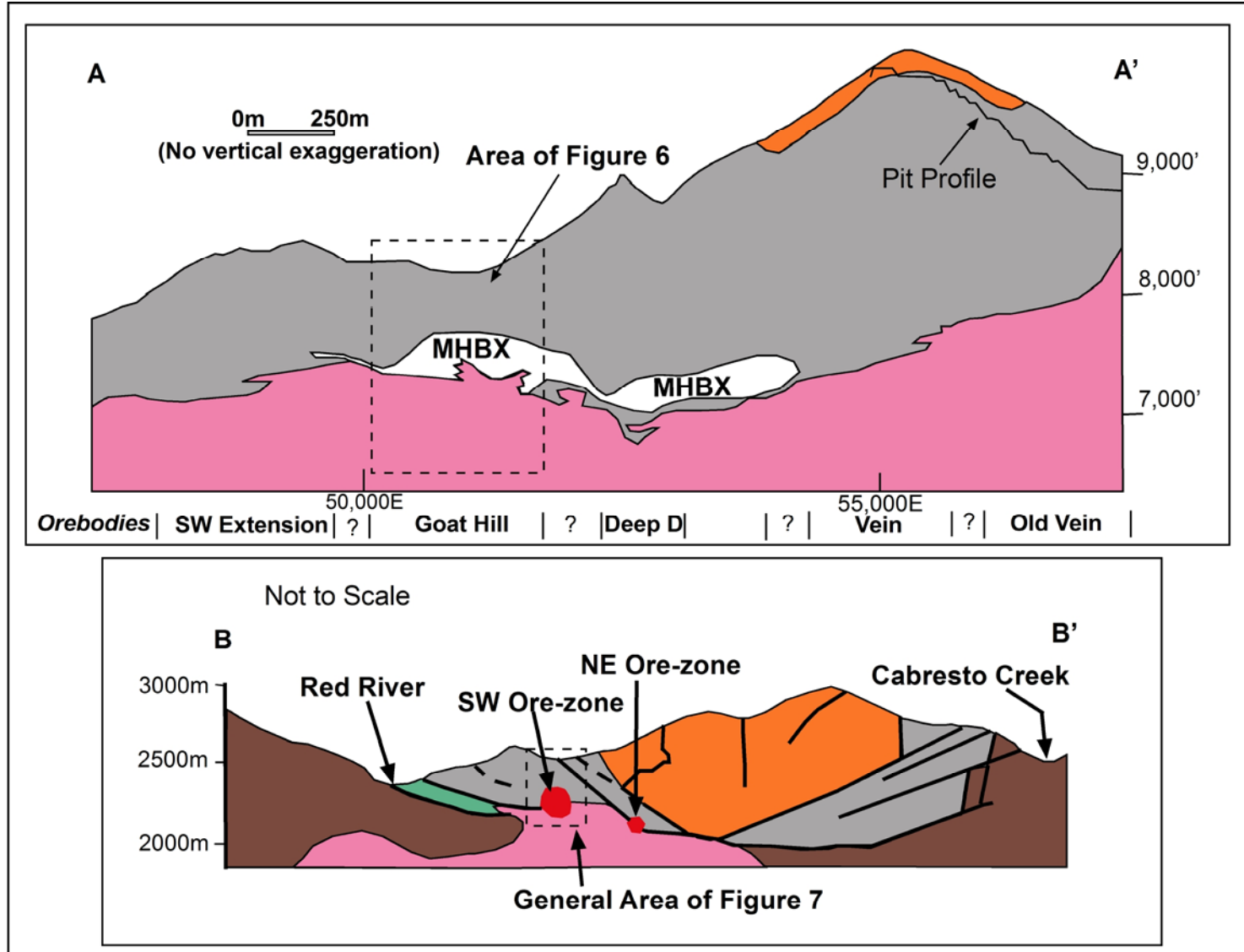


Figure 4. Respective cross-sections from Figure 3. Modified from Ross, 2002. General areas for Figures 6 and 7 in dashed boxes.

1958, the Old Underground Mine had produced 0.375 million tons (Mt) of ore at >4% MoS₂ (Ross, 2002; Ross et al., 2002).

Extensive exploration began in 1953, which included surface mapping, assay, and drilling program. Exploration efforts soared by 1956, which led to the 1957 discovery and delineation of a low-grade, large tonnage molybdenite orebody, mineable by the open-pit method (Carpenter, 1968; Schilling, 1956). In 1964, a new mill and modern flotation plant were constructed and pre-mining stripping began in preparation for the commencement of open-pit mining (Schilling, 1956; Carpenter, 1968). Open-pit mining of stockwork veins of the Upper Sulphur Gulch commenced in 1965 and ceased in 1982 (Schilling, 1956; Bloom, 1981; Walker, pers. comm., 2004). Between 1965 and 1982, the open pit produced 81 Mt of molybdenum ore at 0.191% MoS₂ (Ross, 2002; Ross et al., 2002; Walker, pers. comm., 2004).

In 1975, joint exploration efforts by Molycorp, Inc. and Kennecott, led to the discovery and delineation of several, deeper mineable orebodies in the Southwest ore zone and Northeast ore zone (Schilling, 1956; Martineau et. al., 1977; Bloom 1981). Molycorp-Kennecott subsequently sold its interest in the Questa project to the Union Oil Company of California (UNOCAL) in late 1977 (Martineau et. al., 1977; Bloom, 1981). Development of a large underground mine below the Goat Hill Gulch in the Southwest ore zone was initiated, leading to the commencement of underground mining by the blockcaving method in 1983 (Schilling, 1956; Bloom, 1981). Mining ceased in 1986 due to a dip in the market prices for molybdenum, but by 1989, production recommenced in the underground mine (Schilling, 1956). Mining of a magmatic-hydrothermal breccia (MHBX) and cross-cutting stockwork veinlets of the Goat Hill orebody ceased in 2000

with a total production of 21.11 Mt of ore at 0.318% MoS₂. The Goat Hill orebody has not been exhausted.

Presently, underground mining efforts are being performed on the D-orebody of the Southwest ore zone, adjacent to the Goat Hill orebody. The blockcaving mining method was commenced in 2001 on the D-orebody, producing an average ore grade of 0.338% MoS₂, and consisting of MHBX and crosscutting stockwork veinlets (Ross, 2002; Ross et al., 2002).

Possible future mining may consist of proven and probable reserves, including the currently mined D-orebody, of 63.54 Mt of ore at 0.338% MoS₂ with a 0.25% MoS₂ cutoff grade (Ross, 2002; Ross et al., 2002).

Rocks and Geologic History of the Questa Area

Precambrian felsic intrusions and amphibolite grade metamorphic rocks comprise the basement complex of the Questa area (Carpenter, 1968; Smith, 1983; Meyer, 1991; Ross, 2002; Ross et al., 2002). The metamorphic rocks are members of an arc-complex that was accreted onto the Wyoming craton during the early Proterozoic (Reed et al., 1987). A steeply dipping Precambrian shear zone along the present day Red River valley separates two Precambrian terranes - the Taos terrane metaigneous suite to the south (mafic schists and gneisses, amphibolite, and felsic schist) and the younger metasediments of the Questa terrane to the north (Meyer, 1991; Ross, 2002; Ross et al., 2002). Precambrian quartz-monzonite to granite plutons that intruded the accreted package also occur in the area (Meyer, 1991).

Shallow subduction of the Farallon oceanic plate underneath the North American continental plate during the late Cretaceous-early Eocene prompted uplift in northern

New Mexico and southern Colorado forming the Sangre de Cristo Mountains (Meyer, 1991; Kelley et. al 1992). Erosion of the Laramide highlands during the Paleocene and Eocene produced the locally derived sandstones and conglomerates of the Sangre de Cristo formation in the Questa area (Meyer, 1991). The Sangre de Cristo formation only occurs in a few locations in the mine area.

During the mid-Oligocene to early Miocene, crustal melting, crustal fractionation, and magma mixing caused by subduction of the Farallon plate provided a source for the calc-alkaline intermediate volcanism of the Latir volcanic field (Leonardson et. al., 1983; Johnson and Lipman, 1988; Meyer, 1991). The Latir volcanism is slightly younger than that of the neighboring San Juan volcanic field of southern Colorado. The Latir volcanic field consists of a series of stratovolcanoes, from which emanated lava flows and flow breccias consisting of andesite to quartz-latitude in composition. The volcanic rocks of the Latir field are interbedded with volcanically derived sedimentary rocks. In the Questa area, the andesite volcanic package (both flows and volcanoclastics) that overlies the Precambrian basement is approximately 1 to 2 km thick (Martineau et al., 1977; Meyer, 1991; Ross, 2002; Ross et al., 2002).

Thermal weakening of the crust by Oligocene volcanism caused the late Oligocene onset of a NE-SW trend of regional crustal extension from the Southern Rocky Mountains to Mexico - the Rio Grande Rift (Leonardson et. al., 1983; Meyer, 1991). The onset of peralkaline magmatism in the Questa area coincided with the initiation of the Rio Grande Rift (Johnson and Lipman, 1988; Johnson et. al., 1990). Extensional rift-related fractures aided in localizing the emplacement of a 20x35 km composite batholith that underlies the entire mining district (Leonardson et. al., 1983; Meyer, 1991). Following

emplacement of the batholith, eruption of the >500 km³ high silica rhyolite ashflow Amalia Tuff initiated collapse of the Questa caldera (Leonardson et. al., 1983; Johnson and Lipman, 1988; Meyer, 1991; Ross, 2002; Ross et al., 2002). The Amalia Tuff is dated at 25.7 ± 0.1 Ma (Johnson and Lipman, 1988; Czamanske et. al., 1990; Ross, 2002). At approximately the same time of eruption, an intrusive suite genetically related to the Amalia Tuff intruded the margins and floor of the caldera as quartz-latitude to rhyolite porphyry in composition (Meyer and Foland, 1991; Meyer, 1991).

One million years following the eruption of the Amalia Tuff, three syn-mineralization high silica granite plutons intruded the southern margin of the Questa caldera – the Bear Canyon, Sulphur Gulch, and Red River plutons, respectively, from west to east (Leonardson et al., 1983; Czamanske et al., 1990; Ross, 2002; Ross et al., 2002). These plutons are believed to be cupola members of the massive batholith underlying the mining district (Czamanske et. al., 1990). In addition, the plutons are similar in trace element composition to the Amalia Tuff and are believed to be possible remnants of non-erupted Amalia Tuff magma (Johnson et. al., 1989). The intrusions consist of distinct granitic to aplitic phases (Czamanske et. al., 1990). The aplitic phase of the Sulphur Gulch pluton is believed to be the source intrusion for the molybdenum mineralization of the Central deposit (Czamanske et. al., 1990; Meyer and Foland, 1991). The southern caldera margin, emplacement of the stocks along the margin, and the trend of mineralization are most likely controlled by the Precambrian shear zone with the N70E to N75E orientation (Smith, 1983; Meyer, 1990; Meyer 1991; Ross, 2002; Ross et al., 2002).

Following mineralization, a rhyolite porphyry, often called the Goat Hill porphyry stock, intruded the mine area. In addition, lamprophyre to latite dikes intruded the area, post-dating all rocks, mineralization, and alteration in the area. (Meyer, 1991).

Early extension of the Rio Grande Rift ceased approximately 17-10 Ma, leading to initiation of extension of the modern-day Rio Grande Rift (17-10 Ma) (Meyer, 1991). During this time, the western margin of the Questa caldera was faulted into the rift. Rift-filling Quaternary sediments of the Santa Fe group are the youngest rocks in the area (Meyer and Foland, 1991). A general stratigraphic column of the area is available in Figure 5.

Goat Hill Orebody

The Goat Hill orebody, located in the Southwest ore zone of the Central deposit at the Questa Mine, occurs between the western-most orebody (Southwest Extension) and the D-orebody of the Southwest ore zone (Figure 4). The Goat Hill orebody is hosted in Tertiary andesite (Tan) and partially in an aplitic source intrusion. It consists of a magmatic-hydrothermal breccia (MHBX) and later qtz-mo stockwork veinlets that exceed the confines of the MHBX. MHBX-related molybdenite mineralization contributed approximately 40% of grade (0.2% MoS₂ cutoff) to the orebody, whereas the later stockwork veinlets contributed the remaining 60% of the molybdenite mineralization (Ross, 2002; Ross et al., 2002).

The earliest alteration that occurred within Goat Hill orebody was a pre-mineralization/pre-brecciation propylitization of the Tertiary andesite, associated with interaction of the country rock with meteoric water. The assemblages associated with this early alteration consist of any combination of biotite+/- chlorite+/-epidote+/-

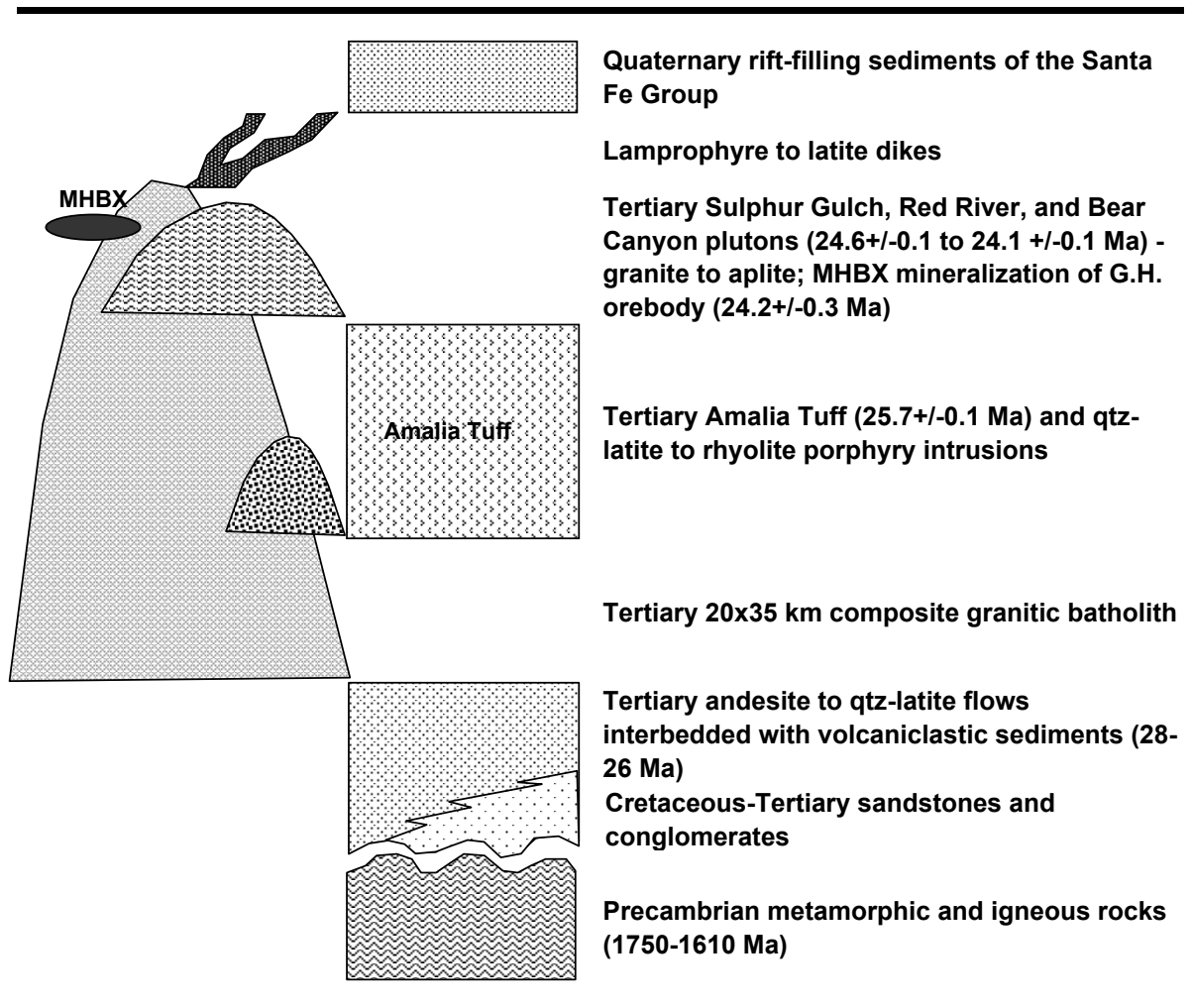


Figure 5. General stratigraphic column of the Questa-Red River area. Thicknesses not to scale. In part modified from Ross, 2002. Thicknesses and dates from Leonardson et al. (1983), Johnson et al. (1989), Czamanske et al. (1990), and Meyer (1991).

magnetite+/-calcite+/-pyrite. Potassic alteration associated with the intrusion of the source aplite further altered the Tan, replacing the rock with biotite, quartz, and potassium feldspar. Later quartz-sericite-pyrite (QSP) alteration overprinted earlier alteration. Lastly, local argillic alteration occurred in fracture zones (Leonardson et al., 1983; Meyer, 1991).

The Goat Hill Magmatic-hydrothermal Breccia (MHBX)

The MHBX was formed by hydraulic fracturing of andesite and premineral dikes by ore-bearing fluids that evolved from a crystallizing water-saturated granitic magma that was emplaced at depths of 3 to 5 km (lithostatic pressures of 0.8-1.4 kbars) below surface (Ross, 2002; Ross et al., 2002; Molling, 1989; Cline and Bodnar, 1994).

Volumetrically, the breccia body is $>6 \times 10^6 \text{ m}^3$ breccia body that is greater than or equal to 100 m thick, 200 meters wide, and 650 meters long. It is located above and southward of the apex of an aplitic stock, which is believed to be the source for the mineralizing fluids (Figures 6 and 7). The upper contact of the breccia dips 18° to the north and is thought to follow a pre-breccia fabric, either representing a fracture zone or volcanic bedding, in which the magmatic-hydrothermal fluids were focused (Ross, 2002; Ross et al., 2002).

Ross defined 5 distinct stratified facies (A-E) within the MHBX based upon matrix mineralogy, clast alteration, and breccia texture (Table 2). Facies A is adjacent to the source aplite intrusion, and is divided into 3 subfacies (A₁, A₂, and A₃). Facies E occurs most distal to the source intrusion. Matrix mineralogy reported by Ross consists of aplite, potassium feldspar (Kspar), quartz (qtz), molybdenite (mo), fluorophlogopite (bt), calcite (ca), and fluorite (fl). Breccia clast alteration reported by Ross consists of

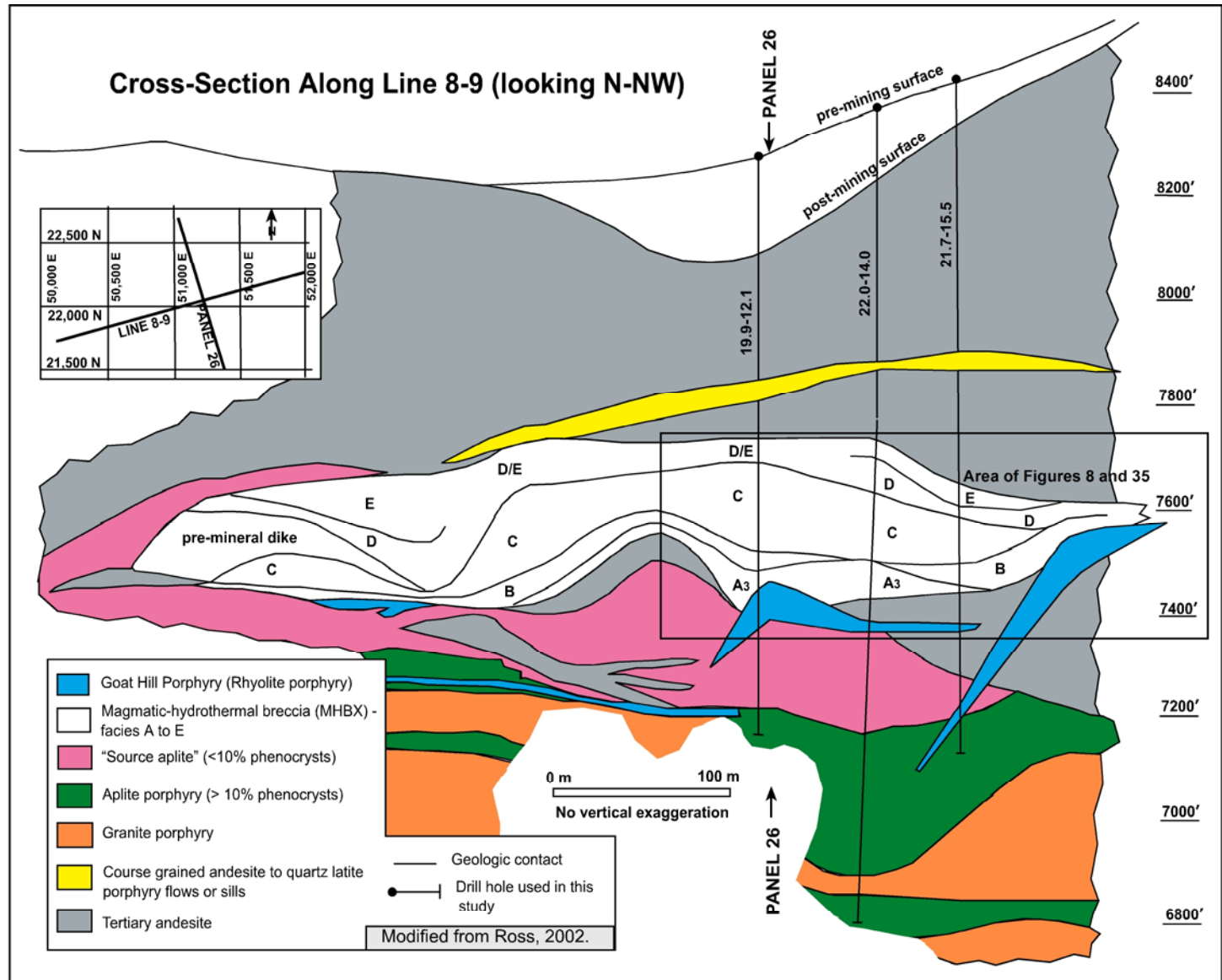


Figure 6. Long-section along Line 8-9.

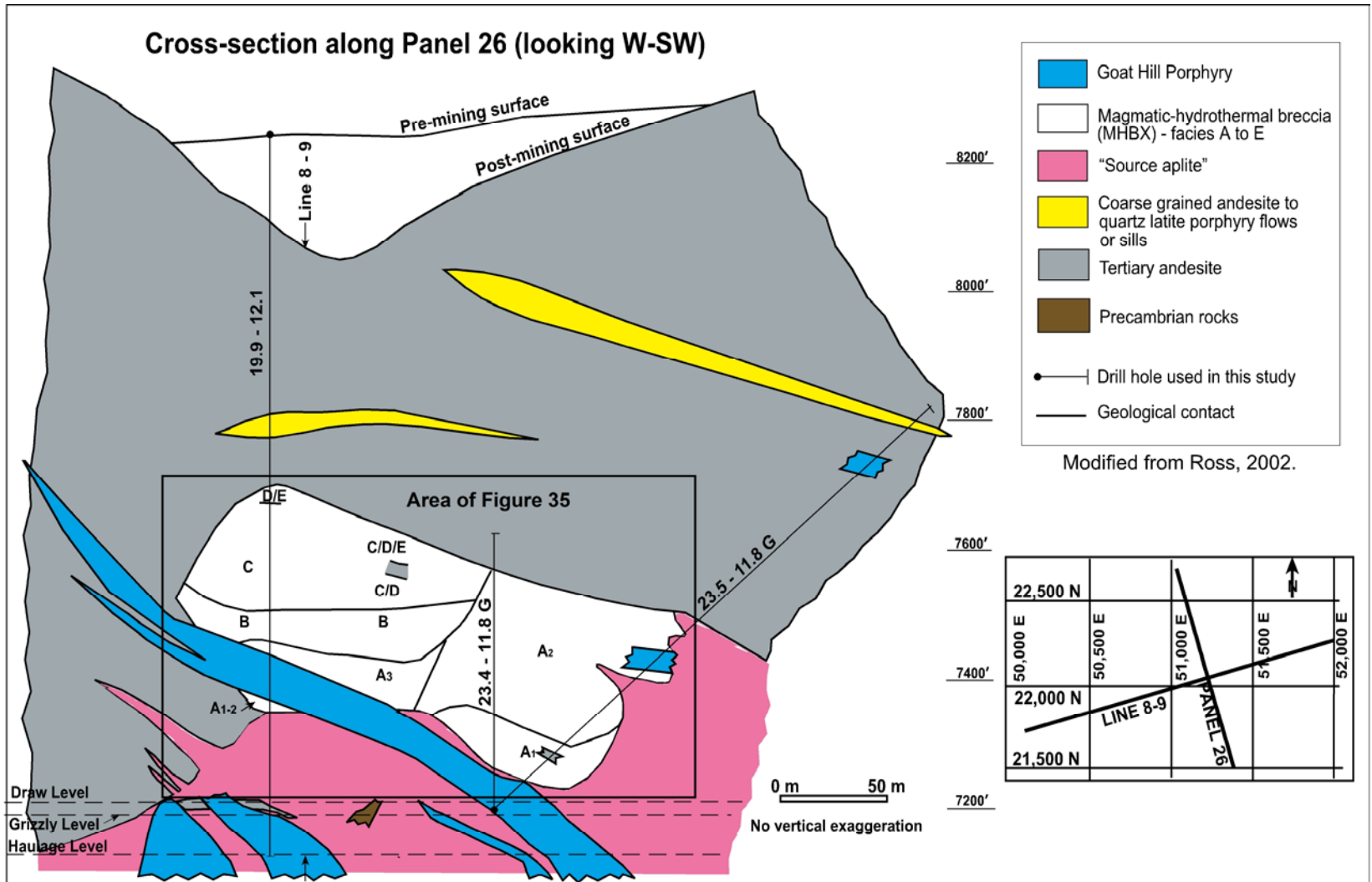


Figure 7. Short-section along Panel 26.

Table 2. Magmatic Hydrothermal Breccia (MHBX) Classification by Ross

| MATRIX | | | ANDESITE FRAGMENTS | | | | |
|----------------|----------|------------------------------------------------|----------------------------------------------------------|-----------------------|------------------------------------------|------------------|---------------|
| <i>Facies</i> | <i>%</i> | <i>Composition</i> | <i>alteration</i> | <i>shape</i> | <i>corrosion</i> | <i>size (cm)</i> | <i>fabric</i> |
| E | 5 - 30 | qtz, bt ₂ , cc, +/- mo, +/-fl | q-s-p | angular to round | hydrothermal linked with bt ₂ | 0.1 - 10 | - |
| D | ? | qtz, bt ₂ , cc, +/- mo, +/-fl, vugs | q-s-p ovrprnt. bt ₁ | angular to round | hydrothermal linked with bt ₂ | 0.1 - 10 | shingle BX |
| C | 5 - 50 | qtz, bt ₂ , kfp, cc, +/-mo, +/-fl | bt ₁ , q-s-p ovrprnt. bt ₁ , q-s-p | angular to subangular | none | 0.1 - 10 | shingle BX |
| B | 5 - 30 | qtz, kfp | bt ₁ | angular | none | <1 - >10 | mosaic |
| A ₃ | 5 - 40 | qtz-kfp, minor apl. porph. | bt ₁ | angular | none | <1 - >10 | mosaic |
| A ₂ | 10 - 95 | qtz-kfp, >aplite porph. | bt ₁ core, kfp margin | angular | none | 2 - 20 | mosaic |
| A ₁ | 50 - 95 | apl. porph., minor qtz+/-kfp | bt ₁ core, kfp margin | digested to angular | magmatic | 3 - 30 | inclusion BX |

Abbreviations: apl. porph. = aplite porphyry, BX = breccia, bt₁ = dark biotite associated with a pre-MHBX alteration event, bt₂ = pale matrix biotite, cc = calcite, fl = fluorite, kfp = K-feldspar, mo = molybdenite, qtz = quartz, ovrprnt. = overprinting, q-s-p = quartz-sericite-pyrite. Note: Most of the alteration is pre-MHBX, except some kfp overprinting earlier bt₁, and q-s-p.

From Ross et. al., 2001.

biotite alteration, Kspar flooding, quartz-sericite-pyrite (QSP) alteration, and QSP overprinting biotite alteration. It was proposed that the differences in the breccia facies is due to evolution of the magmatic-hydrothermal fluid away from its source, differing intensities of water/rock interaction, and/or differing breccia forming processes (Ross, 2002; Ross et al., 2002). A detailed explanation of the breccia forming mechanisms in the MHBX can be found in Ross, 2002 and Ross et al., 2002.

MHBX-related grade contribution was defined by Ross (2002) within the eastern portion of the Goat Hill (Figure 8). This is also the area of study for this paper. The MHBX-related grade contribution in the Goat Hill is concentrated in the C, D, and E facies, where QSP alteration is prevalent, with a grade range of 0.2-0.5%, 0.4-0.5%, and 0.2-0.5% MoS₂, respectively.

Previous Fluid Inclusion Studies

Previous fluid inclusion studies have been performed on Climax-type porphyry Mo deposits in attempts to determine the geochemistry and genetic origin of the fluids that deposited the molybdenum ore. The previous studies discussed in this paper cover Climax and Henderson of the Colorado Mineral Belt (COMB), and the area of study for this paper - Questa, New Mexico.

Climax, Colorado

Hall et. al. (1974) performed a fluid inclusion study on 120 samples from the Climax mine in Colorado. Three distinctive types of fluid inclusions were observed. Type I fluid inclusions of Hall et. al. (1974) are the most abundant, have a moderate salinity (0.7-12 eq. wt. % NaCl), contain 15-25% vapor, and contain zero to two non-salt daughter minerals. Type II fluid inclusions of Hall et. al. are gas-rich (50-75% vapor)

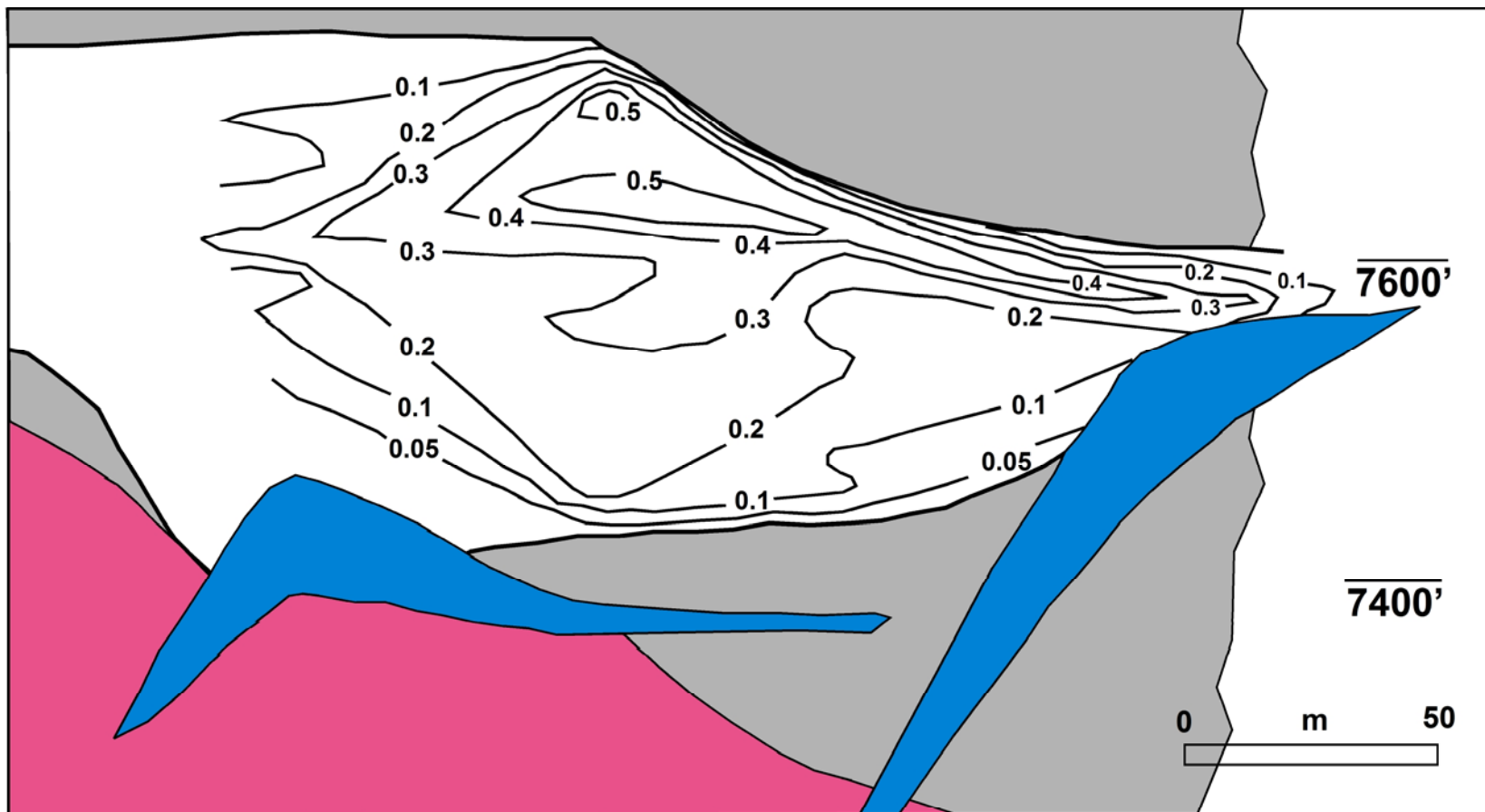


Figure 8 - MHBX grade distribution (in wt. % MoS₂). See figure 6 for location and lithologic symbols. Modified from Ross, 2002.

and have a final temperature of homogenization greater than 350°C. Some Type II inclusions containing liquid CO₂ were observed, but are not common. Type III fluid inclusions of Hall et. al. are liquid rich (10-15% vapor) higher salinity inclusions (~35 eq. wt. % NaCl) containing halite daughter minerals and other translucent daughters.

Final temperatures of homogenization (T_h) range from 200-600°C with a mode at 250-350°C. Only gas-rich inclusions exhibited a T_h above 400°C. As found in other studies of porphyry systems, both copper and molybdenum, the recognition of primary and secondary inclusions, paragenetic relationships, and associations with a particular intrusion, stage of mineralization, or alteration, have been obscured by the complex array of fluid inclusion types and their great abundance in all samples of this deposit. This mixing of fluid inclusion types was found to be the reflection of multi-stages of mineralization, typical of Climax-type systems. Gas-rich inclusions did not co-exist with liquid-rich inclusions. Therefore, no evidence of boiling was observed in the samples from the Climax deposit. Consequently, Hall et al. (1974) interpret the fluids to have been either above or below the liquid/vapor boiling curve.

Mo mineralization was determined to be at 360°C and 250 bars, with an equivalent depth of mineralization of 10,000 feet. Mineralization was interpreted to be predominantly from the moderately saline inclusions. Based upon this data, and that of their light stable isotope study, Hall et al. (1974) concluded that the fluid depositing the molybdenum ore was not purely magmatic, but was a fluid formed by the mixing of magmatic and meteoric fluids.

Henderson, Colorado

Kamilli (1978) and White et al. (1981) reported findings of a fluid inclusion study performed on the Henderson Mine in Colorado. The fluid inclusions observed at Henderson were in open-space filling veins, the equivalent to the Goat Hill MHBX at Questa. Secondary fluid inclusions were dominant over primary inclusions at Henderson. However, as seen in other porphyry systems, numerous fluid inclusions could not be grouped in any distinguishable group. Abundant evidence of boiling was observed at Henderson. The fluid inclusions observed contained abundant daughter minerals, with halite, hematite, carbonate, and molybdenite being most recognizable and common. Three principle types of fluid inclusions with corresponding salinities were observed at Henderson: liquid-rich at 0-5 eq. wt. % NaCl, vapor-rich at 10-20 eq. wt.% NaCl, and liquid-rich containing halite daughters at 30-65% eq. wt.% NaCl. Final temperatures of homogenization ranged from >600°C in early stages of mineralization to 250°C in the final stage of mineralization, with a principal peak at 400°C. Inclusions containing halite daughters often had final temperatures of homogenization by halite dissolution (Tshl) at 100-200°C greater than vapor bubble disappearance (vbd). This temperature difference between Tshl and Tlv (liquid-vapor homogenization) requires pressures much greater than any realistic lithostatic load. This is thought to be indicative of overpressures caused by exsolution and evolution of hydrothermal fluid under the projected lithostatic conditions of 350-585 bars. Hence, it was thought a pressure correction should be applied to these highly saline and also the less saline inclusions. This correction would raise the average temperature of molybdenite mineralization to 500-650°C, a temperature reflecting purely magmatic origin.

Carten (1987) described two different fluid types observed in fluid inclusions related to the mineralization at Henderson: a chlorine-rich peralkaline fluid and fluorine-rich peraluminous fluid. As in other studies, Carten also found most of the fluid inclusions to be secondary in origin, in which each type of fluid was trapped in separate secondary planes. Those fluid inclusions related to the chlorine-rich peralkaline fluid contained halite+hematite+manganosiderite+sylvite+erythrosiderite daughter minerals, with a salinity of 62 eq. wt.% NaCl in the earlier chlorine-rich fluids to 16-20 eq. wt.% NaCl in the later chlorine-rich fluids. The temperature of vapor bubble disappearance ($280\pm 35^{\circ}\text{C}$) for the chlorine-rich fluids was substantially less than the temperature of dissolution of halite. This fact, in addition to the absence of cogenetic low-salinity vapor-rich inclusions led to the conclusion that the high salinity liquid was derived directly from the silicic melt. The fluorine-rich peraluminous fluid described by Carten (1987) was parent to fluid inclusions that contained micalike daughter minerals that occupied approximately 50% of the fluid inclusion by volume. No chloride daughters were observed. The fluid inclusions consisted of an aqueous liquid that homogenized at $346\pm 30^{\circ}\text{C}$ with a temperature of final ice melting (T_{mice}) of $-3.4\pm 1.9^{\circ}\text{C}$. The micalike daughter minerals observed in these inclusions dissolved at $400\text{-}550^{\circ}\text{C}$. This fluorine-rich, peraluminous fluid is thought to represent the ore-fluid in which the molybdenum partitioned.

Seedorf and Einaudi (2004) conducted a reconnaissance fluid inclusion study at Henderson for the purpose of assigning approximate temperatures of formation to the various mineral assemblages and incorporating those temperatures into a model of the geochemical evolution of the hydrothermal system. The mineral assemblages at

Henderson were grouped by the temperature in which they formed – high, moderately high, moderate, or low temperature. Molybdenite mineralization is associated with the high and moderately high temperature mineral assemblages. The moderately high, moderate, and low temperature mineral assemblages were grouped as the “lower temperature” assemblages, which were divided further into two subgroups based upon their position – above intrusive centers and on the flanks of the Seriate center (one of three intrusive centers that are composed of 12 rhyolitic stocks at Henderson). The fluid inclusion study was conducted on the “lower temperature” assemblages. As in earlier fluid inclusions studies at Henderson, and other porphyry systems, determining fluid inclusion paragenesis proved difficult, due to ambiguity caused by numerous superimposed populations. The moderately high, moderate, and low temperature assemblages resulted in temperatures of formation of 600-460°C, 530-310 °C, and low 390-200 °C, respectively. The inclusions from mineral assemblages above the intrusive centers demonstrated salinities of 28-65 eq. wt.% NaCl+/-KCl. Inclusions from mineral assemblages on the flanks of the Seriate center demonstrated salinities <29 eq. wt.% NaCl+KCl. High salinities (29-36 eq. wt.% NaCl) found in inclusions associated with sericite and intermediate argillic alteration led to the conclusion that cooling of evolved, magmatic fluids, rather than meteoric input, was the mechanism for sericitic and intermediate argillic alteration.

Questa, New Mexico

Bloom (1981) performed a reconnaissance study on fluid inclusions related to mineralization and associated alteration at Questa, and Hudson Bay Mountain and Endako in British Columbia. The samples collected and analyzed at Questa were from

the open pit at the 8480 bench. As seen in other studies, complex overlapping of fluid inclusion populations and types often made it difficult to locate primary inclusions and/or to distinguish between primary and secondary inclusions. Bloom identified five distinct fluid inclusion types at Questa: [liquid(l)>vapor(v)+/-hematite(hm)] type A, [l<v+/-hm+/-halite(hl)] type B, [l>v+hl+/-hm] type C, [l>v+hl+sylvite+/-hm+/-mo+/-unknowns] type D, and [l_{H2O}+l_{CO2}+v_{CO2}] type E. Hypersaline (33.5-51 eq. wt.% NaCl; 10-19% eq. wt. % KCl; 40-70% NaCl+KCl) Type D fluid inclusions are suggested to be associated with early, fluorine-rich biotite-stable potassic alteration. Type D inclusions exhibited predominantly a final T_h by halite dissolution with a range of 320°C to >600°C uncorrected and a mode at 390°C. Bloom suggests that the bulk of molybdenite mineralization coincided with quartz-sericite-pyrite or phyllic alteration and with the moderately saline (30-60 eq. wt.% NaCl) type C fluid inclusions or the low to moderately saline (5-15 eq. wt.% NaCl) type A fluid inclusions. Type C fluid inclusions homogenized by T_{s,hl} or vapor bubble disappearance with a range from 300->600°C and a mode at 390°C. Type A inclusions homogenized by vapor bubble disappearance and also exhibited a final T_h of 300->600°C with a mode at 390°C. Pressures varied during mineralization from lithostatic to hydrostatic load with intermittent overpressures. Hence, a universal pressure correction could not be applied. Local or intermittent boiling is evident, however significant boiling is not probable due to the lack in abundance of co-existing vapor-rich inclusions.

Bloom suggests that the various fluid inclusion data is evidence for evolution from magmatic to meteoric conditions. The hypersaline type D solution was a precursor to the bulk of mineralization and evolved directly from the granitic source magma.

Fluids re-equilibrated with the granitic source intrusion, or the dissolution of halite precipitated by earlier hypersaline type D solutions along the halite trend, are possible origins of saline type C inclusion fluids. Fracturing events causing adiabatic cooling may be a possible mechanism of cooling the hydrothermal solutions from near magmatic temperatures (390°C mode). Further fracturing in the system permitted the influx of meteoric water, a source for the low salinity type A fluid inclusions.

Smith (1983) performed a reconnaissance fluid inclusion study and a study on the solution geochemistry of molybdenum at Questa. As in other studies discussed, Smith found the determination of paragenesis between fluid inclusion populations to be difficult due to superimposed populations of fluid inclusion types. Four types of primary fluid inclusions were observed: two-phase l>v that homogenize by vapor bubble disappearance, two-phase l<v that homogenize by liquid disappearance, three-phase l>v+hl+/-hm+/-mo that homogenize by vapor disappearance or dissolution of halite, and multiphase l>v+hl+sylvite+/-hm+/-mo+/-anhy+/-opaques(op). A wide range of homogenization temperatures were measured: 300-500°C, 520-555°C, and 580-600°C. Salinities demonstrated a bimodal distribution of 5-20 eq. wt.% NaCl and 25-65 eq. wt.% NaCl. Liquid-rich secondary inclusions were observed in almost every sample with a T_h range of 200-370°C.

Smith (1983) found that the hypersaline inclusions containing halite and sylvite only occurred in quartz-biotite veins which predate molybdenite mineralization and therefore represent the earliest fluids. Smith concluded that halite-bearing saline inclusions found in quartz veins associated with potassic and sericitic alteration may represent fluids generated from earlier hypersaline fluids by the exchange of K for Na

during potassic alteration. The halite-bearing saline inclusions and the liquid-rich two-phase inclusions are believed to be associated with molybdenite mineralization. Smith could not establish the paragenesis of the vapor-rich inclusions due to their coexistence with all other inclusion types. Co-existence of liquid-rich and vapor-rich fluid inclusions was interpreted to represent boiling. In the case of boiling fluids, $T_h=T_t$ (temperature of trapping) and no pressure correction was necessary. The pressure of the boiling fluids was approximately 180 bars for this case. Smith states that local or sporadic boiling is evident, however most inclusions were not trapped at P-T-V conditions that allowed boiling. For the inclusions that represented non-boiling fluids, pressures were calculated to range from less than 100 bars for 500 bars. Temperatures of halite dissolution occurred within 40°C of vapor bubble disappearance in fluid inclusions which homogenized by halite dissolution. Smith calculated a pressure of approximately 330 bars for these inclusions.

Smith (1983) delineated the following geochemical factors that would favor molybdenite mineralization. Molybdenite is transported in saline, high temperature fluids. A decrease in the temperature of the fluid from 350 °C-250 °C would result in a 98% decrease in molybdenite solubility. A decrease in pressure from 500 bars to 65 bars at 350 °C would decrease molybdenite solubility by 60%. An increase in pH and decrease in oxygen fugacity would aid in molybdenite deposition. Dilution of saline hydrothermal fluids by meteoric water would decrease molybdenite solubility. Molybdenite deposition would occur in response to wall-rock interaction with the fluids associated with potassic alteration, i.e. the formation of fluorine-rich micas, or the alteration of igneous biotite to magnesium-rich hydrothermal biotite.

Cline and Bodnar (1994) performed a fluid inclusion study on samples collected from andesite in the MHBX footwall at the 7120 ft haulage level of the Deep “D”-orebody. Cline and Bodnar chose these samples because they were thought to be representative of system sealing following brecciation and aqueous fluid exsolution that prohibited fluid influx following ore deposition. These samples were also chosen due to the high fluorine content of the MHBX matrix phlogopite, which is interpreted by Cline and Bodnar to be an indicator that no alteration by post magmatic fluorine-poor fluids has occurred. Cline and Bodnar only analyzed inclusions in the quartz-biotite-molybdenite matrix zone with silica- and potassium feldspar-flooded clasts (Ross (2002) C, D or E zones), which excludes other zones of the MHBX. In addition, predominantly only large inclusions in clear quartz adjacent to the fluorophlogopite were analyzed. Sampling and analysis of only these zones and specific inclusions more than likely limited this study in terms of proper representation of the ore fluids and fluid evolution.

Again, as in other studies of this deposit type, no distinction between primary and secondary fluid inclusions could be made, most likely due to superimposed inclusion populations and types. Three fluid inclusion types representing three distinct fluids were identified in this study at Questa: liquid-rich low salinity type I inclusions that homogenize by vapor bubble disappearance, vapor-rich type II that homogenize to liquid, vapor, or by critical behavior, and high salinity liquid-rich type III fluid inclusions in which approximately 80% homogenize by halite dissolution and the remainder homogenize by vapor bubble disappearance. Type I fluid inclusions exhibited a final T_h range of 150-370°C and a salinity range of 0-12 eq. wt.% NaCl. Near critical type II fluid inclusions exhibited a wide range of homogenization temperatures and salinities of 360-

500°C and 2-26 eq. wt.% NaCl, respectively. Saline type III fluid inclusions homogenized between 200° and 500°C with a mode at 360° to 400°C. Type III salinities varied from 31 to 57 eq. wt. % NaCl.

Based upon phase equilibria constraints (inclusions that homogenize by halite dissolution are required to have been trapped in the liquid-stable, vapor-absent field) and lack of low-density inclusions co-existing with liquid-rich brine inclusions, Cline and Bodnar concluded that these fluids were not boiling and the different fluid inclusion types were not formed by aqueous fluid immiscibility. Instead, Cline and Bodnar suggest that the fluids originated by exsolution directly from the crystallizing silicic melt and different pressure regimes yielded the three different fluid types with their respective homogenization temperatures and salinities. The system consisted of an increasing pressure regime with MHBX formation which yielded the moderate salinity fluids and moderate pressures, system sealing causing a high pressure setting and high salinity inclusions, overpressures yielding high salinity inclusions where $T_{lv} \ll T_{shl}$, and a low pressure post-brecciation setting which yielded the low salinity fluids and/or the low salinity, lower temperature fluids may have exsolved directly from the silicic melt prior to MHBX formation. Based upon all of these criteria, Cline and Bodnar suggest that the system at Questa was purely magmatic, with no meteoric input.

Cline and Vanko (1995) include similar data and interpretations that were presented in Cline and Bodnar (1994) of the previous year. High fluorine content of the biotite suggests that only magmatic fluids played a part in the formation of the orebody, in that post-magmatic (meteoric) fluorine poor fluids would have exchanged OH⁻ complexes for fluorine. No definitive criteria to distinguish primary and secondary

inclusions were observed. Three types of fluid inclusions were identified: liquid-rich, low salinity type I inclusions that homogenize by vapor-bubble disappearance (150-370°C), vapor-rich type II inclusions that homogenize to a liquid (370->470°C), vapor (390-500°C), or by critical behavior (370-420°C), and high salinity type III inclusions in which 80% homogenize by the dissolution of halite (220-490°C, mode at 350-420°C) and the remainder by vapor-bubble disappearance (230-420°C). No CO₂ was detected in any of the fluid inclusions.

Cline and Vanko chose not to discuss type I inclusions due to their lack of abundance. Cline and Vanko suggest that either the high salinity fluid or the low-salinity near-critical fluid transported and precipitated the concentrated ore metals. Based upon the lack of co-existing low-salinity vapor-rich and high-salinity fluid inclusions and the fact that the inclusions which homogenized by halite dissolution could not have co-existed with a low salinity fluid stably, Cline and Vanko concluded that these fluids are a result of direct exsolution from the crystallizing silicic melt rather than aqueous fluid immiscibility. Cline and Vanko also use pressure fluctuations to explain the broad range of homogenization temperatures and salinities. Pressure fluctuations occurred as the system sealed, resulting in overpressures and eventually in brecciation. At low pressures, low salinity type I fluids were produced. As the system began to seal itself off, moderate pressures yielded moderately saline type III inclusions. At high pressures, high temperature and high salinity type III fluid inclusions were produced. Eventual overpressures leading to fracturing and brecciation produced type III brines where $T_{lv} \ll T_{shl}$. After brecciation, the pressure is dramatically reduced, producing low salinity, perhaps near critical fluids.

Klemm (2004) performed a preliminary fluid inclusion study on free-grown vuggy quartz from the D facies of Ross (2002a and 2002b). Klemm divided the observed fluid inclusions into 3 groups: i) l=v, variable CO₂, low to moderate salinity (5-12 eq. wt. % NaCl), opaque daughters present; ii) high salinity brine (31-46 eq. wt.% NaCl) with several daughters (both ots and op); and iii) vapor-rich inclusions. Klemm identified two distinct brine fluids: an early brine with a salinity of 38-46 eq. wt.% NaCl and Th>450°C by vbd, and a late brine with a salinity of 32-40 eq. wt.% NaCl with a Th range of 270-350°C. The early brine co-exists with the vapor-rich fluid inclusions, evidence of boiling. Klemm analyzed individual fluid inclusions with an LA-ICPMS for Na, K, Mn, Fe, Mo, and Cu. The early brines contained up to 1000 ppm of Mo. Mo was below detection limits in the late brines. Klemm concluded that early single-phase low salinity type I inclusions represent fluid that exsolved directly from the crystallizing magma. Klemm also concluded that Mo precipitated from the brine by temperature decrease, since Mo concentrations decrease dramatically by over an order of magnitude with decreasing Th.

METHODS

Fourteen samples from the Goat Hill orebody, two samples from each zone of the MHBX defined by Ross (2002a and 2002b) (A₁, A₂, A₃, B-E), were collected from 5 different drillholes (19.9-12.1, 21.7-15.5, 22.0-14.0, 23.4-11.8G, 23.5-11.8G) for petrographic and fluid inclusion analysis (See Figure 5 and Figure 6). The presence of quartz was the primary criteria for sample selection. Quartz was the main mineral of interest due to its abundance in the orebody, known association/cogenesis with molybdenite, general transparency, abundant fluid inclusion content, and fairly high insusceptibility to leakage and necking-down of the fluid inclusions.

Petrographic Analysis

Prior to fluid inclusion analysis, a petrographic analysis was performed on each of the 14 samples for mineralogy, alteration, and paragenetic relationships. A 1 inch x 2 inch x ½ inch billet was cut for each sample and sent to Quality Thin Sections (QTS) in Tucson, Arizona for sample preparation. Sample preparation consisted of mounting a mirror slice of the doubly polished fluid inclusion thick section for each sample onto a microscope slide and polishing the thin section to 30 microns. The petrographic thin sections were analyzed under both reflected and transmitted light with a Nikon OPTIPHOT-POL petrographic microscope. Photographs were taken using a Nikon AFX microscope mounted camera.

Fluid Inclusion Analysis

After analyzing the samples petrographically for mineralogy, alteration, and paragenetic relationships, fluid inclusion analyses were performed. The fluid inclusion thick sections were doubly polished and cut by QTS into a 0.2-0.5 mm thick mirror slice of the corresponding petrographic section. The fluid inclusion wafers were removed from their microscope slides with acetone prior to analysis. In addition, the fluid inclusion wafers were broken into approximately 4x4 mm chips, so that they may fit on the fluid inclusion microscope stage. The chips were analyzed petrographically for fluid inclusion paragenetic relationships, distribution, content or phases present, size, and shape prior to microthermometric measurements.

Microthermometric measurements were made using a Linkam THMS-600 heating/freezing stage that was mounted on a petrographic microscope and associated automatic temperature controller. Microthermometric analysis is the measurement of the

temperature in which phase changes occur within a fluid inclusion during heating or cooling from room temperature. Phase changes that may occur in a fluid inclusion during cooling are T_e (temperature of the eutectic or first ice melting), $T_{m_{ice}}$ (temperature of final ice melting), $T_{m_{CO_2}}$ (temperature of melting of solid CO_2), and $T_{m_{cl}}$ (temperature of melting of CO_2 or CH_4 clathrate). Phase changes that may occur in a fluid inclusion during heating are $T_{h_{CO_2}}$ (temperature of homogenization of CO_2), T_{lv} , T_{Shl} , T_{Sylv} (temperature of the dissolution of sylvite), and final T_h (temperature where only one phase remains). These measurements and observations can then be used to derive estimates of the PVTX conditions of the fluids at the time of trapping. The aforementioned phase changes were looked for during microthermometric measurements for this study.

The calibration of the instrument was checked in the beginning of each session on the fluid inclusion stage utilizing a pure water standard. In addition, each week the instrument calibration was checked using a pure water standard (mid temperature, $T_{m_{ice}} = 0^\circ C$), CO_2 -water standard (low temperature, $T_{m_{CO_2}} = -56.6^\circ C$), and potassium chromate standard (high temperature, $T_{SK_2CrO_4} = 398^\circ C$). The analytical error of the instrument is $\pm 0.1^\circ C$ for temperatures at or below $25^\circ C$ and $\pm 2.0^\circ C$ for temperatures around $400^\circ C$.

Following the calibration check, microthermometric measurements were performed on the 176 fluid inclusions. Due to the possibility of stretching of the fluid inclusions during the heating process, freezing measurements were taken first. Freezing measurements were performed on fluid inclusions that did not contain a halite or sylvite daughter mineral, and any inclusion suspected or known to contain a CO_2 phase.

Inclusions were cooled rapidly to -110°C and heated at a $20\text{-}0.1^{\circ}\text{C}/\text{min}$ ramp speed, depending on the proximity to the target temperatures. The slowest ramp speed was used when approaching the target temperature. All phase changes and corresponding temperatures were recorded. After freezing measurements were obtained, the fluid inclusions were heated until the final phase change (final T_h) or decrepitation occurred. The inclusions were heated at a ramp speed of $2\text{-}0.5^{\circ}\text{C}/\text{min}$. All phase changes and corresponding temperatures were recorded. Salinity was calculated from either the temperature of final ice melting ($T_{m_{\text{ice}}}$) or the temperature of halite dissolution (T_{shl}) utilizing the MacFlinCor computer program of Brown and Hagemann, 1994. All measured or calculated fluid inclusion data was recorded and tabulated in Appendix A.

RESULTS

Petrography

MHBX Clasts and Clast Alteration

The MHBX clast alteration was found to evolve from the bottom of the breccia (A-facies) to the top and distal edges (E-facies) as similarly noted by Ross, 2002. Petrographic analysis revealed biotite alteration and Kspar flooding in facies A; biotite alteration and kspar flooding in B; biotite, QSP overprinting biotite alteration (often with a “spotty” texture), QSP alteration, and kspar flooding in C; QSP and QSP overprinting biotite alteration in D; and QSP alteration in E. The minerals identified in the MHBX clasts consist of fluorophlogopite, quartz, sericite, Kspar, rutile, fluorite, pyrite, molybdenite, calcite, topaz, kaolinite, apatite, magnetite, and chalcopyrite (Figure 9). In addition, late stage sericite, calcite, and fluorite veins were observed in the clasts. A

| MINERAL | A1 Clast | A2 Clast | A3 Clast | B Clast | C Clast | D Clast | E Clast |
|-------------------------|-----------------|-----------------|-----------------|----------------|----------------|----------------|----------------|
| aplite | x | No clasts in | | | | | |
| apatite | | petrographic | | x | | x | |
| calcite | | sections | | x | | | |
| chalcopyrite | | | | | | x | |
| fluorite | x | | x | x | | x | x |
| fluorophlog (bt) | | | x | x | x | x | x |
| kaolinite | | | | x | x | x | |
| kspar | | | x | x | x | | |
| molybdenite | | | | x | x | x | x |
| magnetite | | | | | | x | |
| pyrite | | | x | x | x | | x |
| quartz | x | | x | x | x | x | x |
| rutile | | | x | x | x | x | x |
| sericite | x | | x | x | x | x | x |
| topaz | | V | x | x | x | x | x |

Figure 9. Facies distribution of minerals in MHBX clasts.

paragenesis diagram for the MHBX clasts is available as Figure 10. A detailed petrographic analysis for each sample used in this study is available in Appendix B.

MHBX Matrix

The MHBX matrix was found to evolve mineralogically from the bottom of the breccia and closest to the source intrusion to the top and distal edges of the breccia, as similarly noted by Ross, 2002. The major matrix components observed consist of aplite, quartz, potassium feldspar, and minor to trace molybdenite in the A facies, quartz, potassium feldspar and minor molybdenite in B, quartz, potassium feldspar, fluorophlogopite, molybdenite, fluorite, calcite, and anhydrite in C, quartz, fluorophlogopite, molybdenite, fluorite, calcite, and anhydrite in D, and quartz, fluorophlogopite, molybdenite, fluorite, and calcite in E (Figure 11). Anhydrite had not been observed in the samples collected from facies E, however it has been noted in the E facies in the drillcore examined for this study. Gypsum occurring as a matrix material, as observed in facies C and D, can either be an alteration product of anhydrite, or as a matrix constituent. Both of these cases have been observed. Other matrix minerals that were observed in thin section are rutile, pyrite, sericite, kaolinite, topaz, and apatite. In addition, late stage calcite, fluorite, sericite, and gypsum veins were observed to have cross-cut the matrix. A paragenesis diagram for the MHBX matrix is available as Figure 12.

Other Observations

Other mineralogic observations were made during petrographic analysis. Molybdenite has an affinity for K-feldspar, fluorophlogopite, and fluorite in this ore deposit. It was noted by Smith (1983) that fluoride coming out of solution as a result of

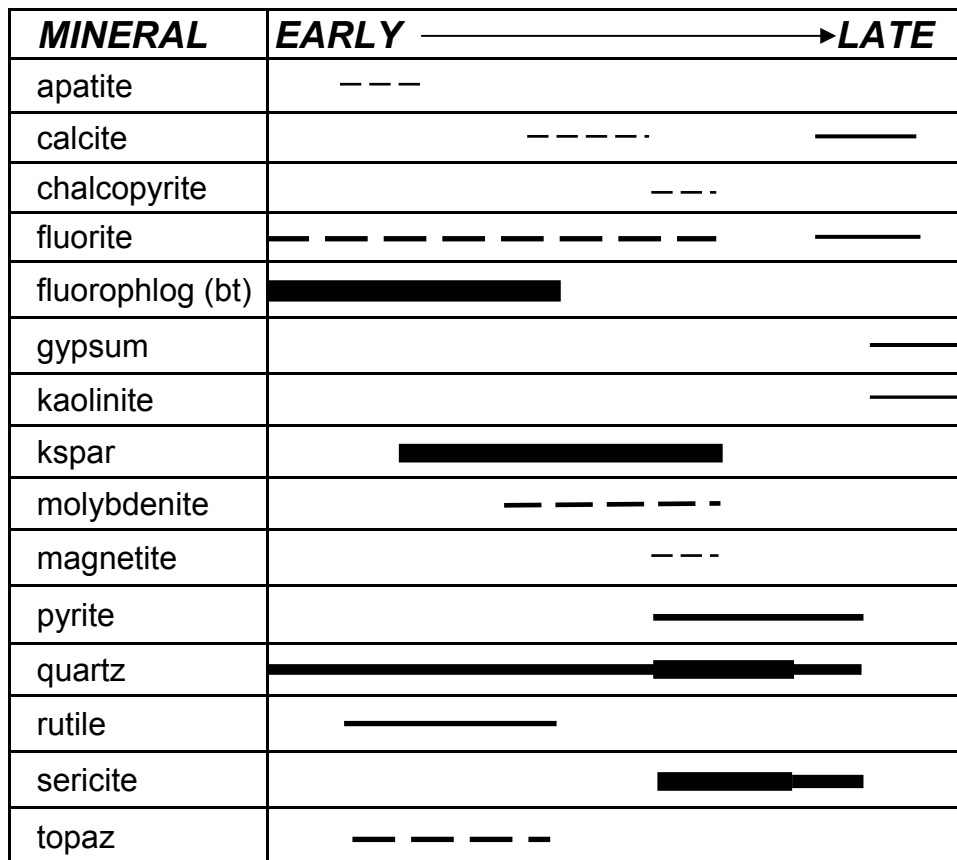


Figure 10. MHBX clast paragenesis. Thickness of line represents abundance of mineral.

| MINERAL | A1 Matrix | A2 Matrix | A3 Matrix | B Matrix | C Matrix | D Matrix | E Matrix |
|-------------------------|------------------|------------------|------------------|-----------------|-----------------|-----------------|-----------------|
| aplite | x | x | x | | | | |
| anhydrite | | | | | x | x | |
| apatite | | | | x | x | | |
| calcite | x | | | x | x | x | x |
| fluorite | x | x | x | x | x | x | x |
| fluorophlog (bt) | | x | x | x | x | x | x |
| gypsum | | | | | x | x | |
| kaolinite | x | x | x | x | x | x | |
| kspar | x | x | x | x | x | x | |
| molybdenite | x | x | x | x | x | x | x |
| pyrite | x | x | x | x | x | x | x |
| quartz | x | x | x | x | x | x | x |
| rutile | x | x | x | x | x | x | x |
| sericite | x | x | x | x | x | x | x |
| topaz | x | | | x | x | x | x |


 - very fine grained and/or minor amount of mineral compared to other facies.

Figure 11. Facies distribution of minerals in MHBX matrix.

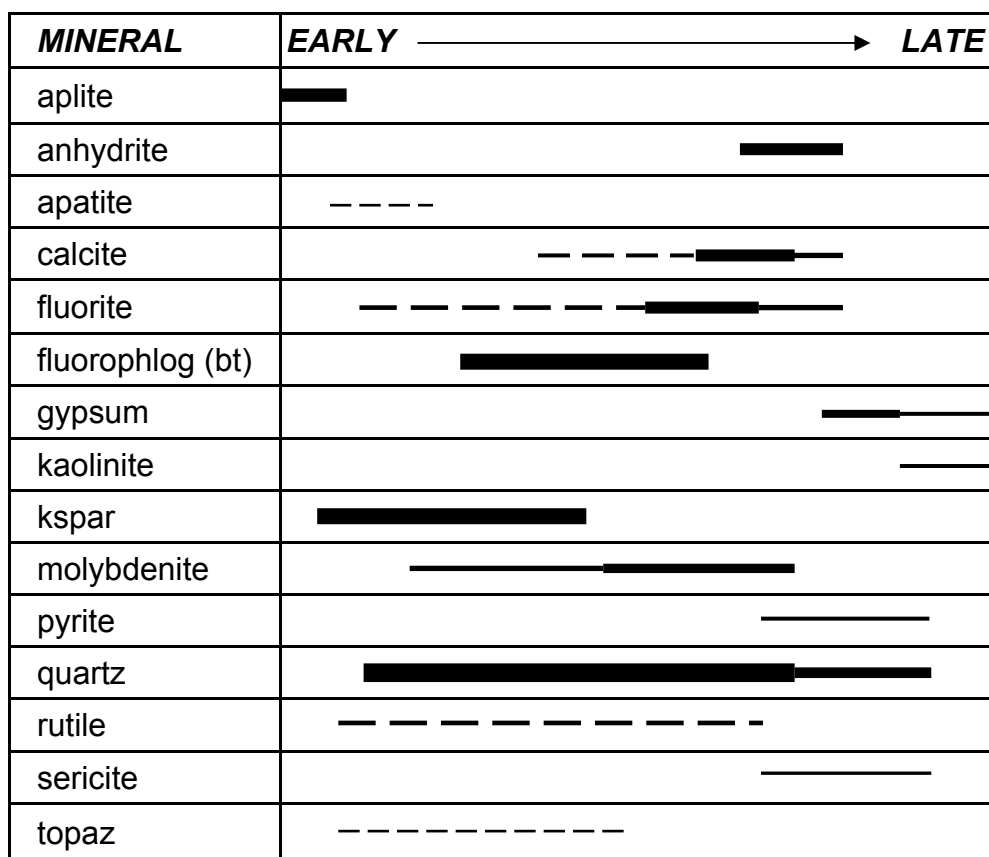


Figure 12. MHBX matrix paragenesis. Thickness of line represents abundance of mineral.

potassic alteration would cause molybdenite precipitation. Within the MHBX matrix, molybdenite often occurs with the coarse-grained fluorophlogopite and Kspar, and almost always occurs with very fine-grained disseminated fluorite that can only be seen microscopically. Molybdenite not only occurs as a matrix component in the MHBX, but as a disseminated phase within QSP altered and/or K-feldspar flooded clasts of the C, D, and E facies. Fluorophlogopite is most abundant in the breccia where there is little to no biotite in the clasts (C, D, and E facies). Fluorophlogopite occurs mostly along the matrix/clast interface growing outward into the matrix from the clast substrate. Fluorophlogopite has an affiliation with rutile, topaz, and fluorite. Fluorophlogopite grains within the matrix often contained abundant rutile inclusions. In some cases, fluorophlogopites were partially altered to entirely altered to sericite, or possessed minute sericite selvages on the edges of the grains. Similar to fluorophlogopite, Kspar most often occurred along the matrix/clast interface growing from the clast substrate into the matrix. On occasion, Kspar was found to be partially or entirely altered to sericite and kaolinite. Topaz grains often contained fluorite. Rutile and pyrite were often found in association. Coarse-grained (macroscopic) fluorite and anhydrite were not observed to coexist. The fluorite in the Goat Hill is either green or purple in color, as is the anhydrite.

Fluid Inclusions

Fluid inclusion analyses resulted in a very broad range of fluid inclusion temperatures and salinities as seen in Figures 13 and 14 (change subsequent figure numbers accordingly). The following sections will break down these results in terms of primary, pseudosecondary, and secondary paragenesis, types, and MHBX facies.

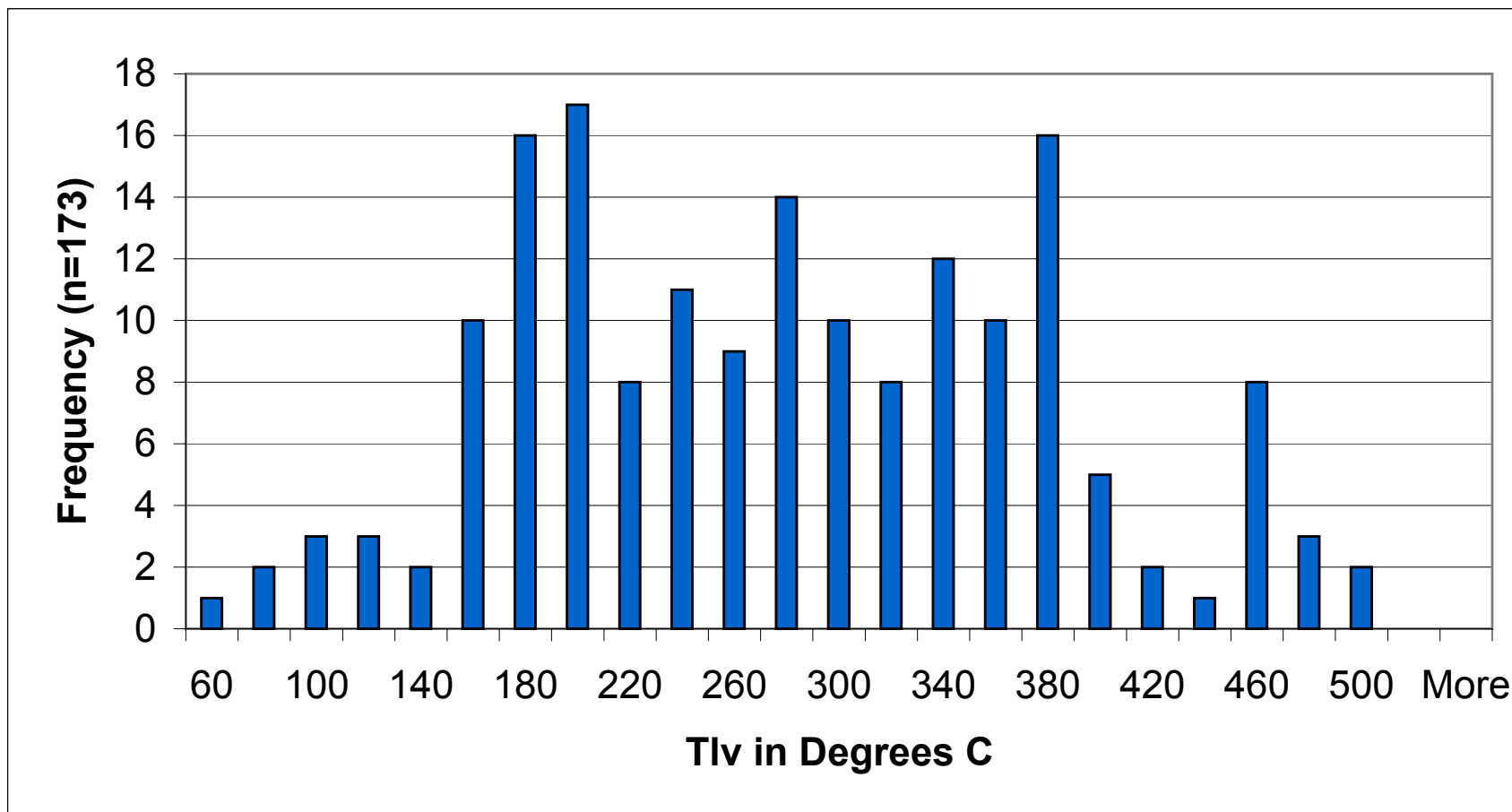


Figure 13. Tlv distribution for all fluid inclusions with a measurable Tlv.

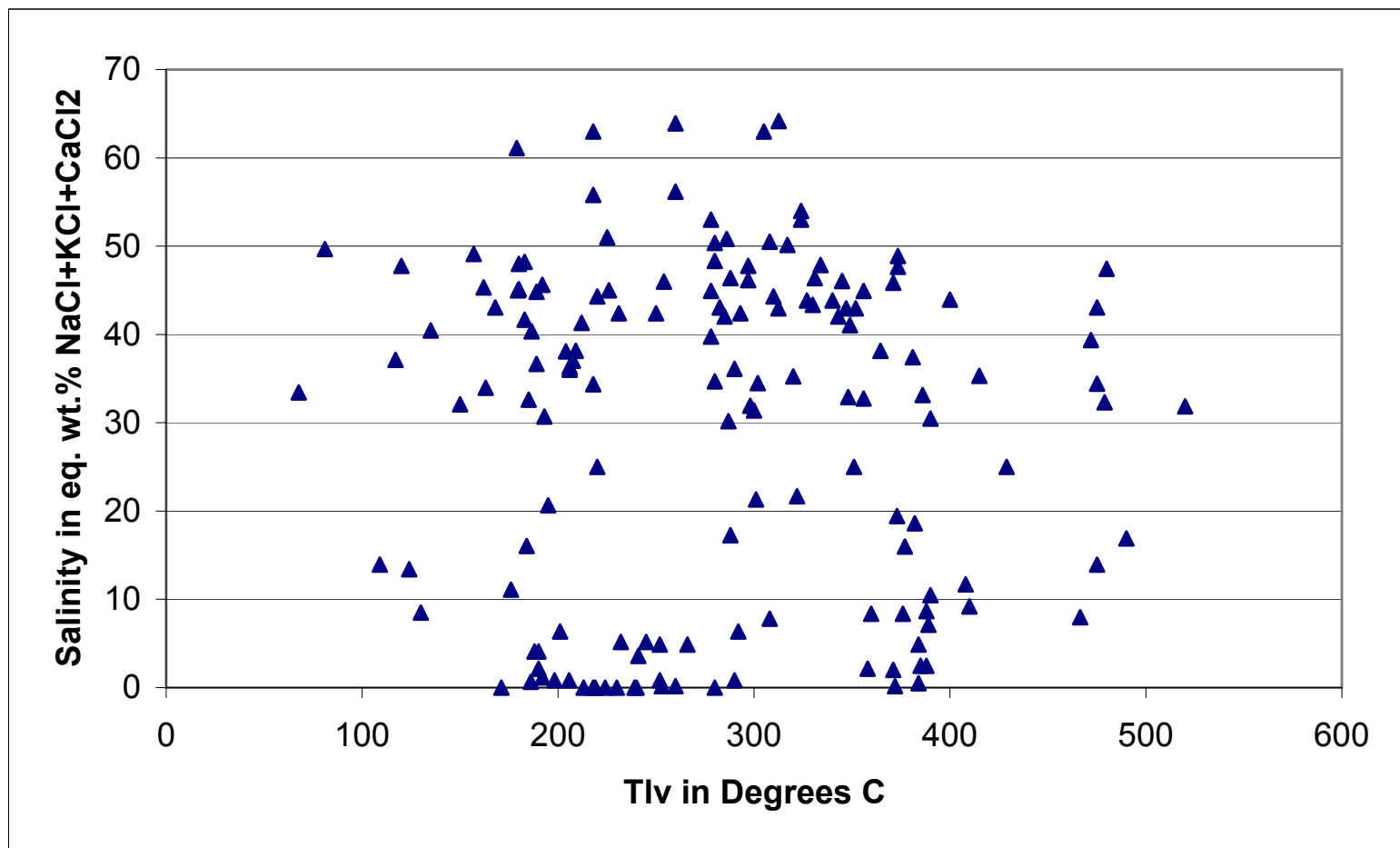


Figure 14. Tlv vs. salinity diagram for all inclusions with Tlv and salinity data.

Paragenesis

Due to the ambiguity of superimposed fluid inclusion populations, classifying individual fluid inclusions as primary, pseudosecondary, or secondary proved to be difficult, leading to an indeterminable paragenetic origin for most inclusions (Figure 15). However, fluid inclusion paragenetic origin was identified whenever possible based upon criteria summarized by Roedder (1979, 1984). Primary inclusions were identified by their occurrence along crystal growth planes or solitary location. Secondary inclusions were identified by their occurrence as arrays that cross-cut all growth zones of a crystal, often in healed fractures (Figure 16). Pseudosecondary inclusions were identified by their occurrence as arrays that cross-cut a crystal, but do not completely cut across all growth zones within the crystal. The paragenetic origin assigned to each individual inclusion can be found in Appendix A – Raw Fluid Inclusion Data.

The Tlv ranges for the known primary, pseudosecondary, and secondary inclusions were 120-467°C, 81-475 °C, and 88-253 °C, respectively (Figures 17 and 18). The fluid inclusions in which the paragenetic origin was indeterminate had a Tlv range of 67.6-520 °C. The salinity ranges for known primary, pseudosecondary, and secondary inclusions were 8-34 eq. wt.% NaCl, 0-53 eq. wt.% NaCl, and 0-8.5 eq. wt.% NaCl, respectively (Figure 18). Inclusions labeled indeterminate demonstrated a salinity range of 0-64 eq. wt.% NaCl.

Types

Based upon visible phases at room temperature, four major fluid inclusion types were identified at Questa (Table 3). Type I inclusions contain liquid and vapor, and are divided into three subtypes (a, b, and c). Type Ia fluid inclusions are liquid-rich and

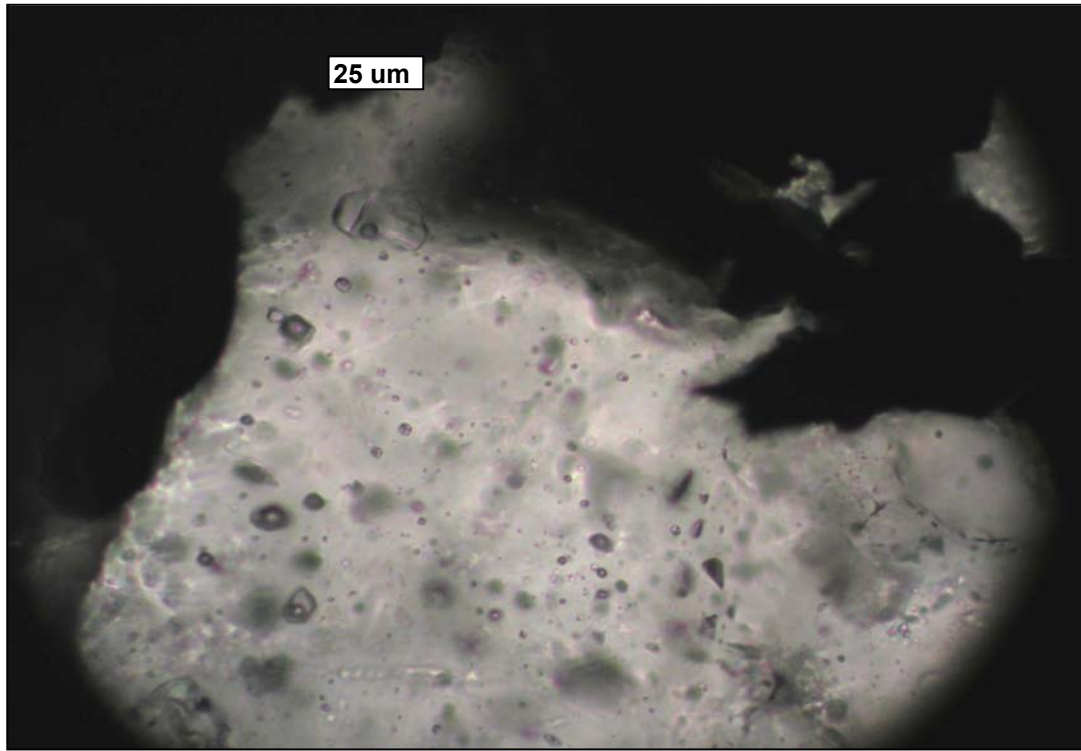


Figure 15. Superimposed fluid inclusion populations in A1 matrix. Superimposed populations lend to difficulty in assigning paragenetic origin to inclusions. Photo taken at 25°C prior to freezing or heating.



Figure 16. Secondary fluid inclusion plane in A3 matrix. Photo taken at 25°C prior to heating or freezing.

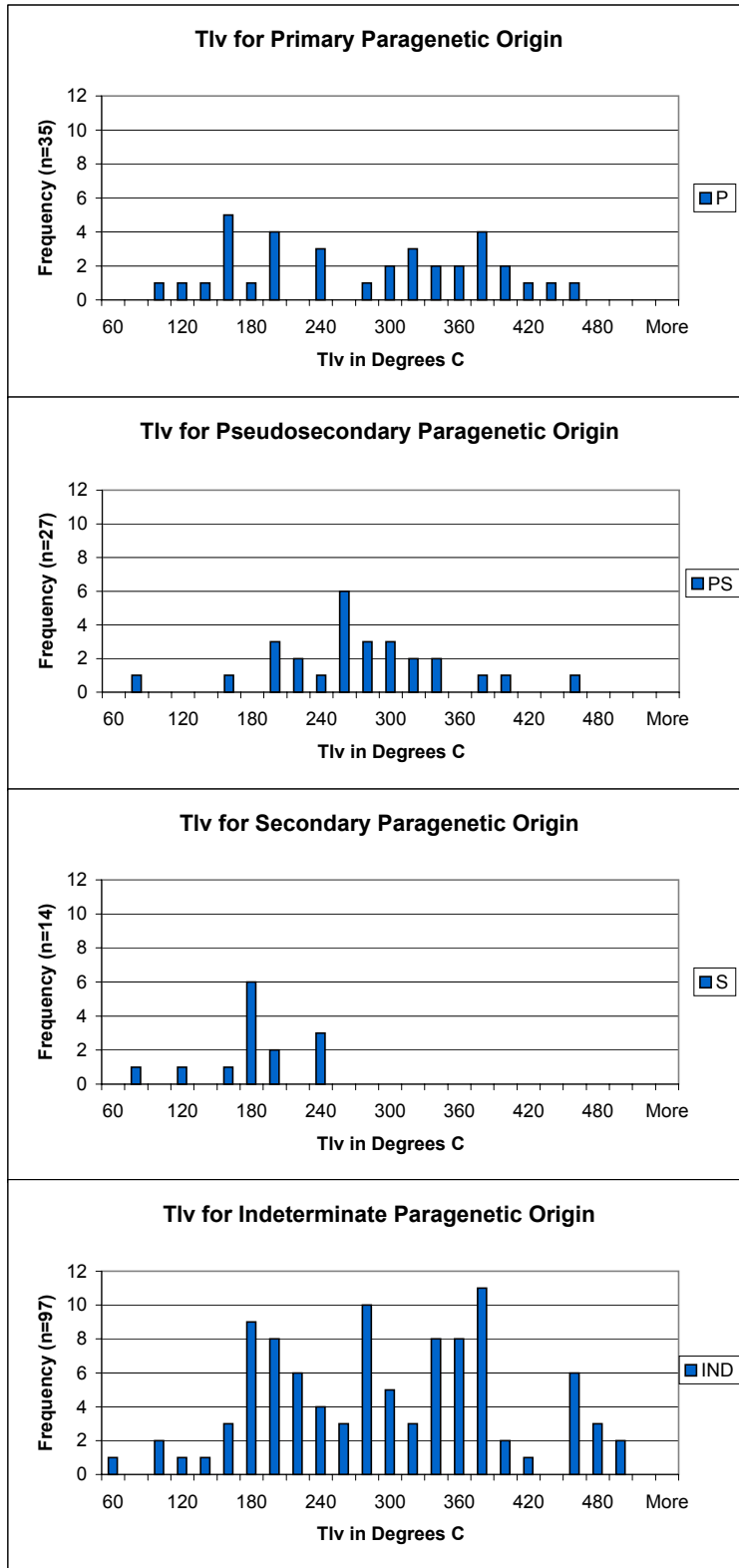


Figure 17. Tlv histograms for each assigned paragenetic species.
 IND - indeterminate P - primary PS - pseudosecondary
 S - secondary

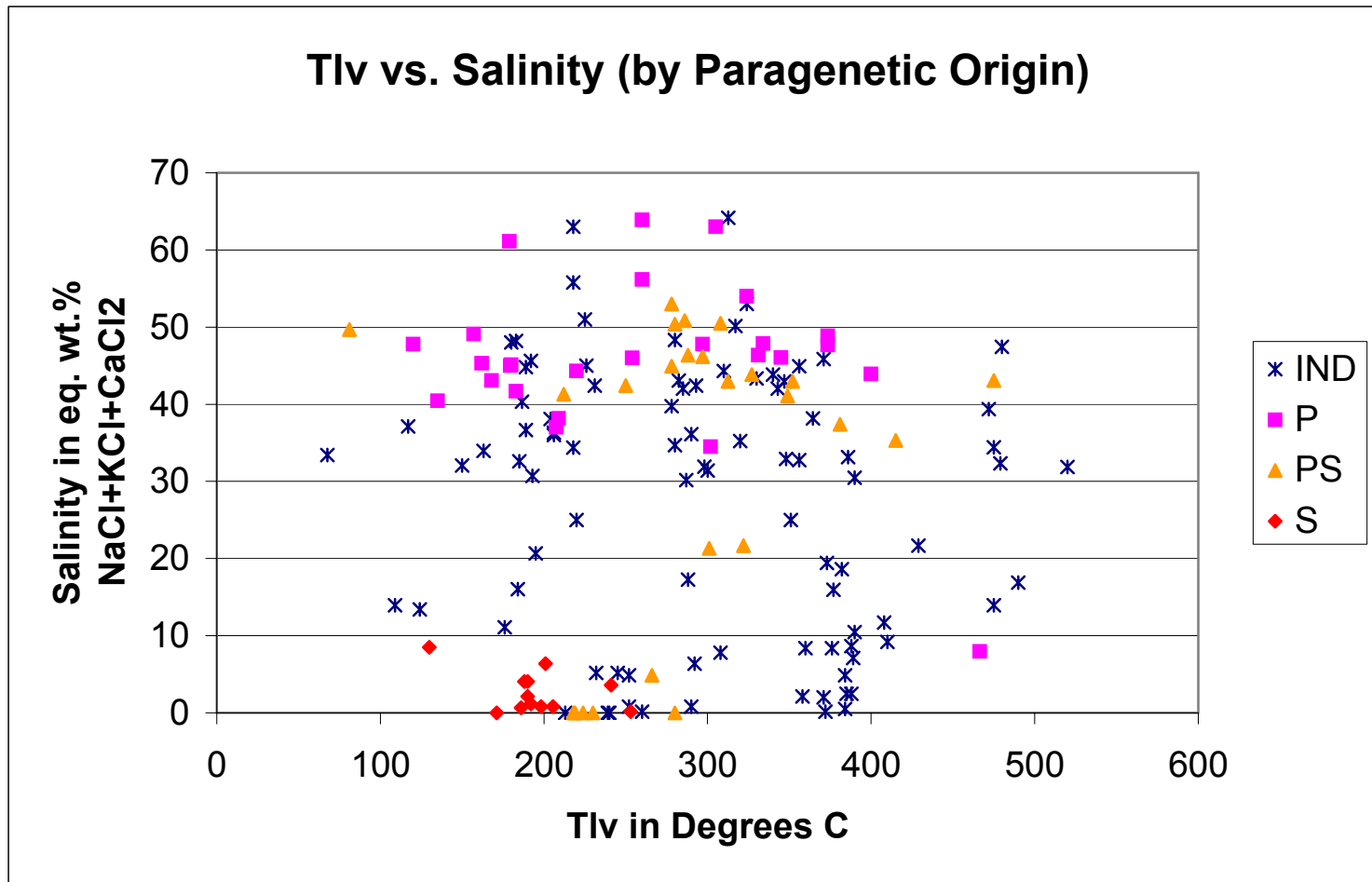


Figure 18. Tlv vs. Salinity diagram for each assigned paragenetic species.
 IND - indeterminate P - primary PS - pseudosecondary S - secondary

l = liquid v = vapor s = solid (daughters) op = opaques ot = other translucent daughters vbd = vapor bubble disappearance
 hm = hematite hl = halite sylv = sylvite anhy = anhydrite cb = critical behavior ld = liquid disappearance d = decrepitation
 otd = dissolution of other translucent daughters Th = temperature of homogenization


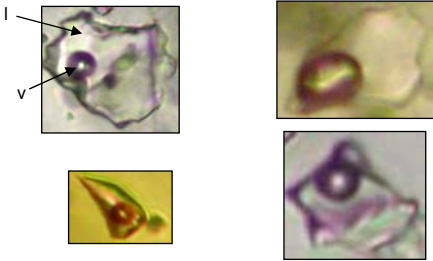
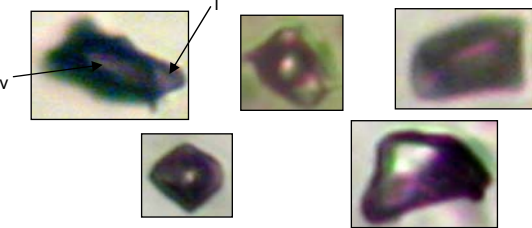
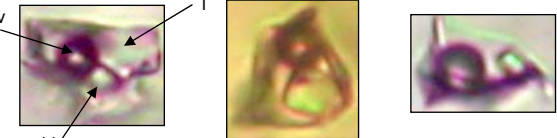
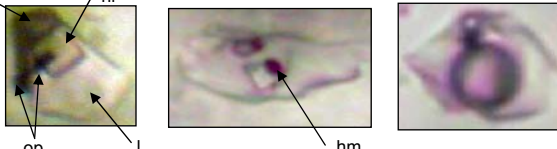

| Most Common Fluid Inclusion Types | Examples |
|-----------------------------------------------------------------------------------------------------------------------------------------------------------------------------------------------------------------------------------------------------------------------------------------------------------------------------------------------------|-----------------------------------------------------------------------------------------------------------------------------------------------|
| <p>la l+v+/-s; l>v; s=op or hm; Final Th by vbd or cb. Final Th range of 176-410°C; Tlv range of 87.6-488; Salinity range of 0-23 eq. wt% NaCl; Facies occurrence: A₁, A₂, A₃, B, C, D, E</p> |  |
| <p>lb l+v; l>v; Final Th by vbd, ld, cb, or d Final Th range of 109-490°C; Tlv range of 109-520°C; Salinity range of 0-22 eq. wt.% NaCl; Facies occurrence: A₁, A₂, A₃, B, C, D, E.</p> |  |
| <p>lc l+v; v>=l; Final Th by vbd, ld, or cb Final Th and Tlv range of 360-485°C; Salinity range unknown; Facies occurrence: A₁, A₂, A₃, B, C, D, E.</p> |  |
| <p>lla l+v+s; l>v; s=halite (hl); Final Th by hd, vbd, and d. Final Th range of 290-520°C; Tlv range of 192-520°C; Salinity range of 31-50 eq. wt.% NaCl; Facies occurrence: A₁, A₂, A₃, C, D, E.</p> |  |
| <p>llb l+v+s; l>v; s=hl+/-op+/-hm; Final Th by hd and vbd. Final Th range of 193-530°C; Tlv range of 117-480°C; Salinity range of 30-64 eq. wt.% NaCl; Facies occurrence: A₁, A₂, A₃, B, C, D, E.</p> |  |
| <p>llc l+v+s; l>v; s=hl+other translucent daughters (anhydrite, nahcolite, calcite, unknown)+/-op+/-hm; Final Th by vbd, hd, otd, and d. Final Th range of 229-532°C; Tlv range of 67.6-475°C; Salinity range of 32-64 eq. wt.% NaCl; Facies occurrence: A₁, A₂, A₃, B, C, D, E.</p> |  |
| <p>lld l+v+s; v>l; s=hl+/-op+/-hm+/-ot daughters. Observed facies occurrence: A₁, A₂, C, D.</p> | <p>No pictures available. Type lld. were not used in this study due to difficulty in observing phase changes with this type of inclusion.</p> |

Table 3. Fluid inclusion types.

l = liquid v = vapor s = solid (daughters) op = opaques ot = other translucent daughters vbd = vapor bubble disappearance
 hm = hematite hl = halite sylv = sylvite anhy = anhydrite cb = critical behavior ld = liquid disappearance d = decrepitation
 otd = dissolution of other translucent daughters Th = temperature of homogenization

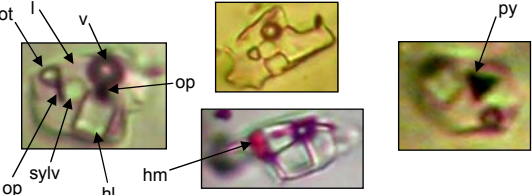
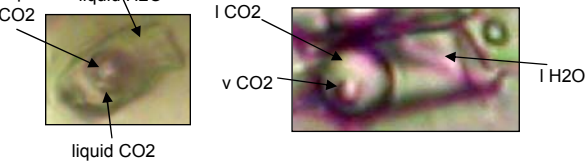
| Most Common Fluid Inclusion Types | Examples |
|-------------------------------------------------------------------------------------------------------------------------------------------------------------------------------------------------------------------------------------------------------------------------|------------------------------------------------------------------------------------------------------------------------------------------------|
| <p>IIIa l+v+s; l>v; s=hl+sylvite+/-hm+/-op+/-ot daughters; Final Th by hd and otd.</p> <p>Final Th range of 258-470°C; Tlv range of 179.5-324°C; salinity range of 35-56 eq. wt.% NaCl; Facies occurrence: A₂, A₃, B, C.</p> |  |
| <p>IIIb l+v+/-s; v>>l; s=hl+sylv+/-hm+/-op+/-anhy+/-ot daughters.</p> <p>Known facies occurrence: A₂ and C.</p> | <p>No pictures available. Type IIIb. were not used in this study due to difficulty in observing phase changes with this type of inclusion.</p> |
| <p>IV lH₂O+/-lCO₂+/-vCO₂; lH₂O>lCO₂+/-vCO₂; Final Th to lH₂O.</p> <p>Final Th range of 130-260; Salinity range of 0-9 eq. wt.% NaCl; Facies occurrence: A₃, B, C.</p> |  |

Table 3 cont'd. Fluid inclusion types.

contain an opaque and/or hematite daughter mineral. Type Ib inclusions, the most abundant of the fluid inclusion types, are liquid-rich with no daughter minerals are present. Type Ic inclusions are vapor-rich and contain no daughter minerals. Type II fluid inclusions contain liquid, vapor, and a halite daughter, and are subdivided into four subtypes (a, b, c, and d). Type IIa inclusions are liquid-rich with a halite daughter mineral, and contain no opaques, hematite, other translucent daughters. Type IIb are liquid-rich with a halite daughter, and contain opaque and/or hematite daughters. Type IIc, the second most abundant of the fluid inclusion types, and the most abundant of the type II inclusions, are liquid-rich fluid inclusions with a halite daughter, and contain other translucent (ot) daughter minerals (nahcolite, anhydrite, calcite and/or unknowns) +/- opaques +/- hematite daughters. Type IId are vapor-rich inclusions containing halite +/- ot +/- op +/- hm daughter minerals. Type IId inclusions were not used in this study due to the difficulty in observing any phase changes with this type of inclusion. Type III fluid inclusions contain liquid, vapor, and halite and sylvite daughter minerals. Type III fluid inclusions are divided into two subtypes (a and b). Type IIIa are liquid-rich, halite and sylvite-bearing inclusions that may or may not contain hematite, opaques, or other translucent daughter minerals. Type IIIb are vapor-rich inclusions that contain halite and sylvite +/- hm +/- op +/- ot daughters. Type IIIb were not used in this study due to the difficulty in observing any phase changes with this type of inclusion. Type IV fluid inclusions, the least abundant of the fluid inclusion types, are carbonic-bearing inclusions that contain liquid water, liquid CO₂, and vapor CO₂ (double bubble). The water phase is greater than the carbonic phases in Type IV inclusions.

Type Ia inclusions homogenized by vapor bubble disappearance (vbd) or critical behavior (cb) with a wide range of Tlv's (88-488°C) and a salinity range of 0-23 eq. wt.% NaCl (Figures 19-22). Type Ib fluid inclusions homogenized by vbd, liquid disappearance (ld), cb, or the inclusions decrepitated (d). Type Ib inclusions demonstrated a wide Tlv range of 109-520 °C and a salinity range of 0-22 eq. wt.% NaCl. Five type I inclusions (two Ia and three Ib) exhibited a $T_{m_{ice}}$ that was below the eutectic temperature of -20.8°C for a pure H₂O-NaCl system. The range in the $T_{m_{ice}}$ for these inclusions was -24.1 to -21.7 °C, suggesting CaCl₂ content. In order to obtain the composition of the fluid in terms of weight percent NaCl and CaCl₂, the melting temperature of hydrohalite and of ice are needed. Only two of the five inclusions produced both of these aspects resulting in salinities of 6% NaCl and 19% CaCl₂ and 12% NaCl and 13% CaCl₂, with a bulk salinity of 25 wt% NaCl+CaCl₂ equivalent for both inclusions. The NaCl/CaCl₂ ratios for the two inclusions are both 0.79 (Shepherd et al., 1985). Type Ic fluid inclusions homogenized by vbd, ld, or cb, with a Tlv range of 360-485 °C. Due to the minute amount of liquid that exists in type Ic fluid inclusions, difficulty in observing the final ice melting temperatures ($T_{m_{ice}}$) resulted in no salinity data for this type inclusion.

Type IIa fluid inclusions homogenized by halite dissolution (hd), vbd, or decrepitated. The Tlv and salinity range for type IIa fluid inclusions were 192-520°C and 31-50 eq. wt.% NaCl, respectively. Type IIb fluid inclusions homogenized by hd or vbd, with a Tlv range of 117-480 °C and a salinity range of 30-64 eq. wt.% NaCl. Type IIc inclusions homogenized by vbd, hd, other translucent daughter dissolution (otd), or

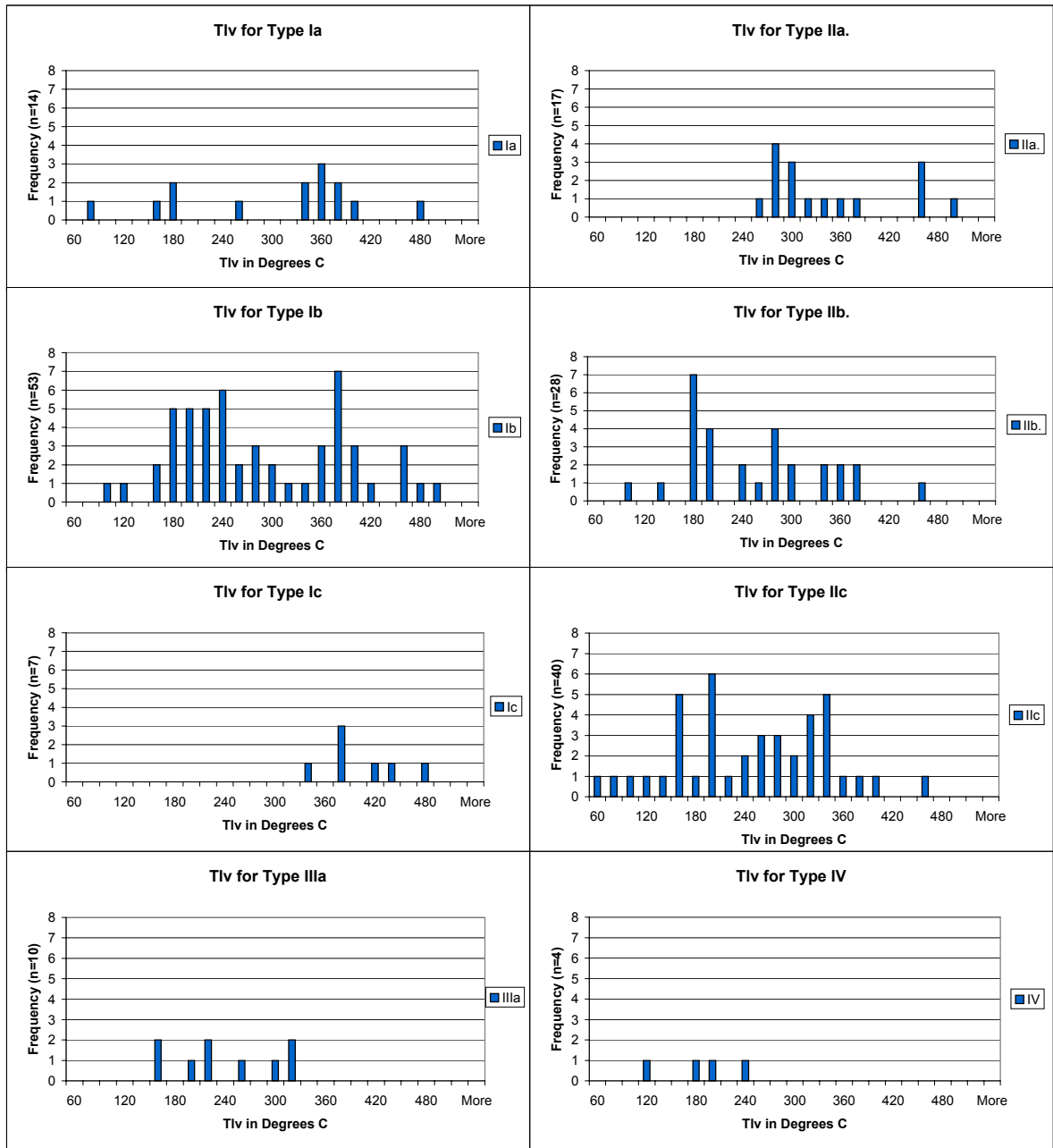


Figure 19. Tlv distribution for each fluid inclusion type and subtype.

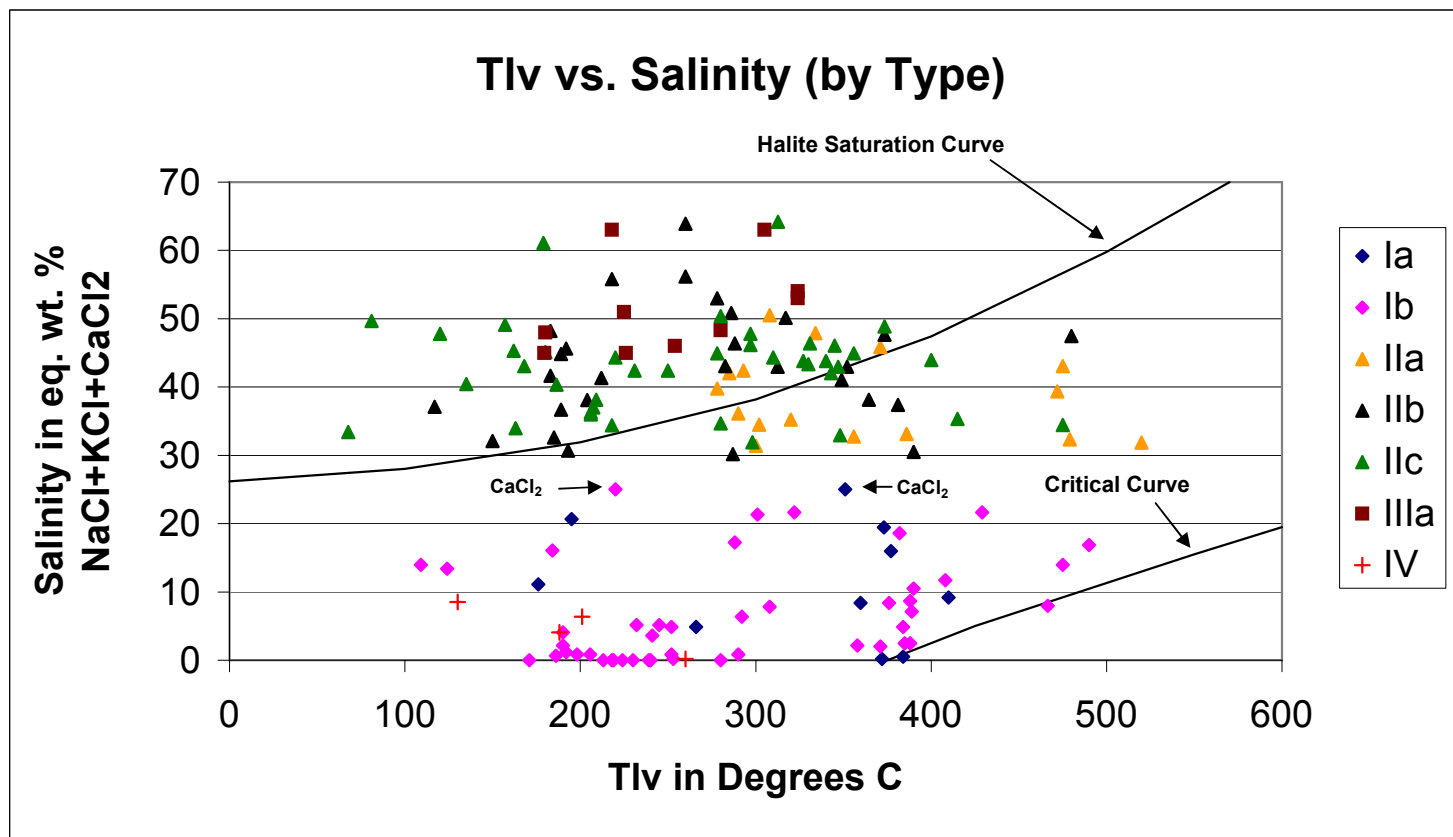


Figure 20. Tlv vs. salinity diagram for types and subtypes. Note the halite saturation curve and the critical curve (Bodnar, 2003 and Roedder, 1984). Inclusions that lie on or above the halite saturation curve homogenized (final Th) by halite dissolution. Inclusions below the curve homogenized (final Th) by a fluid phase change rather than a solid phase change. The critical curve shows critical temperatures, or the minimum temperature at which a fluid of given salinity can separate into two phases, for unsaturated H₂O-NaCl solutions. Inclusions on or near this curve represent critical or near-critical fluids (See Figure 21).

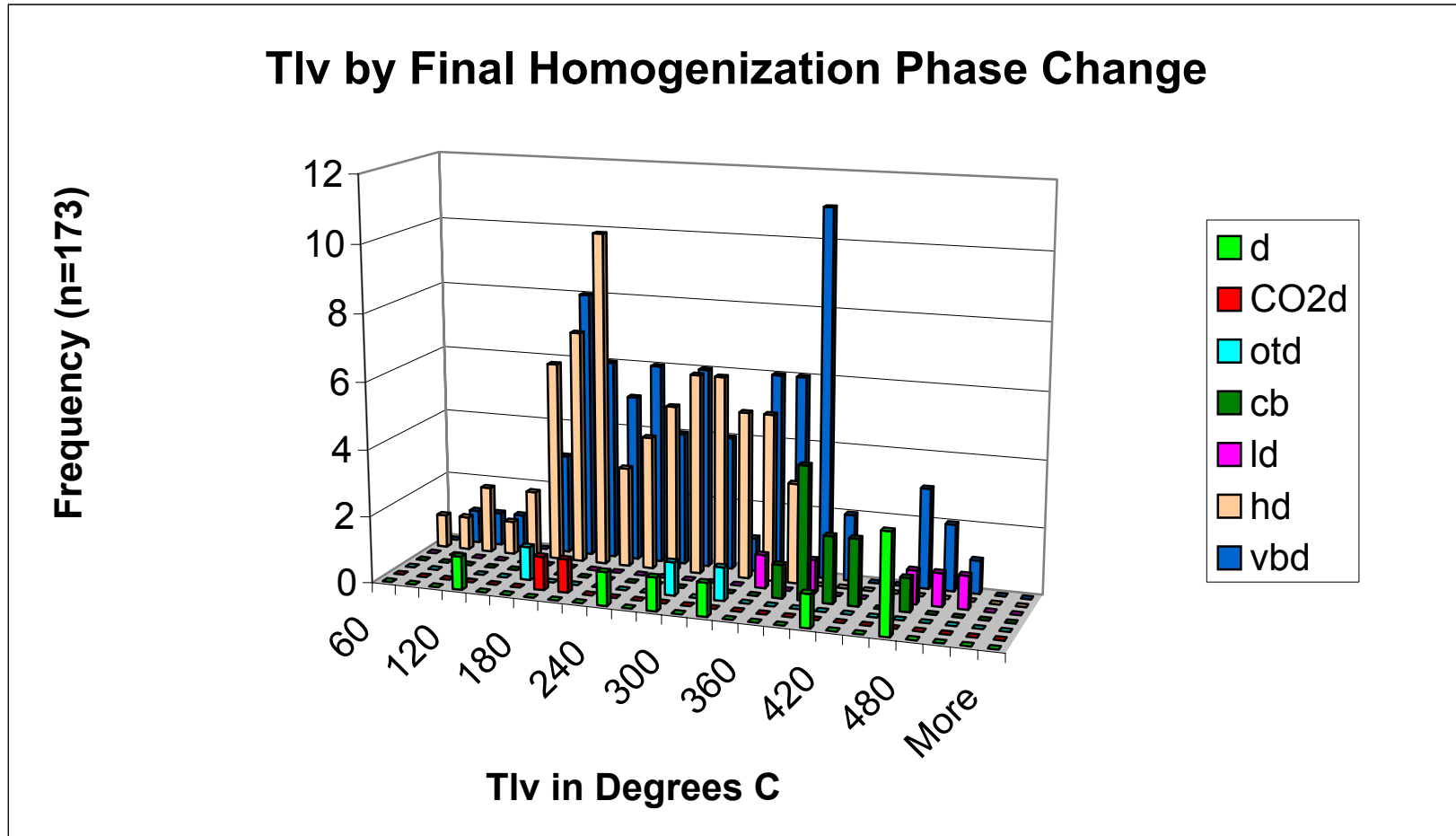


Figure 21. Tlv for each inclusion and its respective phase change for final Th. vbd - vapor bubble disappearance hd - halite dissolution ld - liquid disappearance cb - critical behavior otd - other translucent daughter dissolution CO2d - CO2 disappearance (carbonic inclusions homogenized to a liquid) d - decrepitation

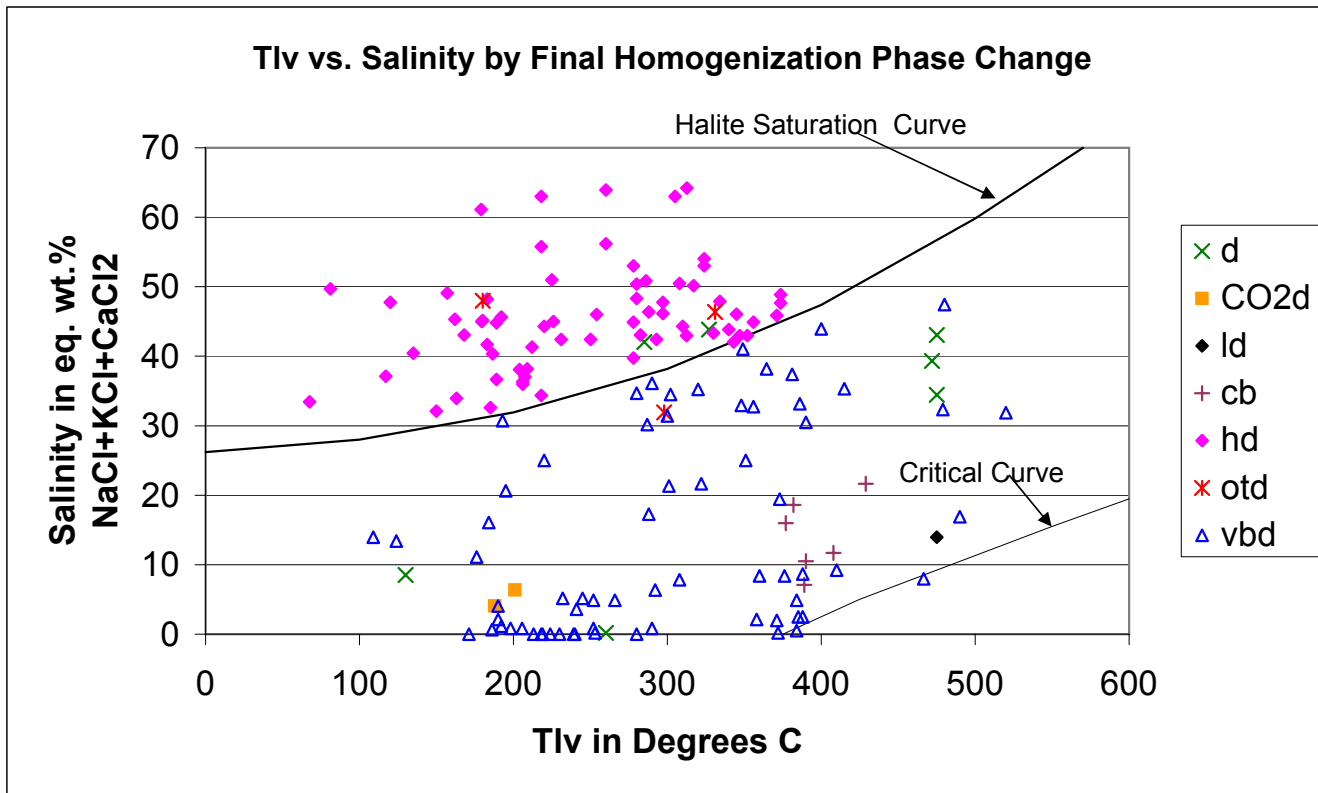


Figure 22. Tlv vs. salinity graph indicating which phase change was exhibited for final homogenization. Note the halite saturation curve and the critical curve (Bodnar, 2003 and Roedder, 1984). Inclusions that lie on or above the halite saturation curve homogenized (final Th) by halite dissolution. Inclusions below the curve homogenized (final Th) by a fluid phase change rather than a solid phase change. The critical curve shows critical temperatures, or the minimum temperature at which a fluid of given salinity can separate into two phases, for unsaturated H₂O-NaCl solutions. Inclusions on or near this curve represent critical or near-critical fluids.

d - decrepitation CO₂d - CO₂ disappearance ld - liquid disappearance vbd - vapor bubble disappearance
 cb - critical behavior hd - halite dissolution otd - other translucent daughter dissolution

decrepitated. Type IIc inclusions demonstrated a Tlv range of 68-475 °C and a salinity range of 32-64 eq. wt.% NaCl.

Type IIIa fluid inclusions homogenized by hd or otd, with a Tlv range of 180-324°C. The salinity for sylvite-bearing type III inclusions ranged from 26% NaCl and 14% KCl to 47% NaCl to 21% KCl, with bulk salinities of 40-68 wt% NaCl+KCl equivalent. The K/Na and NaCl/(NaCl+KCl) ratios for type IIIa inclusions range from 0.35-0.75 and 0.57-0.74, respectively (Table 4)(Roedder, 1984).

Carbonic type IV fluid inclusions homogenized to liquid water or decrepitated at 130-260 °C. Type IV inclusions demonstrated a salinity range of 0-9 eq. wt.% NaCl.

Excluding the two CaCl₂-bearing inclusions, there is a gap in the data on the Tlv vs. salinity graph (Figure 19) between 23 and 30 weight % NaCl+/-KCl+/-CaCl₂ equivalent. This gap occurs in almost all reported data, and is due to two factors – misreporting hydrohalite melting as ice melting, and halite metastability. Between 23.2 and 26.3 wt.% NaCl, hydrohalite is the last phase to melt. This is often misreported as ice melting, giving rise to a gap in data at this salinity (Shephard et al., 1985 Figure 6.1). From 26.3 to 30 wt.% NaCl, inclusions often fail to nucleate a halite daughter crystal, or the daughter is too small to see. For these reasons, data is hardly ever reported for these salinities (Bodnar, 2003).

MHBX Facies Distribution

It was important to also report the fluid inclusion results in terms of the MHBX facies, in order to determine if there was any fluid evolution associated with the prominent mineralogic and alteration evolution of the Goat Hill MHBX, or if there was any geochemical fluid evolution at all. Types Ia, Ib, and Ic occurred within all of the

| Sample ID | Inclusion | Facies | Calculated T* | Measured Tlv | DCalcT-Tlv | Na** | K** | K/Na | NaCl/(NaCl+KCl) |
|----------------|-----------|--------|---------------|--------------|------------|------|-----|------|-----------------|
| AR-106 | 8 | A2 | 437 | 254 | 183 | 63 | 37 | 0.59 | 0.63 |
| AR-93 | 1 | A3 | 399 | 324 | 75 | 68 | 32 | 0.47 | 0.68 |
| AR-93 | 2 | A3 | 370 | 225 | 145 | 72 | 28 | 0.39 | 0.72 |
| AR-8 | 11 | C | 355 | 305 | 50 | 74 | 26 | 0.35 | 0.74 |
| AR-8 | 12 | C | 407 | 180 | 227 | 67 | 33 | 0.49 | 0.67 |
| AR-8 | 15 | C | 362 | 324 | 38 | 73 | 27 | 0.37 | 0.73 |
| AR-131 | 3 | C | 362 | 218 | 144 | 73 | 27 | 0.37 | 0.73 |
| AR-131 | 12 | C | 477 | 226 | 251 | 58 | 42 | 0.72 | 0.58 |
| AR-131 | 15 | C | 485 | 180 | 305 | 57 | 43 | 0.75 | 0.57 |
| Average | | | 406 | 248 | 157 | 67 | 33 | 0.50 | 0.67 |

* Temperature calculated using Na/K geothermometer of Fournier (1981).

$$t^{\circ}\text{C} = \frac{1217}{\log(\text{Na/K})+1.483} - 273.15 \quad t > 150^{\circ}\text{C}$$

** Na and K from NaCl-KCl-H₂O system ternary in Roedder, 1984.

Table 4. Na and K data from sylvite and halite-bearing type IIIa fluid inclusions.

MHBX facies. The CaCl_2 -bearing inclusions of types Ia and Ib occurred in facies A1, A2, B, and E. Type IIa occurs in all facies, except facies B. Types IIb and IIc occurred in all of the MHBX facies. Type IId were noted in facies A1, A2, C, and D. However this inclusion type may have occurred in other MHBX facies, but since this type was not to be analyzed, minor attention was applied to this type. Sylvite-bearing Type IIIa occurred in facies A2, A3, B, and C only. Facies IIIb was noted in A2 and C, but similarly to IIId, was only given minor attention, and may have occurred in other MHBX facies as well. Carbonic type IV inclusions occurred in facies A3, B, and C only.

The A facies exhibited a wide range of Tlvs of 109-475 °C, 87.6-472 °C, 81-520 °C, and 81-520 °C for A1, A2, A3, and combined A facies, respectively. Facies A exhibited a salinity range of 0-50.5, 0-45, and 0-53 eq. wt.% NaCl for A1, A2, and A3 and/or combined A facies, respectively. The B facies exhibited a tighter Tlv range of 188-429 °C and a salinity range of 2-64 eq. wt. % NaCl. Facies C also exhibited a tighter Tlv range of 130-372 °C. The salinity range exhibited by facies C is 0-56 eq. wt.% NaCl. Facies D and E exhibited a Tlv range of 67-467 °C, 117-490 °C, and 68-490 °C, for D, E, and combined D and E, respectively. Facies D and E resulted in a salinity range of 0-61, 0-53, and 0-61 eq. wt.% NaCl for D, E, and combined D and E, respectively. Tlv distribution for all facies is available in Figure 23. A comparative Tlv histogram by facies is available in Figure 24. Tlv vs. salinity is plotted in Figure 25. The subunits of facies A (A1, A2, and A3) can be treated in combination due to the fact that they are a part of one main unit, and also because these units are very similar and often ambiguous to each other. Similarly, facies D and E are treated in combination due to the ambiguity that often occurs with the facies classification of the D and E units (Figures 6 and 7).

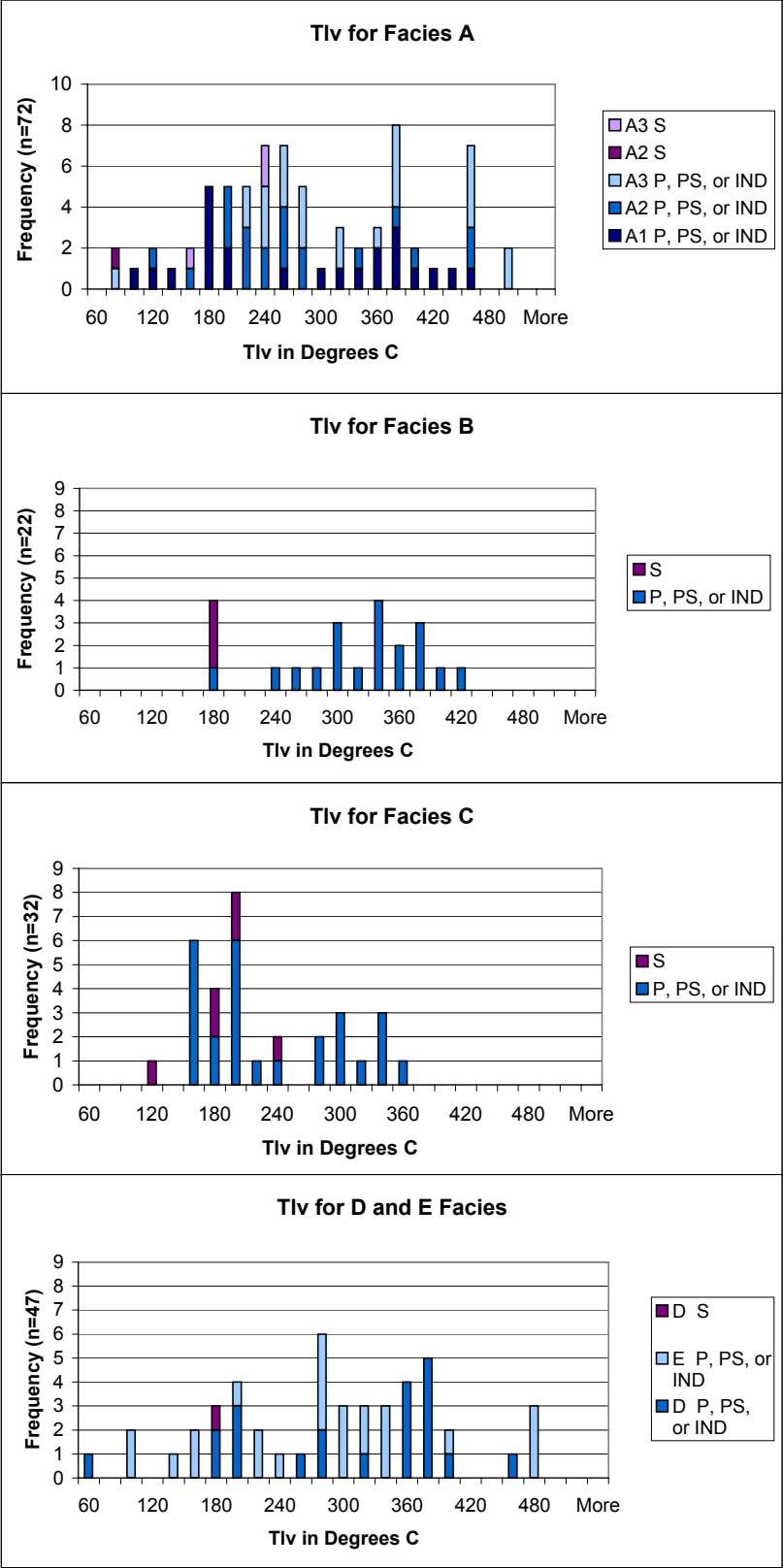


Figure 23. Tlv distribution for facies.
P - primary PS - pseudosecondary S - Secondary IND - Indeterminate

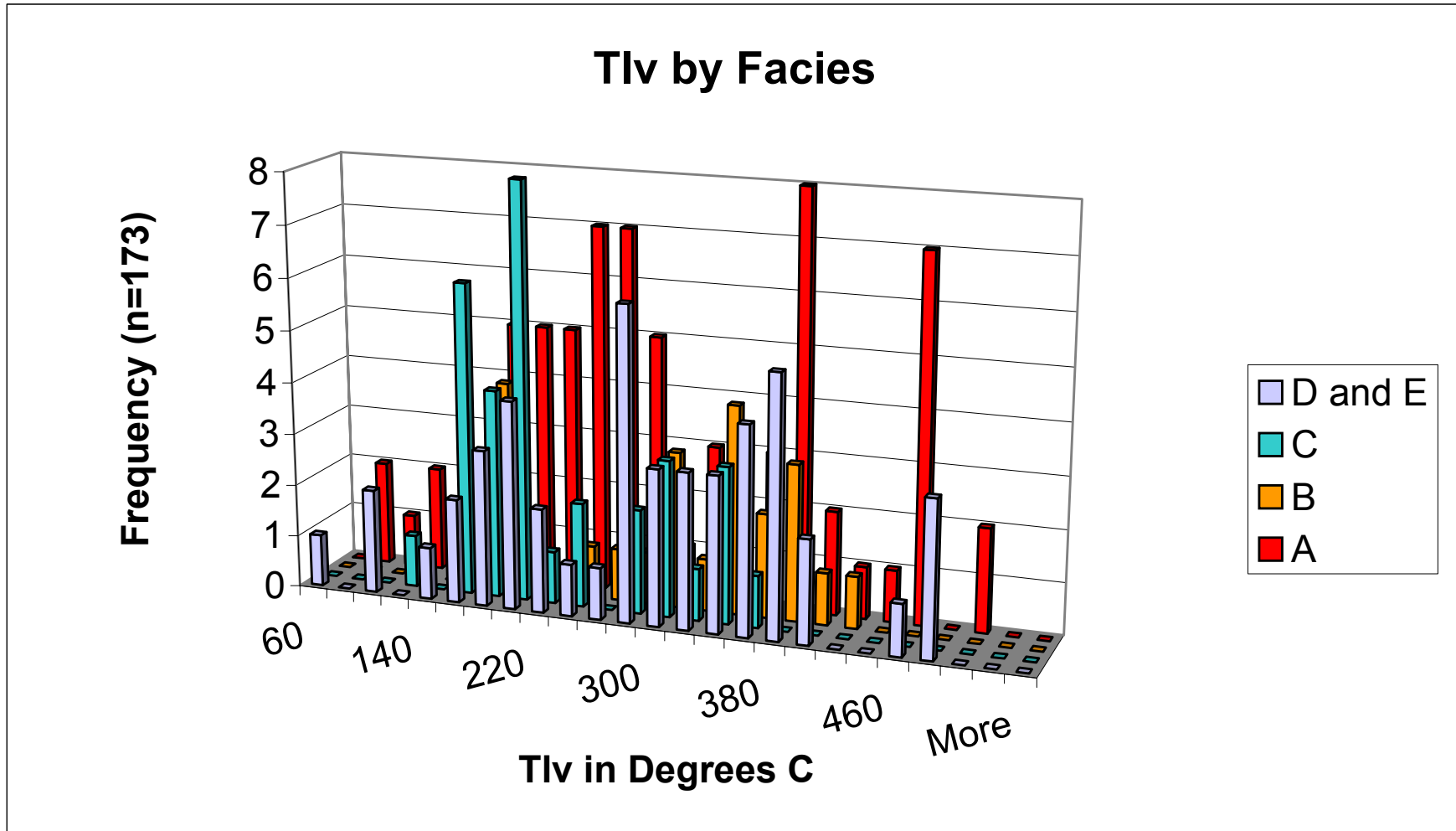


Figure 24. Comparative Tlv histogram by facies.

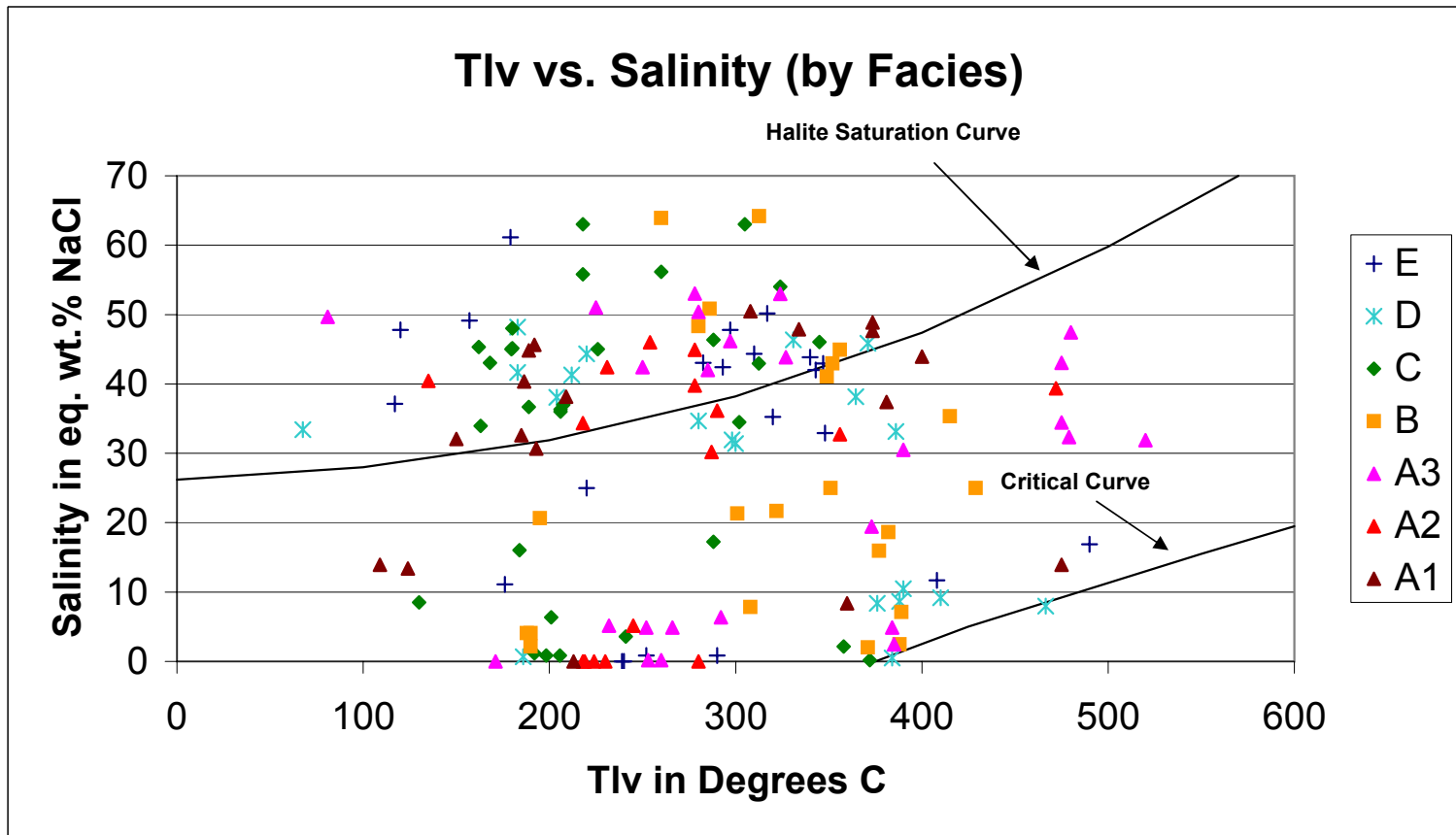


Figure 25. Tlv vs. salinity diagram by facies. Note the halite saturation curve and the critical curve (Bodnar, 2003 and Roedder, 1984). Inclusions that lie on or above the halite saturation curve homogenized (final Th) by halite dissolution. Inclusions below the curve homogenized (final Th) by a fluid phase change rather than a solid phase change. The critical curve shows critical temperatures, or the minimum temperature at which a fluid of given salinity can separate into two phases, for unsaturated H₂O-NaCl solutions. Inclusions on or near this curve represent critical or near-critical fluids.

DATA ANALYSIS AND INTERPRETATION

Final Th vs. Tlv – Trapped Halite

The majority of the fluid inclusions that contained halite daughter minerals (types II and III) demonstrated final Th by halite dissolution (Figures 26 and 27). There are several instances where the dissolution of halite occurred well above (over 100 degrees C) that of vapor bubble disappearance (Figure 28). As various pressure-temperature (P-T) data indicate (Bodnar, 1994; Bodnar & Vityk, 1994; Cline & Bodnar, 1994; Gunter et al., 1983; Bodnar, 2003), the pressures corresponding to these types of fluids are “much greater than any reasonable lithostatic load” (Kamilli, 1978), 2 kbars and above (Figure 28). This places the Goat Hill MHBX much too deep below the surface at formation. Based upon stratigraphic reconstruction, Molling (1989) determined that the source granitic magma was emplaced at depths of 3 to 5 km, corresponding to lithostatic pressures of 0.8-1.4 kbars below surface. Ross (2002) concluded a lithostatic pressure of 1 kbar for the emplacement of the MHBX. Based upon fluid inclusion data, Smith (1983) determined a lithostatic pressure of 180-550 bars for the Goat Hill orebody.

Previous studies on Climax-type deposits have indicated two possibilities for the origin of the inclusions that exhibited a final homogenization by halite dissolution at $>100^{\circ}\text{C}$ above that of vapor bubble disappearance – overpressures, caused by exsolution and evolution of the hydrothermal fluid or by system sealing, (Kamilli, 1978; Cline & Bodnar, 1994; Bloom, 1981), or trapped halite crystals (Bloom, 1981). Overpressure is not indicated by the geologic context of the Goat Hill orebody. The brecciation process and formation occurs almost instantaneously and as a single event, eliminating possibility of system sealing, further brecciation, resealing, and so on (see Ross, 2002 for details on

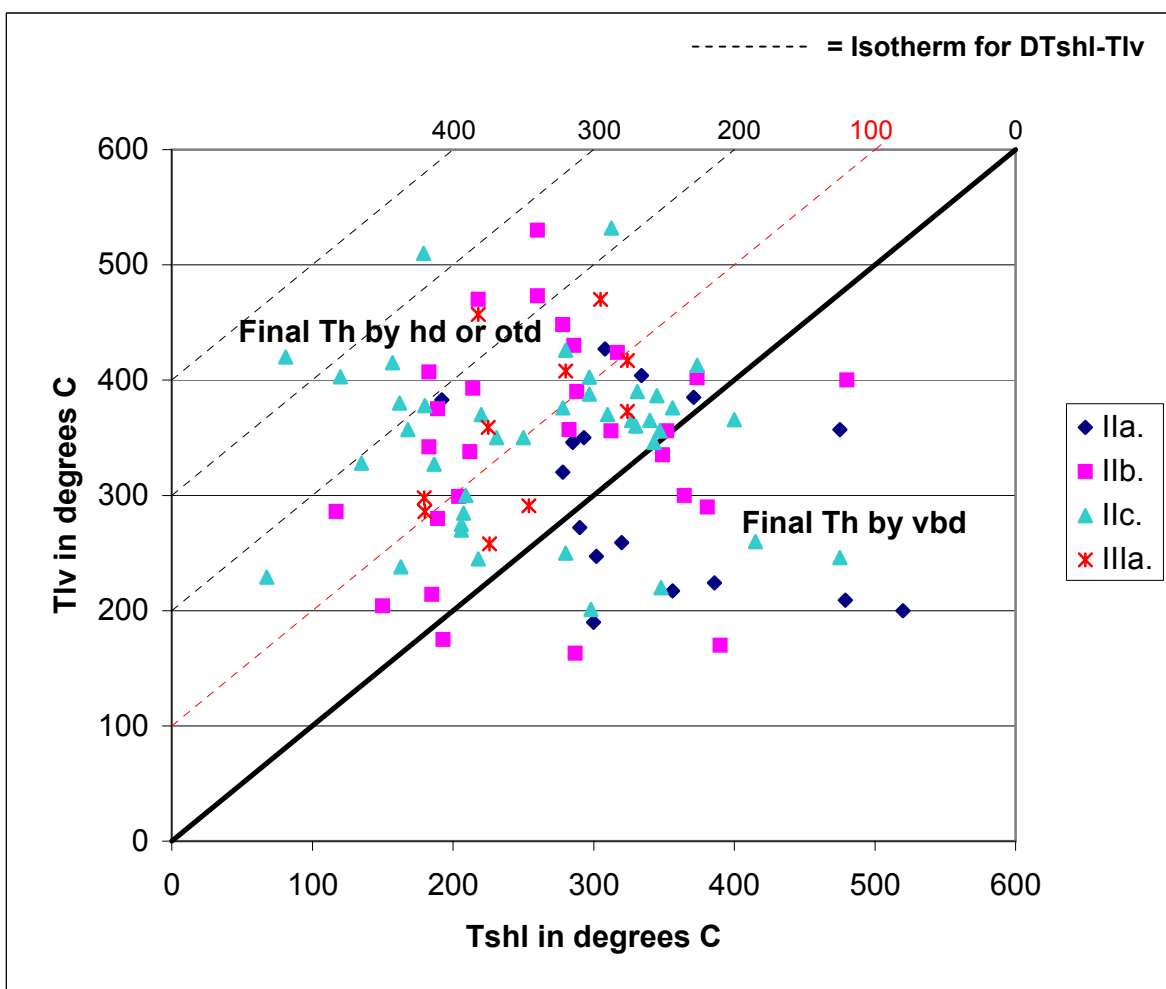


Figure 26. Tlv vs. Tshl diagram in terms of type for inclusions containing a halite daughter. Inclusions above the line homogenized by halite dissolution (hd) or other translucent daughter dissolution (otd), those below the line homogenized by vapor bubble disappearance (vbd). Those inclusions above the red dotted line (100°C isotherm for DTshl-Tlv) have a Tshl >> Tlv and are most likely a representation of inclusions that have trapped halite.

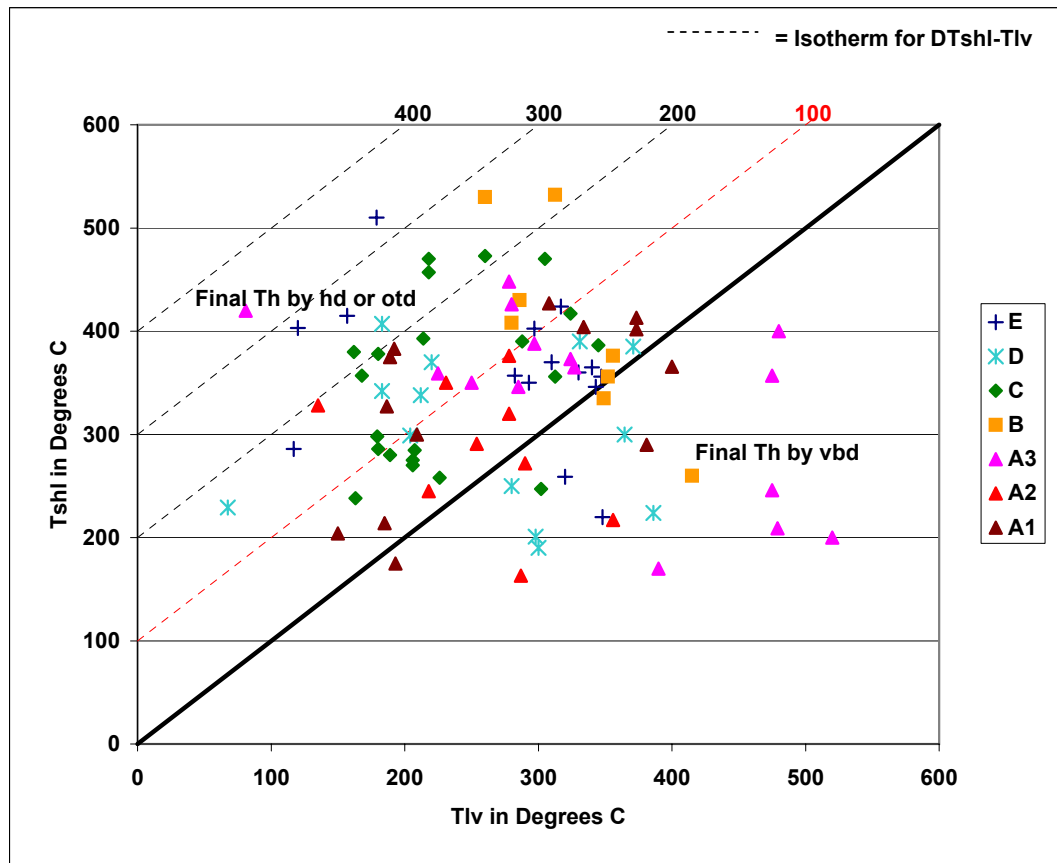


Figure 27. Tlv vs. Tshl diagram in terms of facies for inclusions containing a halite daughter. Inclusions above the line homogenized by halite dissolution (hd) or other translucent daughter dissolution (otd), those below the line homogenized by vapor bubble disappearance (vbd). Those inclusions above the red dotted line (100°C isotherm for DTshl-Tlv) have a Tshl >> Tlv and are most likely a representation of inclusions that have trapped halite.

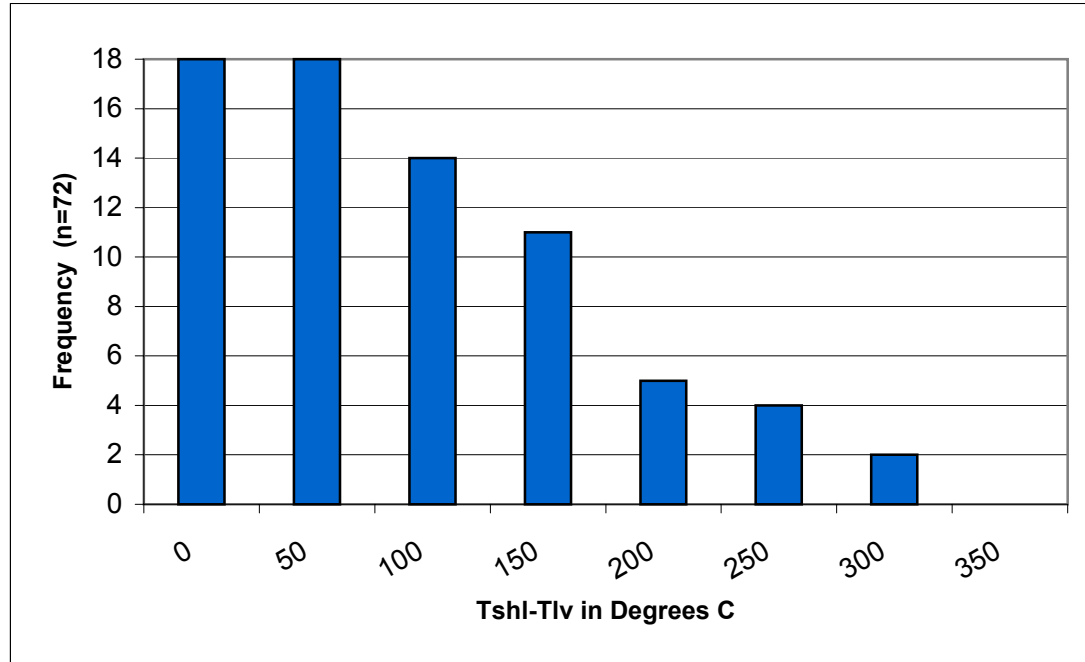


Figure 28. Tshl-Tlv distribution. As seen here, 36 halite-bearing inclusions demonstrated halite dissolution less than 100°C from liquid-vapor homogenization (Tlv) and 36 halite-bearing fluid inclusions demonstrated Tshl at 100-350 degrees C above that of Tlv.

MHBX formation). If exsolution and hydrothermal fluid evolution were the mechanism for overpressures, and accounted for the Tshl>>Tlv inclusions, an evolutionary pattern would be evident from the fluid inclusion data in terms of type and facies. This is not the case. Inclusions that have a final Th by Tshl>>Tlv occur as all possible types (IIa, IIb, IIc, and IIIa) and in all of the facies, with no evident pattern (Figures 26 and 27), hence ruling out exsolution as a control on fluid inclusion PTX.

Entrapment of halite crystals from a heterogeneous fluid that is saturated with respect to halite is another potential mechanism that produced the Tshl>>Tlv inclusions. Entrapment of a halite crystal in an inclusion would provide an over-estimate in salinity and final Th, hence giving way to unrealistic PTX conditions. Several previous studies on other ore deposits such as Naica (Erwood et al., 1979), Capitan Mountains (Campbell et al., 1995), Panguna (Eastoe, 1978), Granisle-Bell (Wilson, 1978), and the Banska Stiavnica district (Kodera et al., 2004), concluded that heterogeneous trapping, or entrapment of a halite crystal, is the mechanism for producing this type of inclusion. Evidence for the trapped halite phenomenon would be solid inclusions of halite in quartz. This feature is hard to recognize due to a close index of refraction for both quartz and halite. There were several instances in this study where solid inclusions in quartz were observed and suspected to be halite (Figure 29, Appendix A), evidence of the trapped halite phenomenon. However, unless the suspected solid inclusions are analyzed for chemistry their composition cannot truly be known. Campbell et al. (2001) identified several solid inclusions of halite in quartz from the Capitan Mountains, NM with an electron microprobe to prove this occurrence. Daughter minerals that did not dissolve upon heating (other translucent daughters, hematite, opaques) can also be an indication of

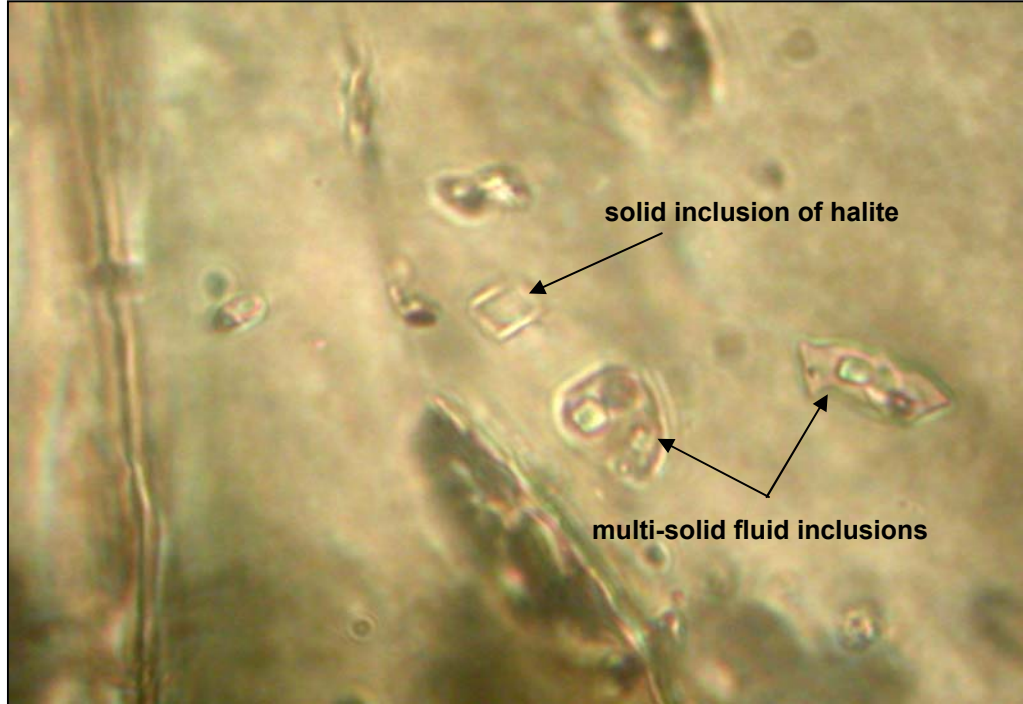


Figure 29. Photograph of solid inclusion of halite in quartz adjacent to multi-solid fluid inclusions, evidence of heterogeneous trapping. Photo taken at 25°C prior to heating.

entrapment rather than in-situ precipitation (Kodera et al., 2004). Only 14 of 48 ot-bearing inclusions contained other translucent daughter minerals that dissolved (Appendix A). In addition, no opaque or hematite daughter minerals were observed to dissolve. Both of these facts further support heterogeneous trapping.

A fluid saturated with respect to halite is not an unlikely occurrence in a hydrothermal system. If pervasive boiling occurs, the fluids can become saturated in halite. In geothermal systems, it has been seen where drillcore is full of halite crystals from boiling of geothermal fluids (Norman, D.I. – NMT E&ES, pers. comm., 2004). Coexisting liquid-rich and vapor-rich fluid inclusions (Ic, IId, and IIIb) were found in several instances in the Goat Hill, evidence of boiling (Appendix A and Figure 30). Based upon phase equilibria constraints, if an inclusion homogenizes by halite dissolution, it had to have formed in the vapor absent field (Figure 31). Liquid-rich high salinity inclusions coexisting with vapor-rich inclusions shows that the liquid-rich high salinity inclusions could not have precipitated halite in-situ, but rather are a result of heterogeneous trapping. Types IId and IIIb inclusions (vapor-rich, but contain halite and/or other minerals) can be a result of boiling and trapping of minerals (heterogeneous trapping) or leakage of the fluid inclusions. The latter does not seem likely considering that these inclusions were identified in several instances in this study. Bloom (1981) also found vapor-rich halite-bearing fluid inclusions, equivalent to type IId of this study. In addition, type Ic fluid inclusions exist, which are a result of boiling, and are considered real.

All type IIIa fluid inclusions homogenized by the dissolution of halite (Figure 20). If the inclusions indeed contained trapped halite rather than in-situ precipitated NaCl,

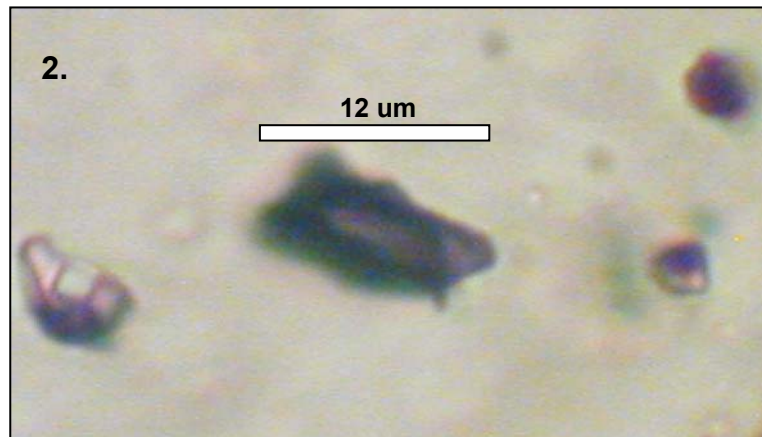
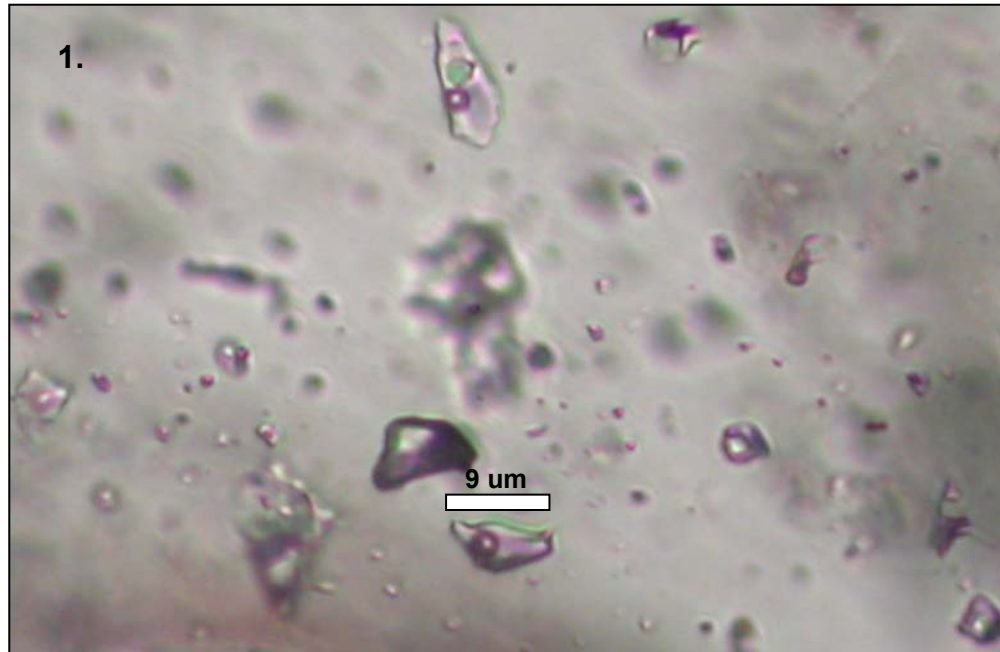


Figure 30. Photographs of coexisting liquid-rich and vapor-rich inclusions, evidence of boiling. Photo taken at 25°C prior to freezing or heating.

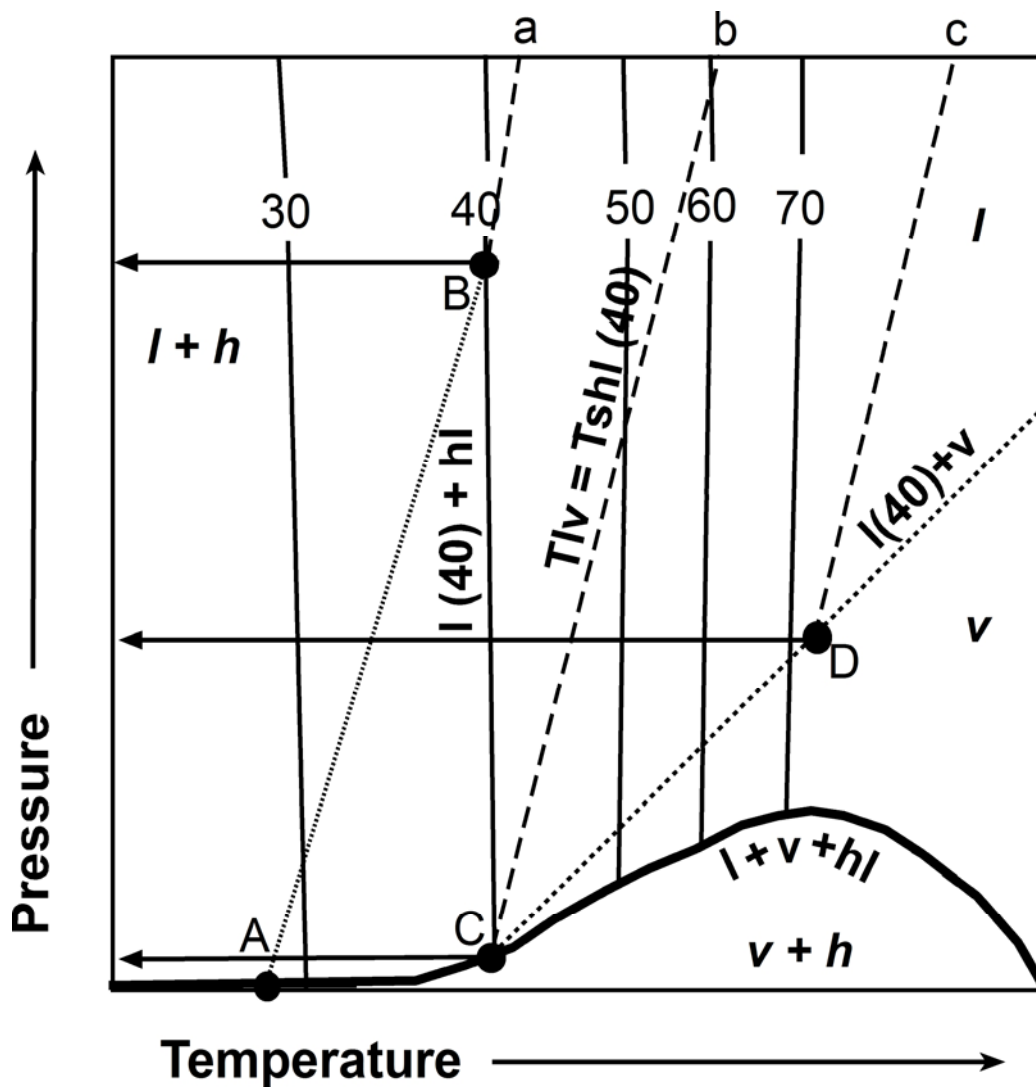


Figure 31. Schematic P-T diagram for the water-NaCl system demonstrating the steepness of the liquidus ($l+h$) for 30-70 wt.% NaCl and the three different modes of halite dissolution for a 40 wt.% NaCl solution. A fluid inclusion with $Tshl \gg Tlv$ will follow the path A (Tlv) - B ($Tshl$) - a (isochoric path after final T_h). Note the high pressure associated with point B that when to scale can lead to unrealistic pressures. A fluid inclusion with $Tshl = Tlv$ will homogenize at C and follow the isochoric path b after homogenization. Note the low pressures associated with point C. An inclusion with $Tshl < Tlv$ will follow the path C ($Tshl$) - D (Tlv) - c (isochoric path after final T_h). Note the moderate pressure for D relative to the pressures of B and C. Modified from Bodnar, 1994 and Shephard et al., 1985.

then the calculated K/Na ratios (0.35-0.75) of type IIIa fluid inclusions would be an underestimate of the K content of the fluid, and an overestimate of the Na content of the fluid. As a result, the calculated temperatures from the Na/K geothermometer would be an overestimate of the temperature of the fluid. The temperatures calculated utilizing the Na/K geothermometer of Fournier (1981) ranged from 355-485°C, with an average of 406°C (Table 4). These calculated temperatures demonstrated an overestimate of 38-305 °C (average of 157 °C) than the measured Tlv for type IIIa inclusions, further supporting that these inclusions contain a trapped halite phase.

Due to the plausibility of heterogeneous trapping and the entrapment of halite, the fluid inclusion data was reported in terms of the homogenization of the liquid-vapor phase (Tlv) (Figures 13 and 14) rather than in terms of the final homogenization temperature (Figures 32 and 33). Reporting in terms of Tlv is more representative of the fluid temperature at the time of trapping.

Temperature and Salinity Distribution – Fluid Evolution

There is a pronounced mineralogic/alteration zonation that occurred in this system, in which the facies classifications are based (Ross, 2002). It was hypothesized that the fluid inclusions in each facies would reflect the mineralogic/alteration zonation or change in terms of an evolutionary pattern in the temperature and salinity data. This is not case, however. As you can see in Figure 24, there is no distinct evolutionary pattern based upon facies. A Pearsons correlation was used in attempts to identify a correlation between facies and type, Tlv, final Th, and salinity, or the lack thereof (Table 5). If the absolute value of a correlation coefficient ($|cc|$) is 0.5 and greater, then it is considered to represent a correlation between the variables. All $|cc|$ s between facies and other

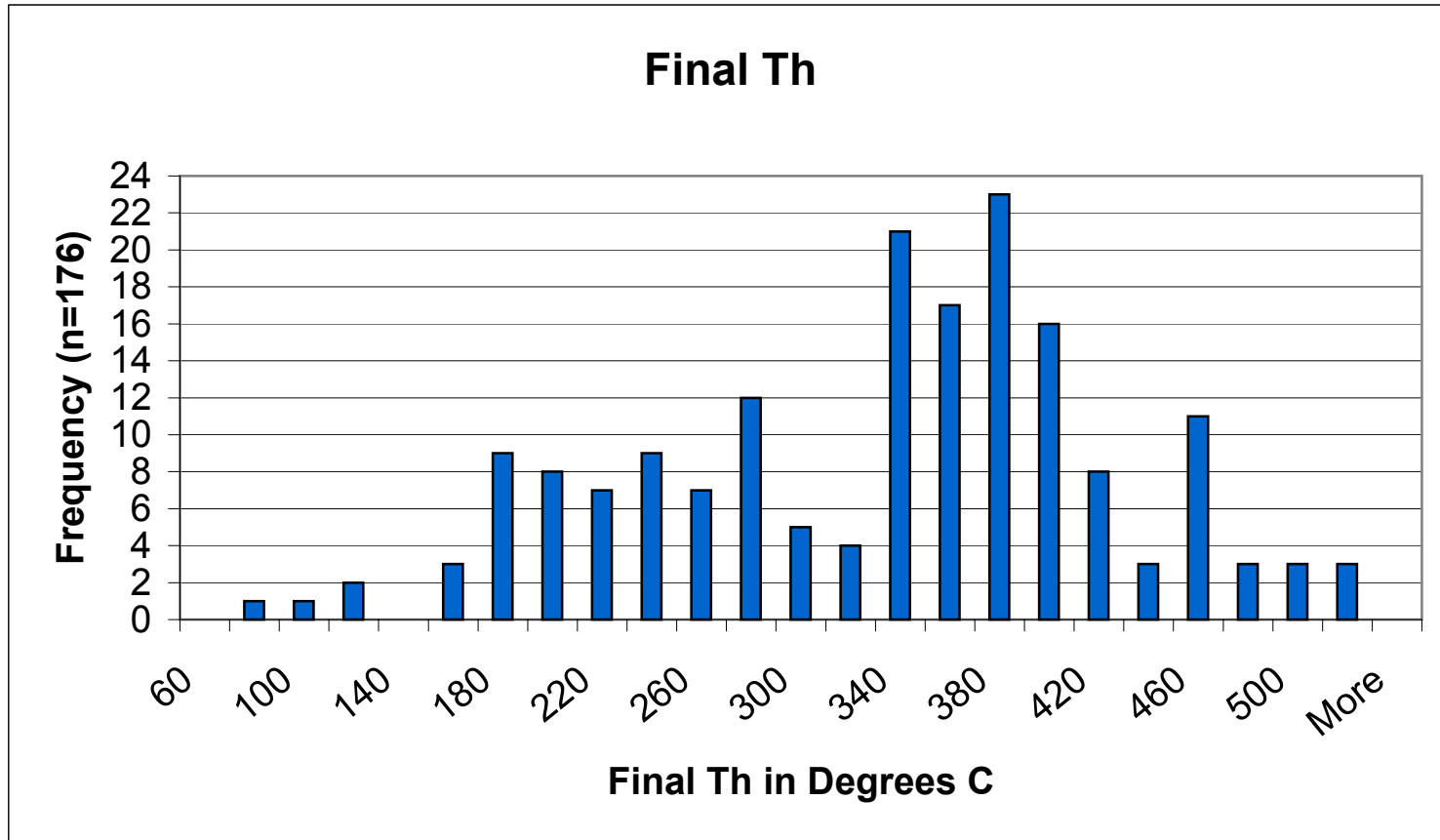


Figure 32. Final Th distribution. Note difference between the bimodal distribution for final Th with modes at 260°C and 380°C compared to the the widespread distribution for Tlv in Figure 12. The final Th is over-estimated for many of the inclusions due to trapped halite and other translucent daughters. Reporting in terms of Tlv is a more accurate representation of homogenization temperatures (Figure 12).

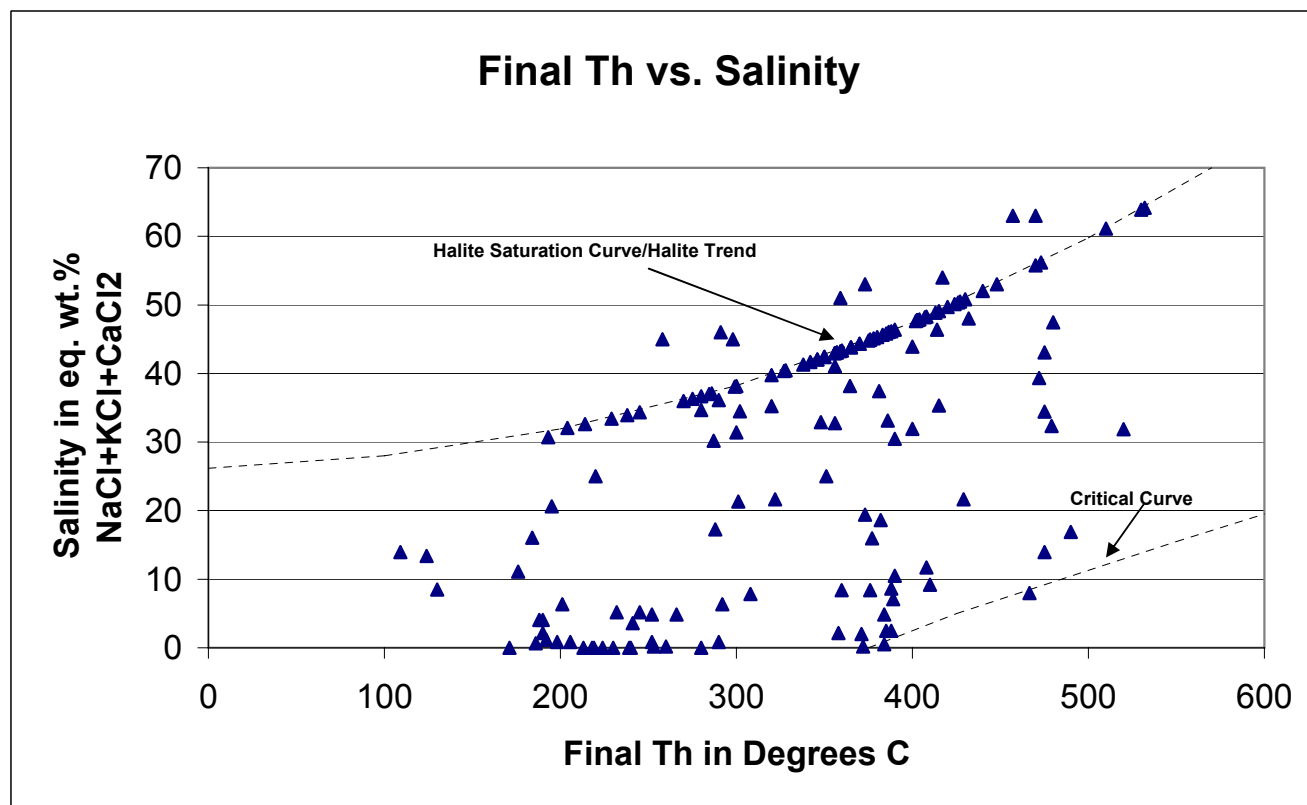


Figure 33. Final Th vs. salinity diagram. All of the inclusions on the halite saturation curve homogenize by halite dissolution. This linear pattern is called the halite trend after Cloke and Kessler (1979). Inclusions above the halite saturation curve contain sylvite (KCl) and also homogenize by halite dissolution. Note the difference in the final Th vs. salinity distribution compared to that of Tlv vs. salinity in Figure 13. The inclusions along and above the halite trend give an over-estimate of final Th and salinity. Presenting data in terms of Tlv is more representative of the temperature of homogenization.

| | Facies | |
|-----------------|----------------------------|-------------------------------------------------------------------|
| Type | 0.0618 153 0.22395 | Correlation coefficient valid cases one-tailed significance |
| Tlv | -0.06347 153 0.21784 | Correlation coefficient valid cases one-tailed significance |
| Final Th | 0.05721 153 0.24117 | Correlation coefficient valid cases one-tailed significance |
| Salinity | 0.05653 153 0.24378 | Correlation coefficient valid cases one-tailed significance |

Table 5. Pearsons correlation data between facies and type, Tlv, final Th, and salinity. Pearsons correlations were obtained utilizing the WinSTAT Statistics for Windows Version 3.1 computer program distributed by Kalmia Co. Inc., 1991-1996.

variables were <0.5 , with values of 0.056-0.063, demonstrating that there is no facies correlation with type, Tlv, final Th, and salinity, and no evolutionary pattern based upon facies.

Some temperature differences between the facies are evident, however (Figure 23). A widespread, almost quad-modal, distribution can be seen in facies A and combined facies D and E. These facies represent the top and bottom or “rind” of the breccia body along the pre-breccia fabric that controlled the shape of the breccia and fluid flow (Figures 6 and 7). Hence, facies A, D, and E were exposed to fluids first, and were exposed to more fluids than facies B and C. Conversely, facies B and C have a tighter temperature distribution. Both B and C are in the middle of the breccia body (Figures 6 and 7), farthest away from the preferential fluid flow path (pre-breccia fabric). B inclusions consist of almost one single population containing no known secondaries, at a moderate to high temperature range (260-429°C). Facies C inclusions consist of a bi-modal temperature distribution, with a lower temperature range than B of 180-372 °C. The lower temperature range of facies C is most likely a reflection of the onset of QSP alteration. Molybdenite will precipitate with a temperature decrease from 350 °C to 200-250 °C (Smith, 1983). Ore grade is concentrated in the C facies (Figure 8)(Ross, 2002). It is hypothesized that the lower temperatures and high grade of facies C are directly related.

In order to find an evolutionary pattern for the fluid inclusions, a smaller scale (individual inclusions) than facies was required. Individual Tlv vs. salinity diagrams for each facies were scrutinized for similarities between the facies (Figure 34). As a result, nine fluid inclusion populations were identified (1-9) (Figure 35; Table 5). The

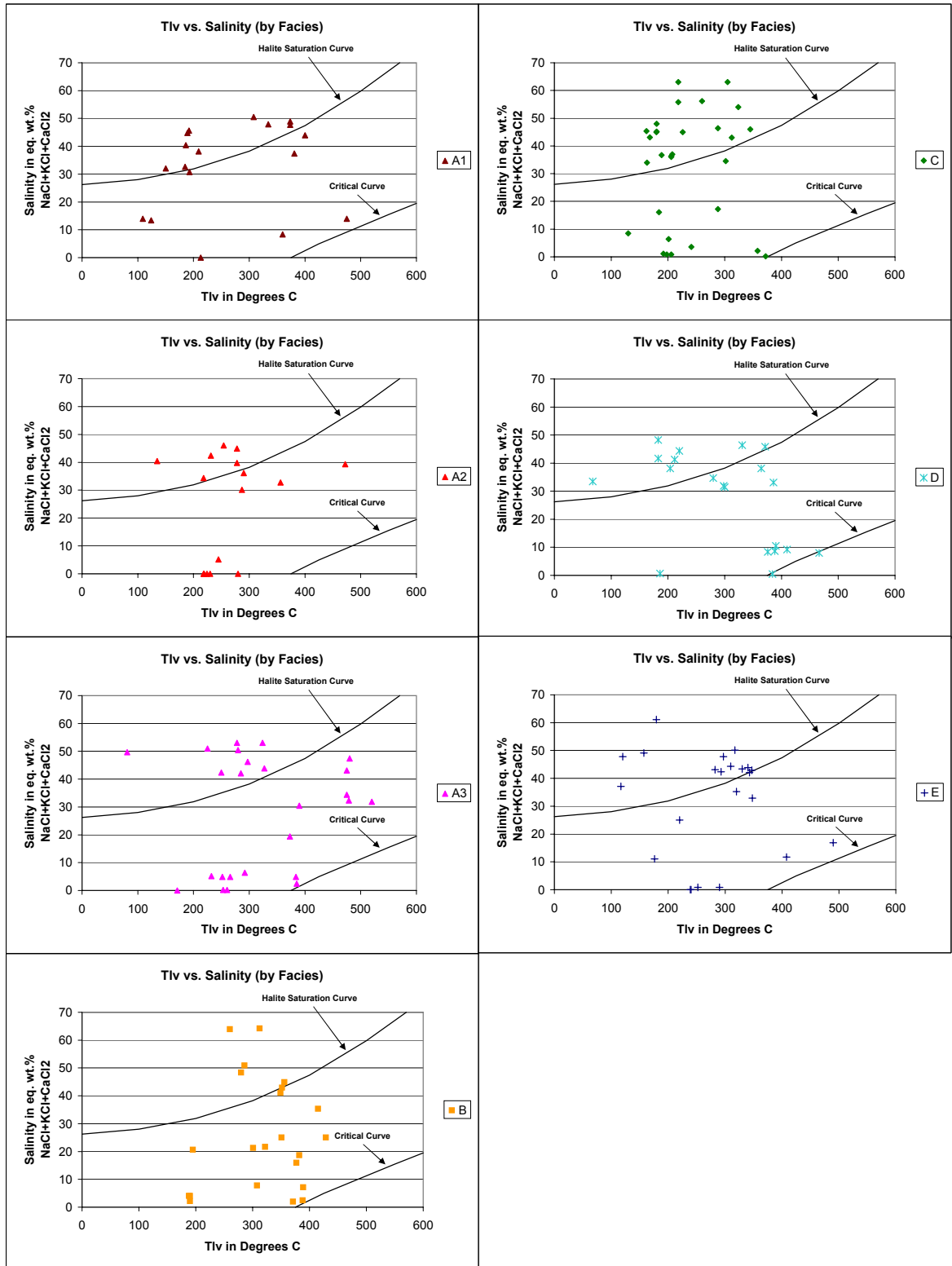
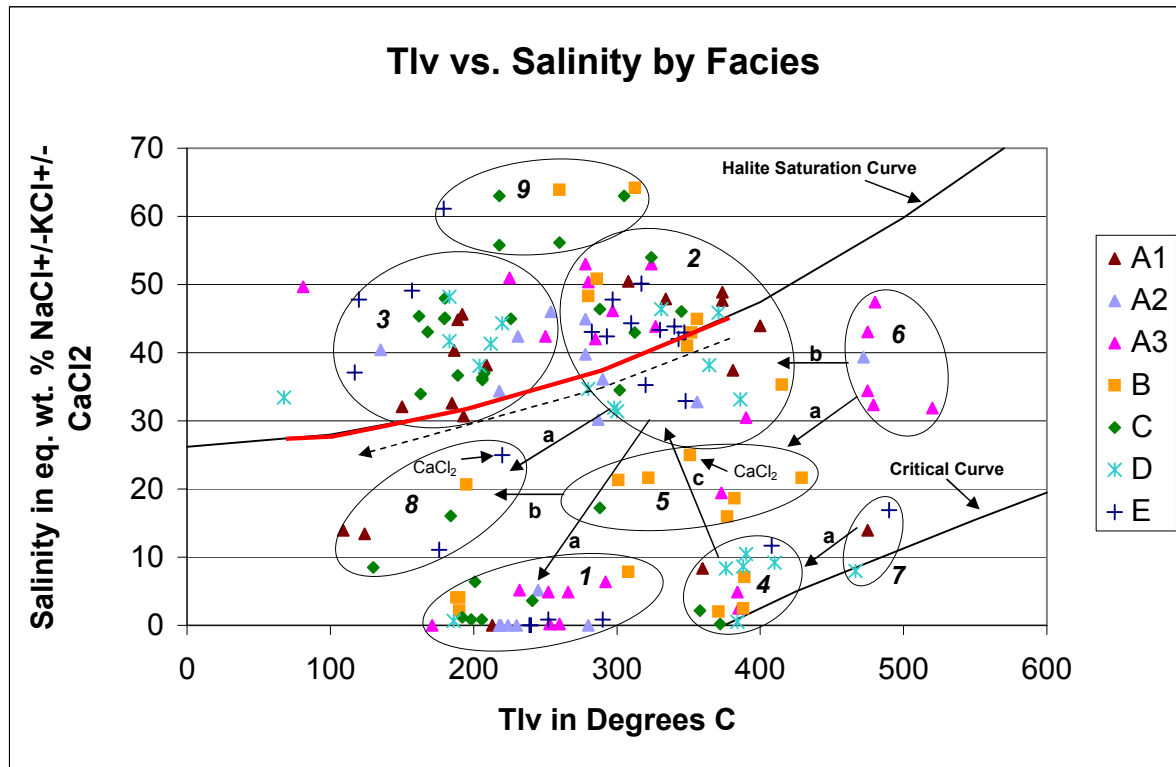


Figure 34. Tlv vs. salinity distributions for individual facies. The similar pattern and location of inclusions between facies led to the distinction of fluid inclusion populations 1 through 9 in Figure 33.



| Population | Facies | Types |
|------------|---------------|---------------------|
| 1 | all | Ia, Ib, IV |
| 2 | all | IIa, IIb, IIc, IIIa |
| 3 | all except B | IIb, IIc, IIIa |
| 4 | all except A2 | Ia, Ib |
| 5 | A3, B, C | Ia, Ib |
| 6 | A2, A3 | IIa, IIb, IIc |
| 7 | A1, D, E | Ib |
| 8 | A1, B, C, E | Ia, Ib, IV |
| 9 | B, C, E | IIb, IIc, IIIa |

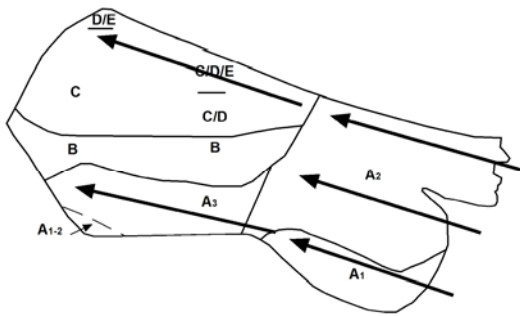
Table 6. Facies and type occurrence for fluid inclusion populations 1-9.

Figure 35. Tlv vs. salinity diagram for individual facies with identified distinct populations of 1 through 9. Inclusions that lie on or above the halite saturation curve (HSC) homogenized (final Th) by halite dissolution. The critical curve shows critical temperatures of unsaturated H₂O-NaCl solutions. Inclusions on or near this curve represent critical or near-critical fluids. The arrows with letters a, b, and c indicate fluid evolution paths by meteoric mixing, simple cooling, or boiling, respectively. The populations above the HSC do not represent a real fluid, due to the trapped halite phenomenon. The populations above the HSC are the result of a fluid at the same temperature on the HSC (represented by the red portion of the curve) and a trapped halite crystal. The dotted arrow represents the cooling path of the saturated fluids of populations 2, 9, and 3 along the HSC, which is the hypothesized mechanism for molybdenite precipitation.

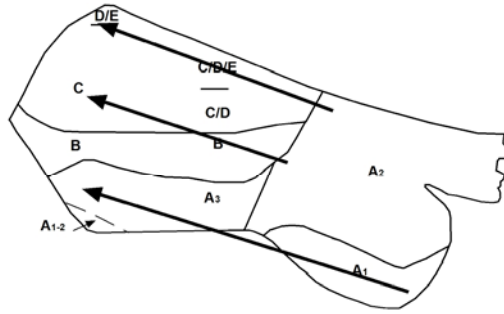
populations on or below the halite saturation curve in Figure 35 (1, a portion of 2, 4-8) are considered to represent fluid evolution, and fluid paths, within the system. The populations above the halite saturation curve (HSC) (the other portion of 2, and populations 3 and 9) are not representative of a real fluid, due to the trapped halite phenomenon. The inclusions/populations above the HSC are the result of a halite saturated fluid along the HSC at the same or corresponding homogenization temperature, and a trapped halite crystal. The salinities of the inclusions above the HSC are a function of the size of the halite crystal that was trapped, and are not real. The fluid inclusions above the HSC can be projected down to the HSC at their same temperature of homogenization, represented by the red portion of the HSC in Figure 35, in order to denote the real fluid in which they originated. The spatial distribution of each population within the MHBX facies, and possible schematic fluid paths for populations below the HSC, were modeled in Appendix C. Fluid flow paths and fluid evolution were summarized based upon the population models of Appendix C (Figure 36). Utilizing the Tlv vs. salinity diagram for the populations in combination with Figures 35 and 36, the following interpretations could be made.

Due to their high, or near magmatic temperatures, modes of homogenization (vbd and ld), and facies occurrence (A, D, and E), populations 6 and 7 are thought to represent the earliest, most pristine fluids. The halite-bearing inclusions in population 6 are below the halite saturation curve, marking that these inclusions do not contain trapped halite, and therefore, are not the result of a boiled-down or highly evolved fluid. Molybdenite is transported, or most soluble, in high temperature, saline fluids (Smith, 1983). This would explain the lower grade for facies A, and further supports population 6 as an earlier, pre-

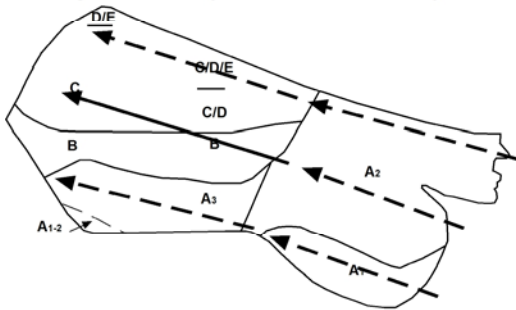
a. Populations 6 & 7



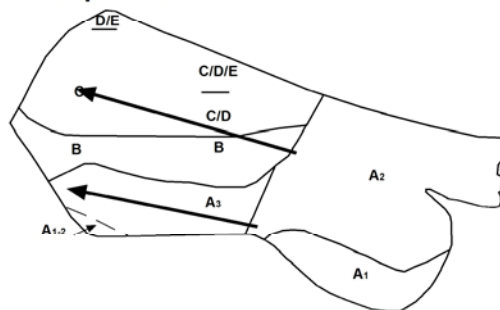
b. Population 4



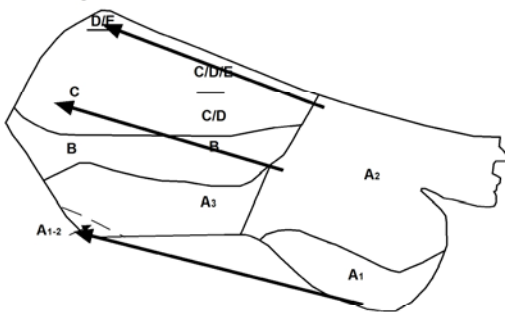
c. Population 2 (on or below HSC*)



d. Population 5



e. Population 8



f. Population 1

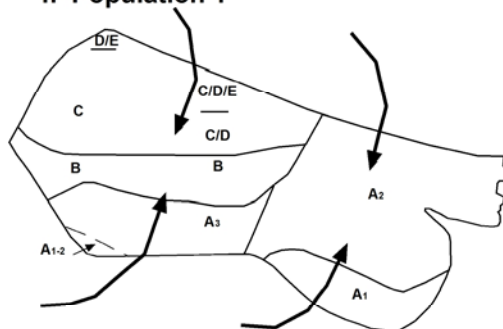


Figure 36. Schematic fluid flow paths for the populations that represent real fluids (on or below the halite saturation curve (HSC)). Drawn in approximate sequential order. Dashed arrows indicate evolution (i.e. cooling), but not necessarily flow. Drawn on MHBX short-section Panel 26. Modified from Ross, 2002. Not to scale. a.) Populations 6&7 most pristine and occur closest to source intrusion (SI) and along pre-breccia fabric. b.) Population 4 was derived from meteoric mixing of fluids from population 7. Occurs farthest from SI, since it would be too hot for any meteoric component (would have been driven off). c.) Population 2 was derived from cooling of population 6. Occurs throughout the breccia. d.) Population 5 was derived from meteoric mixing of fluids from population 6. Occurs farthest from the SI, since any water would have been driven off by the heat. e.) Population 8 was derived from either meteoric mixing of fluids from population 2 or cooling from population 5. Occurs farthest from the SI, since any water would have been driven off by the heat closest to the SI or simple cooling would lead to similar occurrence as population 5. f.) Population 1 was the last stage and is a result of meteoric influx into the entire system.

molybdenite mineralization fluid. Inclusions in population 7 are on or near the critical curve for unsaturated NaCl-H₂O fluids and represent critical or near-critical fluids. A pre-breccia fabric caused by volcanic bedding or a Precambrian shear zone controlled the shape of the breccia body and fluid flow (Ross, 2002). Direction of fluid flow can be recognized in Figures 6 and 7 by the shapes of the breccia, source intrusion, and dikes. Populations 6 and 7 occur in facies A, D, and E, where the first fluid flow occurred as brecciation began (Ross, 2002) (Appendix C, Figure 36a). The fluids of populations 6 and 7 gained minor meteoric input from hydrous minerals of the propylitically altered country rocks (andesite) or a pre-existing fluid, represented by populations 5 and 4, respectively. Note that Populations 4 and 5 do not occur in the facies closest to the source intrusion (A2 +/- A1) in Panel 26 (Figure 36 b and d). This supports that mixing is a likely factor for populations 4 and 5, in that no water would be available in the area closest to the intrusion due to the extreme heat. Population 5 contains inclusions from facies A3, B, and C. Three inclusions in population 5 homogenized by critical behavior. Population 5 also contains a CaCl₂-bearing inclusion. Perhaps the isolation of the population is due to calcium in the other inclusions as well. The origin of the calcium may be the propylitically altered andesite country rock, in which these fluids intruded. Population 5, and the tighter, higher temperature range of facies B, sets facies B apart from other facies (Figure 23). Population 4 contains inclusions from all facies except for A2. Inclusions in population 4 lie on or near the critical curve, representing critical or near-critical fluids. Three of the inclusions in population 4 homogenized by critical behavior. Simple cooling of fluids from population 6 caused by contact with cooler country rocks and/or crystallization/solidification, resulted in population 2 (portion on or

below the HSC), which occurred in all facies. Type IIa inclusions only occur in populations 6 and 2, supporting their relationship (Figure 37). There are no type IIa fluid inclusions in facies B, another factor that sets B apart from other facies. Type IIa inclusions contain no opaque or other translucent daughter minerals, and hence no molybdenite. This may be an indicator that the Type IIa inclusions are not related to the high grade molybdenite mineralization. Population 4 may also be the result of boiling of population 2 (on or below the HSC). Populations 2, 3, and 9 that occur above the HSC, can be projected down to the curve at the same T_h , as previously discussed (represented by the red portion of the curve in Figure 35). Population 9 only occurs in facies B, C, and E. Population 3 occurs in all facies except for facies B. This is another factor contributing to the uniqueness of facies B. In addition, type IIa inclusions (contain no opaque or other translucent daughters) do not occur in population 3. Type IIIa fluid inclusions only occur in populations 2, 3, and 9, and “tie” these three populations together as seen in Figure 37. The sylvite-bearing (KCl) type IIIa inclusions only occur in facies A, B, and C and are associated with potassic alteration. Cooling of fluids represented by the portion of population 2 that occurs below and on the HSC, and of the fluids represented by the projection of populations 2, 3, and 9 onto the HSC, are hypothesized to be the mechanisms for high grade molybdenite mineralization. The cooling of the fluids along the HSC is also considered to be associated with QSP alteration for the MHBX. Simple cooling of population 5 may have been the mechanism resulting in population 8. Population 8 occurs in facies A1, B, C, and E. Population 8 also contains a CaCl_2 -bearing inclusion, leading to the idea that perhaps all of the inclusions in this population are calcium-bearing, further supporting their relationship to

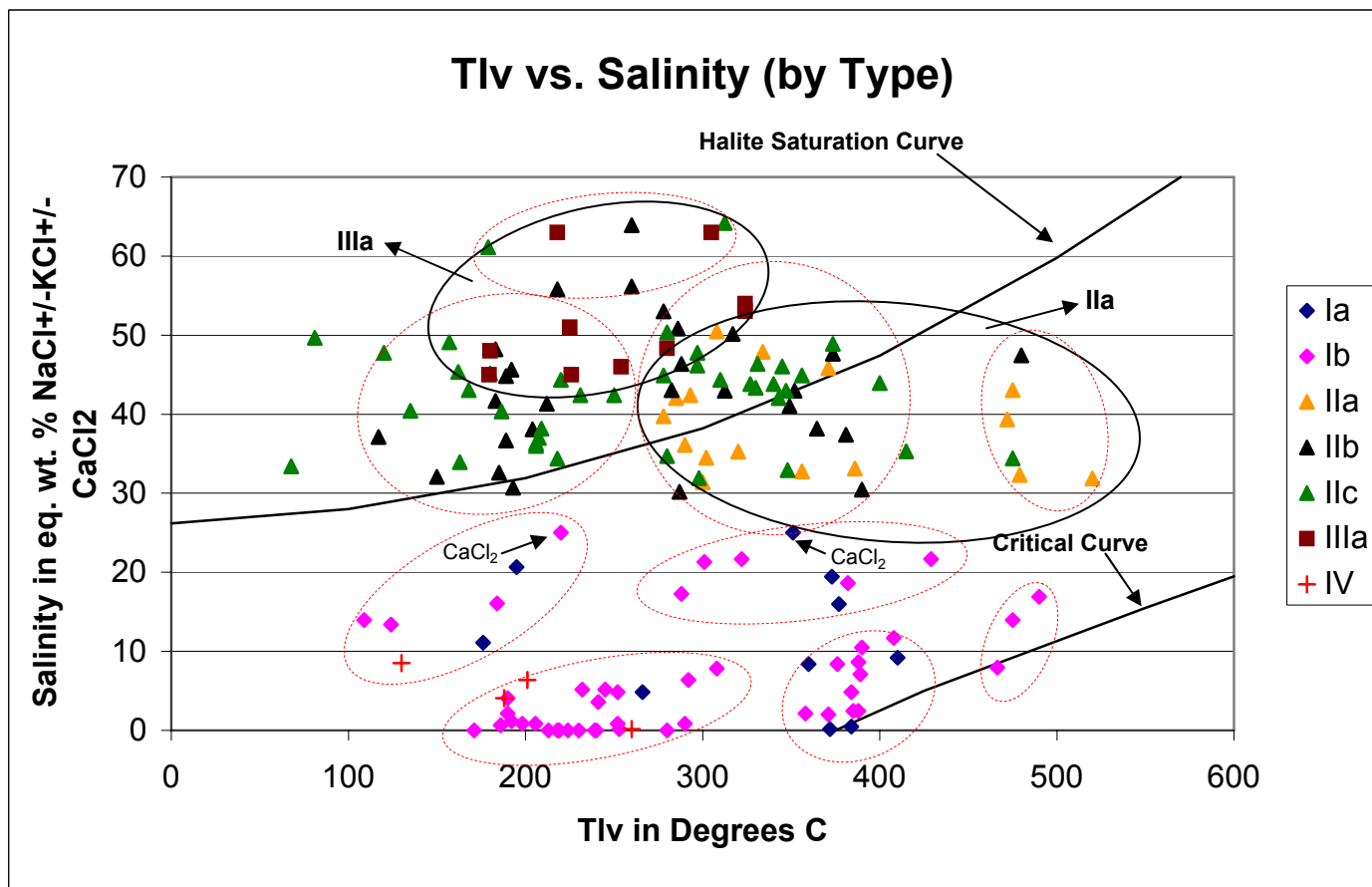


Figure 37. Tlv vs. salinity distribution by type. Red dotted circles are populations 1-9. Black circles are drawn around types IIa and IIIa.

population 5. Population 8 could also have been produced by meteoric mixing with the fluids of population 2 (real and projected onto HSC). Lastly, meteoric water influx and mixing with fluids of population 2 resulted in lower temperature, low salinity population 1. Population 1 contains inclusions from all facies. All of the known secondary inclusions occur in population 1. Only one inclusion containing an opaque daughter mineral occurs in population 1. The secondaries and lack of opaque-bearing inclusions further support a meteoric component to population 1. Population 1 contains three CO₂-bearing inclusions. The CO₂ could have been acquired from meteoric waters percolating through propylitically altered andesites.

Other evolutionary paths for the populations representing real fluids are certainly possible. The importance should be emphasized on the fact that there are 9 discreet populations in the fluid inclusion data. The populations are considered real (but not all represent real fluids), rather than a result of necking down, leakage, etc., because of the fact that previous studies had results reflecting similar populations. Cline and Bodnar (1994) had similar populations that would be equivalent to populations 1, 2, 4, 5, and 8 of this study. Bloom (1981) had populations similar to populations 2, 4, 5, and 6 of this study. Smith (1983) had similar populations that would be equivalent to populations 1, 2, 4, 5, 6, and 8 of this study. Due to data reporting in terms of final Th rather than Tlv in previous studies, populations 3, 9, and the portion of 2 above the HSC could not be compared.

As mentioned in the background section of this paper, quartz-molybdenite veins cross-cut the breccia and contributed a higher percentage of grade than the MHBX. Performing a fluid inclusion study on the veins in each of the facies, as was done for the

MHBX, may aid in further defining the origin and evolution of each of these populations. It is most likely that the veins have contributed to at least one of these populations, and the vein fluid inclusion data may indicate that one or two of these populations can be dropped out of the data-set for the MHBX.

Pressure Corrections

The liquid-vapor homogenization temperatures were not corrected for the effects of pressure. Boiling is evident throughout the breccia facies, hence $T_{lv}=T_t$ (temperature of trapping). The coexistence of liquid-rich and vapor-rich fluid inclusions are evidence of boiling. Trapped halite crystals are a possible consequence of boiling, as previously mentioned. The brecciation event was an instantaneous, single event (Ross, 2002). The Goat Hill MHBX contains no evidence of system sealing and re-brecciation, and resealing, etc., associated with the breccia itself, such as a β (beta), or secondary breccia, that cross-cuts the original breccia. Associated with this single, instantaneous brecciation event would be one pressure regime. All populations of Figure 35 are assumed to be associated with this event. The Goat Hill does contain later quartz-molybdenite veins that cross-cut the MHBX. The quartz-molybdenite veins are most likely the result of system sealing (breccia), pressure increase, and resultant fracturing and vein mineralization of the ore body.

CONCLUSIONS

The Goat Hill magmatic-hydrothermal breccia (MHBX) is composed of five distinct stratified facies (A-E) that were defined based upon matrix mineralogy and clast alteration (Ross, 2002). These five facies reveal a mineralogic/alteration evolution of the MHBX from the bottom of the breccia (facies A) to the top (facies E), with higher

temperature mineral and alteration assemblages at the bottom of the breccia, and lower temperature minerals and alteration at the top and distal edges of the MHBX. Four types of fluid inclusions (I-IV) with a wide range of temperatures and salinities were identified within the facies of the MHBX. The major types consisted of two-phase liquid- and vapor-rich, halite-bearing liquid-rich, halite- and sylvite-bearing liquid-rich, and three-phase carbonic inclusions. Identification of paragenetic origin of the fluid inclusions deemed difficult due to the ambiguity caused by multiple superimposed populations. Fifty percent of the halite-bearing fluid inclusions (types II and III) homogenized by halite disappearance at temperatures of 100 to 350°C greater than that of vapor bubble disappearance, which leads to unrealistic pressures and depths of formation for the MHBX. The unrealistic pressures are not attributed to overpressures, or exsolution and evolution of hydrothermal fluid, as previous authors on Climax-types proposed, but to heterogeneous trapping of halite crystals. Entrapment of halite crystals would provide an over-estimate of salinity and final T_h , and hence unrealistic PTX conditions. Evidence of the trapped halite phenomenon in the MHBX consisted of solid halite inclusions in quartz, “daughter” minerals that did not dissolve upon heating, vapor-rich inclusions containing halite +/- sylvite +/- other translucent minerals +/- opaques +/- hematite, and coexisting high salinity liquid-rich inclusions and vapor-rich inclusions, which is also an indication of boiling. Boiling is a probable mechanism for causing the fluid to become saturated in halite. Due to the plausibility of trapped halite, reporting in T_{lv} , rather than final T_h , is a more representative of the temperature of trapping.

The fluid inclusion data (T_{lv} vs. salinity) for the Goat Hill MHBX does not indicate any evolutionary pattern based upon facies, which is opposite of what had been

hypothesized. This indicates that the fluid evolution of the system is independent of the recognized mineralogic/alteration zonation. The data in terms of Tlv did indicate however, that Facies B and C exhibited a tighter temperature distribution than did that of facies A, D, and E. The data was scrutinized on a smaller scale (individual inclusions) in order to reveal a fluid evolution. Resultantly, nine distinct populations were defined on a Tlv vs. salinity diagram. Three populations occur above the halite saturation curve (HSC), and are not considered to be representative of a real fluid, due to the trapped halite phenomenon. The fluid inclusions from these populations above the HSC are a result of a real fluid along the HSC at their same temperature, and a trapped halite crystal. Fluid evolutionary paths were defined based upon the populations below the HSC, and the projection of the populations above the HSC onto the curve at their same temperatures. The evolution of the fluids was a result of 3 mechanisms - boiling, cooling, and meteoric mixing. Fluid inclusion analyses on the veins of the Goat Hill orebody would aid in delineating any vein contribution to the nine identified populations in the MHBX data set.

A spatial distribution of the fluid inclusions populations was modeled, from which a fluid flow and cooling/crystallization path was defined. The Goat Hill MHBX cooled and crystallized from the inside out, with facies B the least encountered by cooler fluids, followed by facies C. The “rind” (A, D, and E facies) of the MHBX encountered more fluids than the middle facies B and C, due to the pre-breccia fabric that controlled the shape of the breccia and the path of fluid flow.

Based upon the grade distribution (high grade ore zone mostly in facies C), the lower temperature distribution of facies C, and the spatial distribution and fluid

evolutionary paths defined by the populations, both real and projected, it was delineated that cooling of the fluids represented by the portion of population 2 on and below the HSC and the fluids along the HSC projected from populations 2, 9, and 3 was the mechanism for high grade molybdenite mineralization and is also associated with the QSP alteration for the MHBX.

COMPARISON WITH PREVIOUS CLIMAX-TYPE STUDIES

The results and interpretations for previous studies of Climax-type porphyry molybdenum deposits by Hall (1974), Kamilli (1978), White et al. (1981), Carten (1987), Seedorff & Einaudi (2004), Bloom (1981), Smith (1983), Cline & Bodnar (1994), Cline & Vanko (1995), and Klemm (2004) and the results and interpretations of this study are tabulated in Table 7. All previous authors reported data in terms of Final Th, rather than Tlv. All of the listed previous studies observed fluid inclusions equivalent to the liquid-rich type I inclusions of this study. All except Carten (1987) observed fluid inclusions equivalent to the vapor-rich type Ic of this study, yet only Kamilli (1978)/White et al. (1981), Bloom (1981), Smith (1983), and Klemm (2004) reported boiling in the system, as did this paper. Temperatures of 67.6-520°C were reported for this study. None of the previous studies reported temperatures below 150°C. Similar temperature ranges to this study were reported by Hall (1974), Carten (1987), Cline & Bodnar (1994), Cline & Vityk (1995), and Klemm (2004). The studies that reported temperature ranges much higher than this study are Kamilli (1978)/White et al. (1981), Bloom (1981), Smith (1983), and Klemm (2004). Similar salinities to this study were reported by all listed previous studies. The K/Na and NaCl/(NaCl+KCl) ratios calculated for this study are 0.35-0.75 and 0.57-0.74, respectively. The K/Na ratios reported by Bloom (1981) and

| Deposit | Author | Type Equivalent* | Final Th in °C | Salinity | K/Na or NaCl/(NaCl+KCl) | Boiling | Pressure | Ore Association and Deposition | magmatic or meteoric |
|-----------|----------------------------------------|-------------------------------------|----------------------------------------------------------|-------------------------------------------------------------------------------------------------|----------------------------------|-----------------------|-----------------------------------------------------------------------------------------------------|------------------------------------------------------------------------------------------------------------------------------------------------------------------------------------------------------------------------|-------------------------------------|
| Climax | Hall (1974) | Ia, Ib Ic IIc IV | 200-400 350-600 200-400 200-400 | 0.7-12 eq. wt.% NaCl ~35 eq. wt.% NaCl | | no | 250 bars | Mo associated with moderately saline inclusions (35 eq. wt.% NaCl and 360°C) | magmatic with meteoric mixing |
| Henderson | Kamilli (1978) and White et al. (1981) | Ia, Ib Ic IIa | Range of 250 to >600 in all inclusions with a mode @ 400 | 0-5 eq. wt.% NaCl 10-20 eq. wt.% NaCl 30-65 eq. wt.% NaCl | | yes | 350-585 bars | Tshl >> Tlv = overpressures due to exsolution and evolution of the hydrothermal fluid. Pressure correction used for all inclusions. Average temperature of mo mineralization after P correction = 500-650°C. | magmatic |
| | Carten (1987) | Ia IIIa | 346 +/- 30 (F-rich) Tlv (280 +/- 35) << Tshl | 16-20 eq. wt.% NaCl (Cl-rich); ~2-7 eq. wt.% NaCl (F-rich) 62 eq. wt.% NaCl (Cl-rich) | | no | | Mo associated with F-rich fluids; Cl-rich Tlv << Tshl fluids derived directly from silicic melt. | |
| | Seedorff & Einaudi (2004) | I, II, III | 600-460 (mod. high), 530-310 (mod), 390-200 (low)** | 28-65 eq. wt.% NaCl+KCl to <29 eq. wt.% NaCl | | | | Mo mineralization associated with mod. high temperature assemblages at 600-460°C and 28-65 and <29 eq. wt.% NaCl. | magmatic |
| Questa | Bloom (1981) | Ia | 300 to >600, mode at 390 | 5-15 eq. wt.% NaCl | | local or intermittent | Varied from lithostatic to hydrostatic with intermittent overpressures. | Mo mineralization coincided with QSP alteration. Mo mineralization associated with moderately saline (30-60 eq. wt.% NaCl) or low to moderately saline (5-15) eq. wt.% NaCl inclusions @ 300 to >600°C, mode at 390°C. | evolution from magmatic to meteoric |
| | | Ic IIa, IIb | 300 to >600, mode at 390 | 30-60 eq. wt.% NaCl | K/Na < 0.2 assoc. w/QSP alt. | | | | |
| | | IIIa IV | 320 to >600, mode at 390 | | K/Na > 0.2 assoc. w/potassic alt | | | | |
| | | | | | | | | | |
| | Smith (1983) | Ia Ic IIa, IIb IIIa | All: 300-500, 520-555, 580-600, secondaries - 200-370 | All: 5-20 and 25-65 eq. wt.% NaCl | K/Na = 0.23-0.29 | sporadic | boiling - 180 bars non-boiling - 100-500 bars Tlv @ 40°C < Tshl - 330 bars | Halite- and sylvite-bearing (equiv. type IIIa) inclusions predate mo mineralization. Bt-mo mineralization @ 550 °C due to potassic alteration which caused F- to go out of solution and into bt. | mixing of magmatic and meteoric |
| | Cline & Bodnar (1994) | Ia, Ib Ic IIa, IIb, IIc, IIIa | 150-370 360-500 200-500, mode @ 360-400 | 0-12 eq. wt.% NaCl 2-26 eq. wt.% NaCl 31-57 eq. wt.% NaCl | NaCl/(NaCl+KCl) = 0.75-0.78 | no | T and salinity result of severe pressure fluctuations due to repeated system sealing and fracturing | Ore fluids originated by exsolution directly from the crystallizing silicic melt and different pressure regimes yielded the three different fluid types. | magmatic |
| | Cline & Vanko (1995) | Ia, Ib Ic IIa, IIb, IIc, IIIa | 150-370 370-500 220-420 | 0-12 eq. wt.% NaCl 2-24 eq. wt.% NaCl 31-57 eq. wt.% NaCl +/- KCl | NaCl/(NaCl+KCl) = 0.75-0.78 | no | T and salinity result of severe pressure fluctuations due to repeated system sealing and fracturing | Mo transport and precipitation associated with high salinity or near critical fluids. Ore fluids generated by exsolution from silicic melt rather than aqueous fluid immiscibility. | magmatic |

* The equivalent to types of this study.

** Moderately high, moderate, and low = "lower temperature" mineral assemblages of Seedorff and Einaudi (2004).

Table 7. Comparison of Climax-type data and interpretations.

| Deposit | Author | Type Equivalent* | Final Th in °C | Salinity | K/Na or NaCl/(NaCl+KCl) | Boiling | Pressure | Ore Association and Deposition | magmatic or meteoric |
|---------------|--------------|----------------------------------------------------------------------|------------------------------------------------------------------------------------------------------------------------------------------------|-----------------------------------------------------------------------------------------------------------------------------------------------------------------------------------------------------------------------|------------------------------------------------------------------------------------------|------------------|----------------------------------------------------|----------------------------------------------------------------------------------------------------------------------------------------------------------------------------------------------------------------------------------------------------------------------|--------------------------------------------|
| Questa cont'd | Klemm (2004) | Ia Ic Iic and IIIa? IV | >450 (early brine); 270-350 (late brine) | 38-46 eq. wt.% NaCl (early brine); 32-40 eq. wt.% NaCl (late brine) | | yes, early brine | | Low salinity type I inclusions represent fluid that exsolved directly from the crystallizing magma. Mo associated with early brine inclusions (1000 ppm Mo). Molybdenite precipitated by temperature decrease since later brine inclusions are lower in temperature. | |
| | This study | Ia Ib Ic IIa IIb IIc IId IIia IIib IV | Tiv = 87.6-488 Tiv = 109-520 Tiv = 360-485 Tiv = 192-520 Tiv = 117-480 Tiv = 67.6-475 Tiv = 179.5-324 130-260 | 0-25 eq. wt.% NaCl+/-CaCl ₂ 0-25 eq. wt.% NaCl+/-CaCl ₂ 31-50 eq. wt.% NaCl 30-64 eq. wt.% NaCl 32-64 eq. wt.% NaCl 45-63 eq. wt.% NaCl+KCl 0-9 eq. wt.% NaCl | Na/K = 0.35-0.75; NaCl/(NaCl+KCl) = 0.57-0.74 | yes | No overpressures; Tshl>>Tiv due to trapped halite. | Cooling of moderately saline inclusions along the HSC caused high-grade molybdenite mineralization. Also associated with QSP alteration. | system is magmatic with meteoric component |

* The equivalent to types of this study.

** Moderately high, moderate, and low = "lower temperature" mineral assemblages of Seedorf and Einaudi (2004).

Table 7 Cont'd. Comparison of Climax-type data and interpretations.

Smith (1983) are <0.2 (QSP alteration) to >0.2 (K-alteration) and 0.23-0.29, respectively. NaCl/(NaCl+KCl) was reported for both Cline papers at 0.75-0.78 (Cline & Bodnar, 1994; Cline & Vanko, 1995). Pressures were reported as lithostatic with a range of 100-585 bars (Hall, 1984; Kamilli, 1978, White et al., 1981; and Smith, 1983) and fluctuations between hydrostatic and/or lithostatic with intermittent overpressures (Kamilli, 1978; Bloom, 1981; Cline & Bodnar, 1994; and Cline & Vanko, 1995). Kamilli (1978), White et al. (1981), Cline & Bodnar (1994), and Cline & Vanko (1995) account for the Tshl>>Tlv fluid inclusions by overpressures caused by system sealing, and hydrothermal fluid exsolution and evolution. This study discounts overpressures, and uses the idea of trapped halite phenomenon to account for the Tshl>>Tlv inclusions. Carten (1987) reported that the Tlv<<Tshl inclusions represent fluids that were derived directly from the silicic melt. The temperature and salinity of the fluid associated with molybdenite mineralization reported in this study are 117-254 °C and 31-51 eq. wt.% NaCl+/-KCl. The temperatures and salinities associated with molybdenite mineralization reported by previous studies are 360 °C and 35 eq. wt.% NaCl (Hall, 1974), 500-650 °C (Kamilli, 1974 and White et al., 1981), 346+/-30 °C and 2-7 eq. wt.% NaCl (Carten, 1987), 600-460 °C and <29 to 28-65 eq. wt.% NaCl (Seedorff & Einaudi, 2004), 300->600 °C with a mode at 390 °C and 5-15 or 30-60 eq. wt.% NaCl (Bloom, 1981), 550 °C (Smith, 1983), 220-500 °C and 2-24 or 31-57 eq. wt.% NaCl+/-KCl (Cline & Vityk, 1995), and >450 °C and 38-46 eq. wt.% NaCl (Klemm, 2004). In this study, it was reported that molybdenite mineralization was caused by a temperature decrease by simple cooling, and is associated with QSP alteration. Previous studies reported the following associations to molybdenite mineralization: Carten (1987) stated that molybdenite

mineralization is associated with F-rich fluids, rather than Cl-rich fluids; Seedorff & Einaudi (2004) delineated that molybdenite mineralization at Henderson is associated with their moderately high temperature assemblages; Bloom (1981) concluded that molybdenite mineralization coincided with QSP alteration; Smith (1983) concluded that molybdenite mineralization was a result of potassic alteration which caused F⁻ (complex for molybdenum) to come out of solution and into biotite; Cline & Bodnar (1994) and Cline & Vanko (1995) concluded that the origin of the ore fluids is exsolution directly from the crystallizing silicic melt rather than aqueous fluid immiscibility; Klemm (2004) concluded that molybdenite precipitation was a result of a temperature decrease. Kamilli (1978)/White et al. (1981), Seedorff & Einaudi (2004), Cline & Bodnar (1994), and Cline & Vityk (1995) concluded a magmatic origin to the ore fluids. Hall (1974), Bloom (1981), and Smith (1983) concluded both a magmatic and meteoric component to the ore system. In this study, the Goat Hill MHBX was concluded to be a system with both a magmatic and meteoric component.

BIBLIOGRAPHY

- Bloom, M.S., 1981, Chemistry of inclusion fluids; stockwork molybdenum deposits from Questa, New Mexico, Hudson Bay Mountain and Endako, British Columbia: *Economic Geology and the Bulletin of the Society of Economic Geologists*, v. 76, p. 1906-1920.
- Bodnar, R.J., 1994, Synthetic fluid inclusions. XII. Experimental determination of the liquidus and isochores for a 40 wt.% H₂O-NaCl solution: *Geochimica Cosmochimica Acta* 58, p. 1053-1063.
- , 2003, Introduction to aqueous-electrolyte fluid inclusions, *in* Samson, I.M., Anderson, A.J., and Marshall, D., eds., *Fluid Inclusions: Analysis and Interpretation*, Volume 32: Short Course: Vancouver, B.C., Mineralogical Association of Canada, p. 81-100.
- Bodnar, R.J., and Vityk, M.O., 1994, Interpretation of Microthermometric data for H₂O-NaCl fluid inclusions, *in* B., D.V., and M.L., F., eds., *Fluid Inclusions in Minerals: Methods and Applications*: Blacksburg, VA, Virginia Tech, p. 117-130.
- Brown, P.E., and Hagemann, S.G., 1994, MacFlinCor: A computer program for fluid inclusion data reduction and manipulation, *in* de Vivo, B., and Frezzottie, M.L., eds., *Fluid Inclusions in Minerals: Methods and Applications*, Volume Short Course IMA, VPI Press, p. 231-250.
- Campbell, A.R., Banks, D.A., Phillips, R.S., and Yardley, B.W.D., 1995, Geochemistry of Th-U-REE mineralizing magmatic fluids, Capitan Mountains, New Mexico: *Economic Geology*, v. 90, p. 1271-1287.
- Campbell, A.R., Lundberg, S.A.W., and Dunbar, N.W., 2001, Solid inclusions of halite in quartz: evidence for the halite trend: *Chemical Geology (including Isotope Geoscience)*, v. 173, p. 179-191.
- Carpenter, R.H., 1968, *Geology and ore deposits of the Questa molybdenum mine area*, Taos County, New Mexico.
- Carten, R.B., 1987, Evolution of immiscible Cl- and F-rich liquids from ore magmas, Henderson porphyry molybdenum deposit, Colorado [abs.]: *Geological Society of America Abstracts with Programs*, v. 19.
- Carten, R.B., White, W.H., and Stein, H.J., 1993, High-grade granite-related molybdenum systems; classification and origin: *Mineral deposit modeling*, v. 40, p. 521-554.
- Cline, J.S., and Bodnar, R.J., 1994, Direct evolution of brine from a crystallizing silicic melt at the Questa, New Mexico, molybdenum deposit: A special issue on volcanic centers as targets for mineral exploration, v. 89, p. 1780-1802.
- Cline, J.S., and Vanko, D.A., 1995, Magmatically generated saline brines related to molybdenum at Questa, New Mexico, USA, p. 153-174 p.
- Cox, D.P., and Singer, D.A., 1986, *Mineral deposit models*: Reston, VA, U. S. Geological Survey, 379 p.
- Czamanske, G.K., Foland, K.A., Kubacher, F.A., and Allen, J.C., 1990, The (super 40) Ar/ (super 39) Ar chronology of caldera formation, intrusive activity and Mo-ore deposition near Questa, New Mexico, *in* Bauer, P.W., Lucas, S.G., Mawer, C.K.,

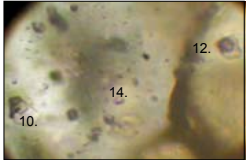
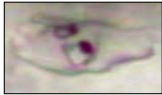





- and McIntosh, W.C., eds., New Mexico Geological Society Forty-first annual field conference, Volume 41, New Mexico Geological Society, p. 355-358.
- Donahue, K.M., 2002, Geochemistry, geology and geochronology of the Victorio mining district, Luna County, New Mexico: Linking skarn and porphyry systems to carbonate-hosted lead-zinc replacement deposits [Master of Science Thesis thesis]: Socorro, New Mexico Institute of Mining & Technology.
- Eastoe, C.J., 1978, A fluid inclusion study of the Panguna porphyry copper deposit, Bougainville, Papua New Guinea: *Economic Geology*, v. 73, p. 721-748.
- Erwood, R.J., Kessler, S.E., and Cloke, P.L., 1979, Compositionally distinct, saline hydrothermal solutions, Naica mine, Chihuahua, Mexico: *Economic Geology*, v. 74, p. 95-108.
- Ford, W.E., 1966, *Dana's Textbook of Mineralogy*, J. Wiley.
- Fournier, R.O., 1981, Application of water geochemistry to geothermal exploration and reservoir engineering, *in* Rybach, L., and Muffler, L.J.P., eds., *Geothermal systems: Principles and Case Histories*, Volume 109-143: New York, John Wiley & Sons.
- Guilbert, J.M., and Park, C.F., Jr., 1986, *The Geology of Ore Deposits*: New York, NY, W. H. Freeman and Company, 985 p.
- Gunter, W.D., Chou, I.-M., and Girsperger, S., 1983, Phase relations in the system NaCl-KCl-H₂O II: Differential thermal analysis of the halite liquidus in the NaCl-H₂O binary above 450°C: *Geochimica Cosmochimica Acta* 47, p. 863-873.
- Hall, W.E., Friedman, I., and Nash, J.T., 1974, Fluid inclusion and light stable isotope study of the Climax molybdenum deposits, Colorado: *Stable Isotopes as Applied to Problems of Ore Deposits*, v. 69, p. 884-901.
- International Molybdenum Association, Website Homepage, 2003, April 10, 2005, <www.imoa.info/RunScript.asp?p=ASP\Pg0.asp>
- Johnson, C.M., Czamanske, G.K., and Lipman, P.W., 1989, Geochemistry of intrusive rocks associated with the Latir volcanic field, New Mexico, and contrasts between evolution of plutonic and volcanic rocks: *Contributions to Mineralogy and Petrology*, v. 100, p. 90-103.
- Johnson, C.M., and Lipman, P.W., 1988, Origin of metaluminous and alkaline volcanic rocks of the Latir volcanic field, northern Rio Grande rift, New Mexico: *Contributions to Mineralogy and Petrology*, v. 100, p. 107-128.
- Johnson, C.M., Lipman, P.W., and Czamanske, G.K., 1990, H, O, Sr, Nd, and Pb isotope geochemistry of the Latir volcanic field and cogenetic intrusions, New Mexico, and relations between evolution of a continental magmatic center and modifications of the lithosphere: *Contributions to Mineralogy and Petrology*, v. 104, p. 99-124.
- Kamilli, R.J., 1978, The genesis of stockwork molybdenite deposits; implication from fluid inclusion studies at the Henderson Mine, The Geological Association of Canada, The Mineralogical Association of Canada, The Geological Society of America (91st annual meeting); 1978 joint annual meeting, Volume 10, Geological Society of America (GSA), p. 431.
- Kelley, S.A., Chapin, C.E., and Corrigan, J., 1992, Late Mesozoic and Cenozoic cooling histories of the flanks of the northern and central Rio Grande rift, Colorado and New Mexico: *New Mexico Bureau Bulletin*, v. 145, p. 39.

- Klemm, L.M., Pettke, T., and Heinrich, C.A., 2004, Early magmatic-hydrothermal evolution of the Questa porphyry-Mo deposit, New Mexico, U.S.A [abstr.], SEG 2004, Predictive Mineral Discovery Under cover: Perth, Western Australia.
- Kodera, P., Lexa, J., Rankin, A.H., and Fallick, A.E., 2004, Fluid evolution in a subvolcanic granodiorite pluton related to Fe and Pb-Zn mineralization, Banska Stiavnica Ore District, Slovakia: *Economic Geology*, v. 99, p. 1745-1770.
- Leonardson, R.W., Dunlop, G., Starquist, V.L., Bratton, G.P., Meyer, J.W., and Osborne, L.W., Jr., 1983, Preliminary geology and molybdenum deposits at Questa, New Mexico, *in* Babcock, J.W., ed., Denver Region Exploration Geologists Society symposium; the genesis of Rocky Mountain ore deposits; changes with time and tectonics: Proceedings of the Denver Region Exploration Geologists Society symposium; the genesis of Rocky Mountain ore deposits; changes with time and tectonics: Wheat Ridge, CO, Denver Reg. Explor. Geol. Soc.
- Lipman, P.W., 1992, Ash-flow calderas as structural controls of ore deposits; recent work and future problems, *in* Thorman, C.H., ed., Application of structural geology to mineral and energy resources of the Central and Western United States, U. S. Geological Survey, p. L1-L12.
- Ludington, S.D., 1986, Descriptive model of Climax Mo deposits: Mineral deposit models, P. 73.
- Ludington, S.D., Bookstrom, A.A., Kamilli, R.J., Walker, B.M., and Klein, D.P., 1995, Climax Mo deposits: Preliminary compilation of descriptive geoenvironmental mineral deposit models, p. 70-74.
- Martineau, M.P., Heinemeyer, G.R., Craig, S.D., and McAndrews, K.P., 1977, Geologic report - Questa Project 1975-1977, Questa Molybdenum Company internal report, p. 161.
- Meyer, J., and Foland, K.A., 1991, Magmatic-tectonic interaction during early Rio Grande Rift extension at Questa, New Mexico: *Geological Society of America Bulletin*, v. 103, p. 993-1006.
- Meyer, J.W., 1990, Structural controls of the Questa molybdenum district, North New Mexico, *in* Bauer, P.W., Lucas, S.G., Mawer, C.K., and McIntosh, W.C., eds., New Mexico Geological Society Forty-first annual field conference, Volume 41, New Mexico Geological Society, p. 5-9.
- , 1991, Volcanic, plutonic, tectonic and hydrothermal history of the southern Questa Caldera, New Mexico [Doctoral thesis]: Santa Barbara, CA, University of California Santa Barbara.
- Meyer, J.W., and Leonardson, R.W., 1990, Tectonic hydrothermal and geomorphic controls on alteration scar formation near Questa, New Mexico, *New Mexico Geological Society Guidebook, 41st Field Conference, Southern Sangre de Cristo Mountains, New Mexico*, p. 417-422.
- Molling, P.A., 1989, Applications of the reaction progress variable to hydrothermal alteration associated with the deposition of the Questa molybdenite deposit, NM [Doctoral thesis]: Baltimore, MD, Johns Hopkins Univ.
- Reed, J., J.C., Bickford, M.E., Premo, W.R., Aleinikoff, J.N., and Pallister, J.S., 1987, Evolution of the Early Proterozoic Colorado Province: constraints from U-Pb geochronology: *Geology*, v. 15, p. 861-865.
- Roedder, E., 1979, Fluid inclusions as samples of ore fluids., *in* Barnes, H.L., ed.,

- Geochemistry of Hydrothermal Ore Deposits. 2nd ed.: Wiley, New York, p. 684-737.
- , 1984, Fluid Inclusions: Mineralogical Society of America, *Reviews in Mineralogy*, v. 12, p. 644.
- Ross, P.S., 2002, Magmatic-hydrothermal Breccia Formation in Porphyry Mo Systems: A Horizontal Stratified Body at Questa, New Mexico: M.Sc. Thesis, Earth Sciences Dept. University of Quebec in Montreal.
- Ross, P.S., Jebrak, M., and Walker, B.M., 2001, A magmatic-hydrothermal breccia formed by hydraulic fracturing under a compressive stress regime at the Questa porphyry molybdenum deposit, *in* Anonymous, ed., Geological Society of America, 2001 annual meeting, Volume 33, Geological Society of America (GSA), p. 420.
- Ross, P.-S., Jebrak, M., and Walker, B.M., 2002, Discharge of hydrothermal fluids from a magma chamber and concomitant formation of a stratified breccia zone at the Questa porphyry molybdenum deposit, New Mexico: *Economic Geology and the Bulletin of the Society of Economic Geologists*, v. 97, p. 1679-1699.
- Schilling, J.H., 1956, Geology of the Questa molybdenum (Moly) mine area, Taos County, New Mexico: Socorro, NM, New Mexico Bureau of Mines and Mineral Resources, 87 p.
- Seedorff, E., and Einaudi, M.T., 2004, Henderson Porphyry Molybdenum System, Colorado: II. Decoupling of Introduction and Deposition of Metals during Geochemical Evolution of Hydrothermal Fluids: *Economic Geology*, v. 99, p. 39-72.
- Shephard, T.J., Rankin, A.H., and Alderton, D.H.M., 1985, *A Practical Guide to Fluid Inclusion Studies*: Glasgow, Blackie & Son Limited, 239 p.
- Sinclair, W.D., 1995a, Porphyry Mo (Climax-type): Selected British Columbia mineral deposit profiles, p. 105-108.
- Sinclair, W.D., 1995b, Porphyry Mo (low-F-type): Selected British Columbia mineral deposit profiles, p. 93-95.
- Smith, R.W., 1983, Aqueous chemistry of molybdenum at elevated temperatures and pressures with applications to porphyry molybdenum deposits [Doctoral thesis]: Socorro, NM, New Mexico Institute of Mining and Technology.
- Theodore, T.G., 1986, Descriptive model of porphyry Mo, low-F: *Mineral deposit models*, p. 120.
- White, W.H., Bookstrom, A.A., Kamilli, R.J., Ganster, M.W., Smith, R.P., Ranta, D.E., and Steininger, R.C., 1981, Character and origin of climax-type molybdenum deposits.
- White, W.H., Carten, R.B., Bookstrom, A.A., and Stein, H.J., 1990, A model for climax-type molybdenum deposits, *in* Boyle, R.W., ed., 8th IAGOD symposium in conjunction with international conference on Mineral deposit modeling, Volume 8, E. Schweizerbart'sche Verlagsbuchhandlung (Naegele u. Obermiller), p. A133-A134.
- Wilson, J.W.J., 1978, Fluid inclusion geochemistry of the Granisle and Bell Copper porphyry deposits, B.C. [MSc thesis]: Toronto, University of Toronto.




APPENDIX A – FLUID INCLUSION RAW DATA

Matrix Fluid Inclusion Data

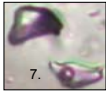



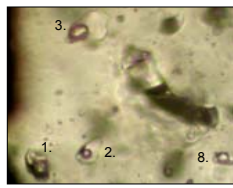
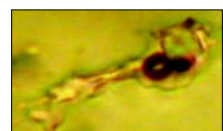
| Sample Comments and Photographs | Sample | Facies | Inclusion | Paragenesis | Assigned Paragenesis | Type | %L CO ₂ | %V CO ₂ | %L | %V | %S | Length in um | Width in um | Phase | Tm _{CO2} | Te | Tm _{hh} | Tm _{ice} | Tm _{clath} | | | | | | | | | | | | | |
|------------------------------------------------------------------------------------------------------------------------------------------------------------------------------------------------------------------------------------------------------------------------------------------------------------------------------------------------------------------|---------|--------|------------------------------------------------------------------------------------------------------------------------------------------------------------------------------------------------------------------------------|-------------|----------------------|-------|--------------------|--------------------|------|------|------|--------------|-------------|--------------------------------------------------------------------------------------------------------------------------------------------------------------------------------------------------------------------------------------------|-------------------|------|--------------------------------------------------------------------------------------------------------------------------------------------------------------------------------------------------|-------------------|---------------------|------|------|---|-------------------------------------------------------------------------------------------------------------------------------------------------------------------------------------------------------------------------------------------------------|--|--|--|--|--|--|----|-------|-------|
|  <p>AR-105 - Inclusions 10, 12, 14</p> <p>Solid inclusions of hl present; evidence of boiling.</p> | AR-105 | A1 | 6 | P | P | llc. | | | | | | | | l+v+s; l>v; s=hl, ops, ots l+v+s; l>v; s=hl, ops l+v+s; l>v; s=hl l+v+s; l>v; s=ops l+v+s; l>v; s=hl, ops, ots l+v+s; l>v; s=hl l+v; v>l l+v; l>v l+v; v>l l+v; v>l l+v+s; l>v; s=hl l+v+s; l>v; s=hl, op | | | | | | | | | | | | | | | | | | |
| | | | 10 | P | P | llb. | | | | | | | 13 | | | | | | | 13 | | | | | | | | | | | | |
| | | | 11 | PS | PS | lla. | | | | | | | | | | | | | | 5 | 5 | | | | | | | | | | | |
| | | | 12 | P or S | IND | la. | | | | | | | | | | | | | | 9 | 9 | | | | | | | | | | | |
| | | | 13 | P | P | llc. | | | | | | | | | | | | | | 13 | 13 | | | | | | | | | | | |
| | | | 14 | PS | PS | lla. | | | | | | | | | | | | | | 5 | 5 | | | | | | | | | | | |
| | | | 15 | P | P | lc. | | | | | | | | | | | | | | | | | | | | | | | | | | |
| | | | 16 | P | P | lb. | | | | | | | | | | | | | | | | | | | | | | | | | | |
| | | | 17 | P | P | lc. | | | | | | | | | | | | | | | | | | | | | | | | | | |
| | | | 18 | P | P | lc. | | | | | | | | | | | | | | | | | | | | | | | | | | |
| | | | 19 | P | P | lla. | | | | | | | | | | | | | | | | | | | | | | | | | | |
| | | | 20 | PS | PS | llb. | | | | | | | | | | | | | | | | | | | | | | | | | | |
| | | |  <p>AR-112 - Inclusion 12</p>  <p>AR-112 - Inclusion 7</p> | AR-112 | A1 | 1 | P or PS | IND | lb. | | | 0.85 | 0.15 | | | | | | | | 6 | 9 | l+v; l>v l+v; l>v l+v+s; l>v; s=hm, op, hl l+v+s; l>v; s=ot, hl l+v+s; l>v; s=hl, hm, op l+v; l>v l+v+s; l>v; s=hl, op, ots l+v+s; l>v; s=hl, mo, op l+v+s; l>v; s=hl, op l+v+s; l>v; s=hl, hm, op l+v; l>v l+v; l>v | | | | | | | | | |
| | | | | | | 2 | P or PS or S | IND | lb. | | | 0.95 | 0.05 | | | | | | | | | | | | | | | | | 25 | 13 | |
| | | | | | | 3 | P or PS | IND | llb. | | | | 0.7 | | | | | | | 0.1 | 0.2 | | | | | | | | | 5 | 5 | |
| | | | | | | 4 | P or PS | IND | llc. | | | | 0.65 | | | | | | | 0.15 | 0.2 | | | | | | | | | 6 | 3 | |
| | | | | | | 5 | PS or S | IND | llb. | | | | 0.75 | | | | | | | 0.05 | 0.2 | | | | | | | | | 6 | 6 | |
| | | | | | | 6 | PS | PS | lb. | | | | 0.9 | | | | | | | 0.1 | | | | | | | | | | 9 | 3 | |
| | | | | | | 7 | P | P | llc. | | | | 0.78 | | | | | | | 0.1 | 0.12 | | | | | | | | | 9 | 9 | |
| | | | | | | 9 | P or PS | IND | llb. | | | | 0.8 | | | | | | | 0.1 | 0.1 | | | | | | | | | 13 | 6 | |
| 11 | PS or S | IND | | | | llb. | | | | 0.85 | 0.07 | 0.08 | | 6 | 5 | | | | | | | | | | | | | | | | | |
| 12 | PS or S | IND | | | | llb. | | | | 0.85 | 0.05 | 0.1 | | 19 | 9 | | | | | | | | | | | | | | | | | |
| 13 | PS or S | IND | | | | lb. | | | | 0.55 | 0.45 | | | 9 | 9 | | | | | | | | | | | | | | | | | |
| 15 | PS or S | IND | | | | lb. | | | | 0.9 | 0.1 | | | 6 | 6 | | | | | | | | | | | | | | | | | |
|  <p>AR-106 - Inclusion 7</p>  <p>AR-106 - Inclusion 11</p> <p>Solid inclusions of hl present; evidence of boiling.</p> <p>Terrible polish; very hard to work with; evidence of boiling.</p> | AR-106 | A2 | | | | 1 | P or S | IND | llc. | | | 0.9 | 0.05 | 0.05 | 9 | 9 | l+v+s; l>v; s=hl, ot l+v+s; l>v; s=hl, ot, hm l+v+s; l>v; s=hl l+v; v>l l+v+s; l>v; s=hl l+v+s; l>v; s=ops, hl, sylv l+v; l>v l+v+s; l>v; s=ot l+v+s; l>v; s=hm, hl, ots | | | | | | | | | | | | | | | |
| | | | | | | 3 | P | P | llc. | | | 0.85 | 0.05 | 0.1 | | | | | | | | | | | | | | | | | 13 | 6 |
| | | | | | | 3a | P or PS | IND | lla. | | | | | | | | | | | | | | | | | | | | | | | |
| | | | 4 | P | P | lc. | | | | 0.45 | 0.55 | | | 11 | 11 | | | | | | | | | | | | | | | | | |
| | | | 6 | P or PS | IND | lla. | | | | 0.5 | 0.25 | 0.25 | | 16 | 16 | | | | | | | | | | | | | | | | | |
| | | | 8 | P | P | llla. | | | | 0.85 | 0.1 | 0.05 | | 6.25 | 18.75 | | | | | | | | | | | | | | | | | |
| | | | 9 | P | P | lb. | | | | 0.75 | 0.25 | | | 34.375 | 34.38 | | | | | | | | | | | | | | | | | |
| | | | 10 | S | S | la. | | | | 0.85 | 0.05 | 0.1 | | | | | | | | | | | | | | | | | | | | |
| | | | 11 | P or PS | IND | llc. | | | | 0.75 | 0.05 | 0.2 | | 18.75 | 18.75 | | | | | | | | | | | | | | | | | |
| | | |  <p>AR-118 - Incl. 1</p>  <p>AR-118 - Incl. 6</p> | AR-118 | A2 | 1 | PS | PS | llc. | | | 0.78 | 0.1 | 0.12 | 12.5 | 6.25 | | | | | | | l+v+s; l>v; s=hl, ots l+v; l>v l+v+s; l>v; s=hl, op l+v+s; l>v; s=hl, hm, ots l+v; v>l l+v+s; l>v; s=hl | | | | | | | | | |
| | | | | | | 2 | PS or S | IND | lb. | | | 0.85 | 0.15 | | | | | | | | | | | | | | | | | | 3.125 | 3.125 |
| 4 | PS or S | IND | | | | llb. | | | | 0.7 | 0.15 | 0.15 | | 6.25 | 3.125 | | | | | | | | | | | | | | | | | |
| 5 | P or PS | IND | | | | llc. | | | | 0.85 | 0.05 | 0.1 | | | | | | | | | | | | | | | | | | | | |
| 6 | P or PS | IND | | | | lc. | | | | 0.65 | 0.45 | | | | | | | | | | | | | | | | | | | | | |
| 7 | PS or S | IND | | | | lla. | | | | 0.7 | 0.15 | 0.15 | | 6.25 | 3.125 | | | | | | | | | | | | | | | | | |
| 8 | PS or S | IND | | | | lla. | | | | 0.85 | 0.05 | 0.1 | | 6.25 | 3.125 | | | | | | | | | | | | | | | | | |

| Sample | Facies | Inclusion | Th _{CO2} | Ts _{syiv} | Ts _{ot1} | Ts _{ot2} | Ts _{hl} | TI-v | Final Th | Final Th by vbd, ld cb, hd, CO2d, d, otd | % NaCl | % KCl | % CaCl ₂ | eq. wt. % NaCl+/- KCl+/-CaCl ₂ | KCl/NaCl | NaCl/CaCl ₂ | comments | | | |
|--------|--------|-----------|-------------------|--------------------|-------------------|-------------------|------------------|-------|----------|---------------------------------------------|--------|-------|---------------------|----------------------------------------------|----------|------------------------|--------------------------------------------|--|-----------------------------------------------------------------------------------------------------------------------------------|---------------------------------------------------------------------------------------------------------------------------------|
| AR-105 | A1 | 6 | | | | | 366 | 400 | 400 | vbd | 43.93 | | | 43.93 | | | Never saw vb disappear. No hh observed. | | | |
| | | 10 | | | | | 402 | 374 | 402 | hd | 47.66 | | | 47.66 | | | | | | |
| | | 11 | | | | | 359 | | | hd | 43.25 | | | 43.25 | | | | | | |
| | | 12 | | | | | 360 | 359.8 | | vbd | 8.38 | | | 8.38 | | | | | | |
| | | 13 | | | | | 413 | 374 | 413 | hd | 48.88 | | | 48.88 | | | | | | |
| | | 14 | | | | | 427 | 308 | 427 | hd | 50.49 | | | 50.49 | | | | | | |
| | | 15 | | | | | 386 | | | cb | | | | | | | | | | |
| | | 16 | | | | | 419 | 419 | | cb | | | | | | | | | | |
| | | 17 | | | | | 443 | 443 | | ld | | | | | | | | | | |
| | | 18 | | | | | 424 | 424 | | cb | | | | | | | | | | |
| | | 19 | | | | | 404 | 334 | 404 | hd | 47.88 | | | 47.88 | | | | | | |
| | | 20 | | | | | 290 | 381 | 381 | vbd | 37.41 | | | 37.41 | | | | | | |
| | | AR-112 | A1 | 1 | | | | | | 213 | 213 | vbd | 0 | | | 0 | | | | vb completed disappeared on freezing, snapped back @ 10c. Decrepitated @ 281 w/ hl almost gone, est. T of Ts hl is 300c. |
| | | | | 2 | | | | | | 109 | 109 | vbd | 13.95 | | | 13.95 | | | | |
| | | | | 3 | | | | | 375 | 189 | 375 | hd | 44.82 | | | 44.82 | | | | |
| | | | | 4 | | | | | 327 | 187 | 327 | hd | 40.35 | | | 40.35 | | | | |
| | | | | 5 | | | | | 383 | 192 | 383 | hd | 45.64 | | | 45.64 | | | | |
| | | | | 6 | | | | | 262 | 262 | | vbd | | | | | | | | |
| | | | | 7 | | | | | 300 | 209 | 300 | hd | 38.16 | | | 38.16 | | | | |
| 9 | | | | | | | 175 | 193 | 193 | vbd | 30.7 | | | 30.7 | | | | | | |
| 11 | | | | | | | 204 | 150 | 204 | hd | 32.08 | | | 32.08 | | | | | | |
| 12 | | | | | | | 214 | 185 | 214 | hd | 32.6 | | | 32.6 | | | | | | |
| 13 | | | | | | | 475 | 475 | | ld | 13.95 | | | 13.95 | | | | | | |
| 15 | | | | | | | 124 | 124 | | vbd | 13.41 | | | 13.41 | | | | | | |
| AR-106 | A2 | | | 1 | | | | 180 | 245 | 218 | 245 | hd | 34.37 | | | 34.37 | | | Decrepitated @ 472c with quite a bit of vb left. Decrepitated @ 419c w/ vb getting smaller. Daughters did not dissolve. | |
| | | | | 3 | | | | | 328 | 135 | 328 | hd | 40.44 | | | 40.44 | | | | |
| | | | | 3a | | | | | 217 | 356 | 356 | vbd | 32.76 | | | 32.76 | | | | |
| | | 4 | | | | | 382 | 382 | | ld | | | | | | | | | | |
| | | 6 | | | | | 315 | 472 | 472 | d | 39.35 | | | 39.35 | | | | | | |
| | | 8 | | | 66 | | 291 | 254 | 291 | hd | 29 | 17 | | 46 | 0.59 | | | | | |
| | | 9 | | | | | 419 | 419 | | d | | | | | | | | | | |
| | | 10 | | | | | 88 | 87.6 | | vbd | | | | | | | | | | |
| | | 11 | | | | | 350 | 231 | 350 | hd | 42.4 | | | 42.4 | | | | | | |
| | | AR-118 | A2 | 1 | | | 295 | | 376 | 278 | 376 | hd | 44.92 | | | 44.92 | | | | Not sure Ts hl is accurate. No vb observed. Estimate of final Th, could not see Tm ice. |
| | | | | 2 | | | | | 245 | 245 | vbd | 5.17 | | | 5.17 | | | | | |
| 4 | | | | | | | 163 | 287 | 287 | vbd | 30.18 | | | 30.18 | | | | | | |
| 5 | | | | | | | 440 | 440 | | hd | 52.04 | | | 52.04 | | | | | | |
| 6 | | | | | | | 465 | 465 | | cb | | | | | | | | | | |
| 7 | | | | | | | 320 | 278 | 320 | hd | 39.76 | | | 39.76 | | | | | | |
| 8 | | | | | | | 272 | 290 | 290 | vbd | 36.12 | | | 36.12 | | | | | | |

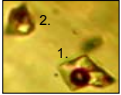


| Sample | Facies | Inclusion | Th _{CO2} | Ts _{sytv} | Ts _{ot1} | Ts _{ot2} | Ts _{hl} | Tl-v | Final Th | Final Th by vbd, ld cb, hd, CO2d, d, otd | % NaCl | % KCl | % CaCl ₂ | eq. wt. % NaCl+/- KCl+/-CaCl ₂ | KCl/NaCl | NaCl/CaCl ₂ | comments | | |
|--------|--------|-----------|-------------------|--------------------|-------------------|-------------------|------------------|------|----------|---------------------------------------------|--------|-------|---------------------|----------------------------------------------|----------|------------------------|----------|--|--|
| AR-118 | A2 | 9 | | | | | | 218 | 218 | vbd | 0 | | | 0 | | | | | |
| | | 10 | | | | | | 173 | 173 | vbd | | | | | | | | | |
| | | 11 | | | | | | 230 | 230 | vbd | 0 | | | 0 | | | | | |
| | | 13 | | | | | | 280 | 280 | vbd | 0 | | | 0 | | | | | |
| | | 14 | | | | | | 219 | 219 | vbd | 0 | | | 0 | | | | | |
| | | 15 | | | | | | 224 | 224 | vbd | 0 | | | 0 | | | | | |
| AR-93 | A3 | 1 | | 74 | | | | 373 | 324 | 373 | hd | 37 | 16 | | 53 | 0.47 | | | |
| | | 2 | | 63 | | | | 359 | 225 | 359 | hd | 36 | 15 | | 51 | 0.39 | | | |
| | | 3 | | | | | | 384 | 384 | vbd | 4.86 | | | 4.86 | | | | | |
| | | 4 | | | | | | | | 537 | d | | | | | | | | |
| | | 5 | | | | | | | 520 | 520 | ld | | | | | | | | |
| | | 6 | | | | | | 357 | 475 | 475 | d | 43.06 | | | 43.06 | | | | |
| | | 7 | | | | | | | 386 | 386 | vbd | | | | | | | | |
| | | 8 | | | | | | | 253 | 253 | vbd | 0.17 | | | 0.17 | | | | |
| | | 9 | | | | | | | 171 | 171 | vbd | 0 | | | 0 | | | | |
| | | 10 | | | | | | | 252 | 252 | vbd | | | | | | | | |
| | | 12 | 30.6 | | | | | | 260 | 260 | d | 0.17 | | | 0.17 | | | | |
| | | 13 | | | | | | | 246 | 475 | 475 | d | 34.43 | | 34.43 | | | | |
| | | 15 | | | | | 370 | 388 | 297 | 388 | hd | 46.16 | | | 46.16 | | | | |
| | | AR-91 | A3 | 1 | | | | | | 420 | 81 | 420 | hd | 49.68 | | | 49.68 | | |
| | | | | 3 | | | | | | 400 | 480 | 480 | vbd | 47.44 | | | 47.44 | | |
| 4 | | | | | | | | | 373 | 373 | vbd | 19.43 | | | 19.43 | | | | |
| 5 | | | | | | | | 200 | 520 | 520 | vbd | 31.87 | | | 31.87 | | | | |
| 6 | | | | | | | | | 252 | 252 | vbd | 4.86 | | | 4.86 | | | | |
| 7 | | | | | | | | | 292 | 292 | vbd | 6.37 | | | 6.37 | | | | |
| 8 | | | | | | | | | 346 | 285 | 346 | d | 42.03 | | | 42.03 | | | |
| 9 | | | | | | 157 | 203 | | 365 | 327 | 365 | d | 43.83 | | | 43.83 | | | |
| 11 | | | | | | 89 | | | 350 | 250 | 350 | hd | 42.4 | | | 42.4 | | | |
| 12 | | | | | | | | | 385 | 385 | vbd | 2.47 | | | 2.47 | | | | |
| 13 | | | | | | | | | 266 | 266 | vbd | 4.86 | | | 4.86 | | | | |
| 14 | | | | | | | | | 448 | 278 | 278 | hd | 53.01 | | | 53.01 | | | |
| 15 | | | | | | | | | 426 | 280 | 426 | hd | 50.37 | | | 50.37 | | | |
| 16 | | | | | | 135 | | | 209 | 479 | 479 | vbd | 32.33 | | | 32.33 | | | |
| 17 | | | | | | | | | 170 | 390 | 390 | vbd | 30.48 | | | 30.48 | | | |
| 18 | | | | | | | | | 232 | 232 | vbd | 5.17 | | | 5.17 | | | | |
| AR-13 | B | | | 1 | | | | | | 308 | 308 | vbd | 7.82 | | | 7.82 | | | |
| | | | | 2 | | | | | | 389 | 389 | cb | 7.11 | | | 7.11 | | | |
| | | 3 | | | | | | 429 | 429 | cb | 21.66 | | | 21.66 | | | | | |
| | | 4 | | | | | | 351 | 351 | vbd | 6 | | 19 | 25 | | 0.41 | | | |
| | | 6 | | | | | | 530 | 260 | 530 | hd | 63.9 | | | 63.9 | | | | |

| Sample Comments and Photographs | Sample | Facies | Inclusion | Paragenesis | Assigned Paragenesis | Type | %L CO ₂ | %V CO ₂ | %L | %V | %S | Length in um | Width in um | Phase | Tm _{CO2} | Te | Tm _{hh} | Tm _{ice} | Tm _{clath} | | |
|------------------------------------------------------------------------------------------------------------------------------------------------------------------------------------------------------------------------|--------|--------|-----------|-------------|----------------------|-------|--------------------|--------------------|------|-------|--------|-----------------------|-------------------------------------------------------|-------------------------------------------------------|------------------------------------|----------------------------|------------------|-------------------|---------------------|-------|--|
|  AR-13 - Incl. 12 | AR-13 | B | 7 | P or PS | IND | Ia. | | | 0.1 | 0.9 | <0.01 | 6.25 | 3.125 | I+v+s; l>v; s=op | | | | -12 | | | |
| | | | 8 | PS or S | IND | Ia. | | | 0.94 | 0.05 | 0.01 | | 9.375 | 6.25 | I+v+s; l>v; s=op | | | | -17.6 | | |
| | | | 9 | PS or S | IND | Ib. | | | | 0.55 | 0.45 | | | 6.25 | 3.125 | I+v; l>v | | | | -1.1 | |
| | | | 10 | P or PS | IND | Iic. | | | | 0.75 | 0.1 | 0.15 | | 6.25 | 6.25 | I+v+s; l>v; s=hm, hl, ot | | | | | |
| | | | 12 | P or PS | IND | IIIa. | | | | 0.75 | 0.05 | 0.2 | | 6.25 | 6.25 | I+v+s; l>v; s=hl, sylv, op | | | | | |
| Evidence of boiling; No pictures available. | AR-169 | B | 1 | PS | PS | Ib. | | | 0.8 | 0.2 | | 7.8125 | 6.25 | I+v; l>v | | | | -18.5 | | | |
| | | | 1a | PS | PS | Ib. | | | 0.8 | 0.2 | | | 12.5 | 6.25 | I+v; l>v | | | | -19 | | |
| | | | 2 | PS | PS | IIb. | | | 0.77 | 0.1 | 0.13 | | 6.25 | 4.688 | I+v+s; l>v; s=hl, mo or bt | | | | | | |
| | | | 3 | S | S | Ib. | | | 0.9 | 0.1 | | | 12.5 | 6.25 | I+v; l>v | | | | -1.3 | | |
| | | | 4 | PS | PS | IIb. | | | 0.73 | 0.12 | 0.15 | | 12.5 | 12.5 | I+v+s; s=hl, hm | | | | | | |
| | | | 5 | PS or S | IND | Ib. | | | 0.55 | 0.45 | | | 9.375 | 9.375 | I+v; l>v | | | | -15 | | |
| | | | 6 | PS or S | IND | Ib. | | | 0.7 | 0.15 | 0.15 | | 6.25 | 3.125 | I+v; l>v | | | | -1.5 | | |
| | | | 7 | PS | PS | IIb. | | | 0.75 | 0.12 | 0.13 | | 6.25 | 3.125 | I+v+s; l>v; s=hl, hm | | | | | | |
| | | | 8 | S | S | Ib. | | | 0.9 | 0.1 | | | 6.25 | 3.125 | I+v; l>v | | | | -2.5 | | |
| | | | 9 | P or PS | IND | IIIa. | | | 0.75 | 0.1 | 0.15 | | 18.75 | 12.5 | I+v+s; l>v; s=hl, sylv, ot, op, hm | | | | | | |
| | | | 10 | PS | PS | Iic. | | | 0.76 | 0.12 | 0.12 | | 9.375 | 9.375 | I+v+s; l>v; s=hl, ot, hm | | | | | | |
| 11 | S | S | IV. | | | 0.075 | 0.025 | 0.9 | | | 7.8125 | 12.5 | ICO ₂ +vCO ₂ +IH ₂ O | unk | | | -2.5 | 6.5 | | | |
| Solid inclusions of hl present; evidence of boiling. | AR-8 | C | 1 | P | P | IIb. | | | | | | 9.375 | 9.375 | I+v+s; l>v; s=hl, op | | | | | | | |
| | | | 2 | P | P | Iic. | | | 0.6 | | | | 6.25 | 6.25 | I+v+s; l>v; s=hl, hm, ot, op | | | | | | |
| | | | 3 | PS or S | IND | Ia. | | | 0.8 | 0.15 | 0.05 | | | | | I+v+s; l>v; s=ot | | | | -0.1 | |
| | | | 4 | PS or S | IND | Ib. | | | 0.9 | 0.1 | | | 6.25 | 6.25 | I+v+s; l>v | | | -24 | | -12.1 | |
| | | | 5 | PS | PS | IIb. | | | 0.55 | 0.2 | 0.25 | | 9.375 | 3.125 | I+v+s; l>v; s=hl, op | | | | | | |
| | | | 6 | P or PS | IND | Ib. | | | 0.87 | | | | 18.75 | 18.75 | I+v; l>v | | | -11 | | -1.3 | |
| | | | 7 | P | P | IIa. | | | | | | | | 12.5 | | I+v+s; l>v; s=hl | | | | | |
| | | | 8 | P | P | Iic. | | | 0.85 | 0.05 | 0.1 | | 15.625 | 15.63 | I+v+s; l>v; s=hl, ots, op | | | | | | |
| | | | 9 | P | P | Iic. | | | 0.78 | 0.12 | 0.1 | | 9.375 | 9.375 | I+v+s; v>l; s=hl, ot | | | | | | |
| | | | 11 | P | P | IIIa. | | | 0.5 | 0.1 | 0.4 | | 15.625 | 15.63 | I+v+s; l>v; s=hl, ops, sylv | | | | | | |
| | | | 12 | P | P | IIIa. | | | 0.8 | 0.15 | 0.05 | | 6.25 | 6.25 | I+v+s; l>v; s=hl, sylv, hm | | | | | | |
| | | | 13 | P | P | Iic. | | | 0.2 | 0.3 | 0.5 | | 12.5 | 12.5 | I+v+s; v>l; s=hl, op, ot | | | | | | |
| | | | 15 | P | P | IIIa. | | | | | | | 15.625 | 15.63 | I+v+s; l>v; s=hl, sylv | | | | | | |
| | | | 16 | P | P | Ic. | | | | | | | 6.25 | 6.25 | I+v; v>l | | | | | | |
| | | | 17 | S | S | Ib. | | | 0.9 | 0.1 | | | 6.25 | 6.25 | I+v; l>v | | | | | -0.5 | |
| | | | 18 | S | S | Ib. | | | 0.95 | 0.05 | | | | | | I+v; l>v | | | | -0.5 | |
| | | | 19 | S | S | Ib. | | | 0.95 | 0.05 | | | | | | I+v; l>v | | | | -0.7 | |
| 21 | P | P | IIb. | | | 0.5 | 0.25 | 0.25 | | 6.25 | 6.25 | I+v+s; l>v; s=hl, ops | | | | | | | | | |
|  AR-131 - Incl. 1  AR-131 - Incl. 3 | AR-131 | C | 1 | S | S | IV. | 0.15 | 0.1 | 0.75 | | | 9.375 | 6.25 | ICO ₂ +vCO ₂ +IH ₂ O | -55.9 | | | -5.5 | 8.5 | | |
| | | | 2 | S | S | Ib. | | | 0.9 | 0.1 | | | 2.0833 | 3.125 | I+v; l>v | | | -24 | | -2.2 | |
| | | | 3 | P or PS | IND | IIIa. | | | 0.6 | 0.07 | 0.33 | | | | | I+v+s; s=hl, sylv, op, hm | | | | | |
| | | | 4 | PS or S | IND | Iic. | | | 0.78 | 0.05 | 0.07 | | 12.5 | 12.5 | I+v+s; l>v; s=hl, ots | | | | | | |
| | | | 5 | S or PS | IND | Iic. | | | 0.85 | 0.075 | 0.08 | | 6.25 | 6.25 | I+v+s; l>v; s=hl, ot | | | | | | |
| | | | 6 | S or PS | IND | Iic. | | | 0.77 | 0.1 | 0.13 | | 12.5 | 3.125 | I+v+s; l>v; s=hl, ot | | | | | | |

| Sample | Facies | Inclusion | Th _{CO2} | Ts _{sytv} | Ts _{ot1} | Ts _{ot2} | Ts _{hi} | Tl-v | Final Th | Final Th by vbd, ld cb, hd, CO2d, d, otd | % NaCl | % KCl | % CaCl ₂ | eq. wt. % NaCl+/- KCl+/-CaCl ₂ | KCl/NaCl | NaCl/CaCl ₂ | comments | |
|--------|--------|-----------|-------------------|--------------------|-------------------|-------------------|------------------|------|----------|---------------------------------------------|--------|-------|---------------------|----------------------------------------------|----------|------------------------|-------------------------------------------------------------------------|--|
| AR-13 | B | 7 | | | | | | 377 | 377 | cb | 15.96 | | | 15.96 | | | ot is most likely nahcolite (NaHCO ₃). no Ts for sylvite | |
| | | 8 | | | | | | 195 | 195 | vbd | 20.65 | | | 20.65 | | | | |
| | | 9 | | | | | | 371 | 371 | vbd | 2 | | | 2 | | | | |
| | | 12 | | | 434 | | | 532 | 532 | hd | 64.18 | | | 64.18 | | | | |
| | | | | | | | 408 | 280 | hd | 48.32 | | | 48.32 | | | | | |
| AR-169 | B | 1 | | | | | | 301 | 301 | vbd | 21.31 | | | 21.31 | | | | |
| | | 1a | | | | | | 322 | 322 | vbd | 21.66 | | | 21.66 | | | | |
| | | 2 | | | | | 430 | 286 | 430 | hd | 50.84 | | | 50.84 | | | | |
| | | 3 | | | | | | 190 | 190 | vbd | 2.14 | | | 2.14 | | | | |
| | | 4 | | | | | 356 | 352 | 356 | hd | 42.96 | | | 42.96 | | | | |
| | | 5 | | | | | | 382 | 382 | cb | 18.62 | | | 18.62 | | | | |
| | | 6 | | | | | | 388 | 388 | vbd | 2.47 | | | 2.47 | | | | |
| | | 7 | | | | | 335 | 349 | 356 | vbd | 41.05 | | | 41.05 | | | | |
| | | 8 | | | | | | 190 | 190 | vbd | 4.07 | | | 4.07 | | | | |
| | | 9 | | | | 310 | | 376 | 356 | 376 | hd | 44.92 | | | 44.92 | | | |
| | | 10 | | | | | | 260 | 415 | 415 | vbd | 35.32 | | | 35.32 | | | |
| 11 | | 31 | | | | 188 | 188 | CO2d | 4.07 | | | 4.07 | | | | | | |
| AR-8 | C | 1 | | | | | 393 | 214 | 393 | hd | | | | | | | | |
| | | 2 | | | | | 378 | 180 | 378 | hd | 45.13 | | | 45.13 | | | | |
| | | 3 | | | | | | 372 | 372 | vbd | 0.17 | | | 0.17 | | | | |
| | | 4 | | | | | | 184 | 184 | vbd | 16.05 | | | 16.05 | | | | |
| | | 5 | | | | | 356 | 313 | 356 | hd | 42.96 | | | 42.96 | | | | |
| | | 6 | | | | | | 358 | 358 | vbd | 2.14 | | | 2.14 | | | | |
| | | 7 | | | | | 247 | 302 | 302 | vbd | 34.49 | | | 34.49 | | | | |
| | | 8 | | | | | 357 | 168 | 357 | hd | 43.06 | | | 43.06 | | | | |
| | | 9 | | | | | 285 | 208 | 284.5 | hd | 37.01 | | | 37.01 | | | | |
| | | 11 | | | 92 | | | 470 | 305 | 470 | hd | 47 | 16 | | 63 | 0.35 | | |
| | | 12 | | | 60 | | | 298 | 180 | 298 | hd | 31 | 14 | | 45 | 0.49 | | |
| | | 13 | | | | | | 387 | 345 | 386.5 | hd | 46.05 | | | 46.05 | | | |
| | | 15 | | | 74 | | | 417 | 324 | 417 | hd | 40 | 14 | | 54 | 0.37 | | |
| | | 16 | | | | | | | 360 | 360 | ld | | | | | | | |
| | | 17 | | | | | | 198 | 198.2 | | vbd | 0.83 | | | 0.83 | | | |
| | | 18 | | | | | | 206 | 205.6 | | vbd | 0.83 | | | 0.83 | | | |
| | | 19 | | | | | | 192 | 192 | | vbd | 1.16 | | | 1.16 | | | |
| 21 | | | | | | 473 | 260 | 473 | hd | 56.17 | | | 56.17 | | | | | |
| AR-131 | C | 1 | 22.9 | | | | | 130 | 130 | d | 8.51 | | | 8.51 | | | Decrepitated @ <130c. | |
| | | 2 | | | | | | 241 | 241 | vbd | 3.6 | | | 3.6 | | | | |
| | | 3 | | | 94 | | | 457 | 218 | 457 | hd | 47 | 16 | | 63 | 0.37 | | |
| | | 4 | | | | 175 | | 238 | 163 | 238 | hd | 33.95 | | | 33.95 | | | |
| | | 5 | | | | 105 | | 270 | 206 | 270 | hd | 35.99 | | | 35.99 | | | |
| | | 6 | | | | | | 275 | 206 | 275 | hd | 36.33 | | | 36.33 | | | |

| Sample Comments and Photographs | Sample | Facies | Inclusion | Paragenesis | Assigned Paragenesis | Type | %L CO ₂ | %V CO ₂ | %L | %V | %S | Length in um | Width in um | Phase | Tm _{CO2} | Te | Tm _{hh} | Tm _{ice} | Tm _{clath} | | | | | | | | | | |
|-------------------------------------------------------------------------------------------------------------------------------------------------------------------------------------------------------------------------------------------------------------------|---------|--------|-----------------------------------------------------------------------------------------------------------------------------------------------------------------------------------------------------------------------------------------------|-------------|----------------------|-------|--------------------|--------------------|---------|-------|-------|-------------------------------|-------------|-------------------------------------|--------------------------|------|--------------------------|-------------------|---------------------|--------|-------|-----------------------------------|-------|----------------------|--|------|--|--|--|
|  AR-131 - Incl. 7  AR-131 - Incl. 12 Solid inclusions of hl present; evidence of boiling. | AR-131 | C | 7 | S or PS | IND | lb. | 0.07 | 0.03 | 0.85 | 0.15 | | 9.375 | 3.125 | l+v; l>v | -55.5 | -21 | | -13.4 | 9 | | | | | | | | | | |
| | | | 8 | P or PS | IND | llb. | | | 0.7 | 0.05 | 0.25 | 6.25 | 3.125 | l+v+s; l>v; s=hl, hm | | | | | | | | | | | | | | | |
| | | | 9 | PS | PS | llb. | | | 0.68 | 0.1 | 0.22 | 12.5 | 6.25 | l+v+s; l>v; s=hl, hm, op | | | | | | | | | | | | | | | |
| | | | 10 | PS or S | IND | llb. | | | 0.85 | 0.05 | 0.1 | 6.25 | 6.25 | l+v+s; l>v; s=hl, op | | | | | | | | | | | | | | | |
| | | | 11 | S | S | IV. | | | 0.9 | | | 12.5 | 9.375 | ICO2+vCO2+lH2O | | | | | | | | | | | | | | | |
| | | | 12 | P or PS | IND | llla. | | | 0.7 | 0.1 | 0.2 | 10.8 | 15.63 | l+v+s; l>v; s=hl, sylv, ot | | | | | | | | | | | | | | | |
| | | | 14 | P | P | llla. | | | 0.83 | 0.05 | 0.12 | 25 | 18.75 | l+v+s; l>v; s=hl, ot, sylv | | | | | | | | | | | | | | | |
| | | | 15 | P or PS | IND | llla. | | | 0.83 | 0.05 | 0.12 | | | l+v+s; l>v; s=hl, sylv, ot, op (mo) | | | | | | | | | | | | | | | |
| | | |  AR-6A - Inclusion 3  AR-6A - Inclusions 6 and 7 Evidence of boiling. | AR-6A | D | 1 | | | P | P | llc. | | | 0.55 | | | | | | 0.2 | 0.25 | 18.75 | 9.375 | l+v+s; l>v; s=hl, ot | | | | | |
| | | | | | | 3 | | | PS or S | IND | llc. | 0.82 | 0.03 | 0.15 | | | | | | 15.625 | 6.25 | l+v+s; l>v; s=hl, ot | | | | | | | |
| | | | | | | 6 | | | PS or S | IND | llc. | 0.7 | 0.15 | 0.15 | | | | | | | | l+v+s; l>v; s=hl, anhy? | | | | | | | |
| | | | | | | 7 | | | S | S | lb. | 0.95 | 0.05 | | | | | | | | | l+v; l>v | | | | | | | |
| | | | | | | 8 | | | P or PS | IND | lla. | 0.85 | 0.1 | 0.05 | | | | | | 6.25 | 6.25 | l+v+s; l>v; s=hl | | | | | | | |
| | | | | | | 9 | | | PS or S | IND | llb. | 0.7 | 0.1 | 0.2 | | | | | | 6.25 | 6.25 | l+v+s; l>v; s=hl, rtl, mo?, anhy? | | | | | | | |
| | | | | | | 11 | | | P or PS | IND | lb. | 0.75 | 0.25 | | | | | | | 6.25 | 6.25 | l+v; l>v | | | | | | | |
| 13 | P or PS | IND | | | | la. | 0.65 | 0.3 | 0.05 | 6.25 | 6.25 | l+v+s; l>v; s=op | | | | | | | | | | | | | | | | | |
| 14 | P or PS | IND | | | | lb. | 0.5 | 0.5 | | 9.375 | 3.125 | l+v; l=v | | | | | | | | | | | | | | | | | |
| 15 | PS or S | IND | | | | llb. | 0.85 | 0.05 | 0.1 | 12.5 | 12.5 | l+v+s; l>v; s=hl, op | | | | | | | | | | | | | | | | | |
| 16 | PS or S | IND | | | | llc. | 0.8 | 0.12 | 0.08 | 12.5 | 12.5 | l+v+s; l>v; s=hl, ot, op | | | | | | | | | | | | | | | | | |
| 17 | PS or S | IND | | | | lb. | 0.6 | 0.4 | | | | | | | | | | | | | | | | | | | | | |
|  AR-78 - Inclusions 1, 2, 3, and 8 Possible solid inclusions of hl. | AR-78 | D | | | | 1 | P or PS | IND | lla. | | | 0.65 | 0.25 | 0.1 | 12.5 | 12.5 | l+v+s; l>v; s=hl | 37 | -24.5 | -23.7 | -23.7 | -5.1 | | | | | | | |
| | | | 2 | P or PS | IND | la. | 0.85 | 0.13 | 0.02 | 12.5 | 6.25 | l+v+s; l>v; s=bt, mo, or rtl | | | | | | | | | | | | | | | | | |
| | | | 3 | P | P | lb. | 0.85 | 0.15 | | 18.75 | 15.63 | l+v; l>v | | | | | | | | | | | | | | | | | |
| | | | 4 | P | P | llc. | 0.7 | 0.1 | 0.2 | 18.75 | 9.375 | l+v+s; l>v; s=hl, hm, ops, ot | | | | | | | | | | | | | | | | | |
| | | | 5 | P or PS | IND | lb. | 0.8 | 0.2 | | 18.75 | 15.63 | l+v; l>v | | | | | | | | | | | | | | | | | |
| | | | 6 | P | P | llb. | 0.77 | 0.1 | 0.13 | 12.5 | 6.25 | l+v+s; l>v; s=hl, op | | | | | | | | | | | | | | | | | |
| | | | 7 | P or PS | IND | llb. | | | | 6.25 | 6.25 | l+v+s; l>v; s=hl, op | | | | | | | | | | | | | | | | | |
| | | | 8 | PS or S | IND | la. | 0.7 | 0.3 | | | | l+v+s; l>v; s=ot | | | | | | | | | | | | | | | | | |
| | | | 11 | PS | PS | llb. | 0.8 | 0.1 | 0.1 | 6.25 | 3.125 | l+v+s; l>v; s=hl, op | | | | | | | | | | | | | | | | | |
| | | | 13 | S or PS | IND | lla. | 0.9 | 0.05 | 0.05 | 6.25 | 6.25 | l+v+s; l>v; s=hl | | | | | | | | | | | | | | | | | |
| | | |  AR-5 - Inclusion 1 (not used in study) Evidence of boiling. | AR-5 | E | 2 | P | P | llc. | | | 0.8 | 0.05 | 0.15 | 12.5 | 12.5 | l+v+s; l>v; s=hl, op, ot | | | | | | -31 | | | -7.5 | | | |
| | | | | | | 3 | PS or S | IND | la. | 0.9 | 0.07 | 0.03 | 6.25 | 6.25 | l+v+s; l>v; s=op | | | | | | | | | | | | | | |
| | | | | | | 4 | P | P | llc. | 0.8 | 0.05 | 0.15 | 15.625 | 15.63 | l+v+s; l>v; s=hl, op, ot | | | | | | | | | | | | | | |
| 5 | PS or S | IND | | | | llb. | 0.85 | 0.05 | 0.1 | 18.75 | 18.75 | l+v+s; l>v; s=hl, op | | | | | | | | | | | | | | | | | |
| 6 | P or PS | IND | | | | lla. | 0.85 | 0.09 | 0.06 | 6.25 | 6.25 | l+v+s; l>v; s=hl | | | | | | | | | | | | | | | | | |
| 6a | P or PS | IND | | | | lc. | 0.5 | 0.5 | | 6.25 | 6.25 | l+v; l=v | | | | | | | | | | | | | | | | | |
| 8 | P or PS | IND | | | | llb. | 0.5 | 0.23 | 0.27 | | | l+v+s; l>v; s=hl, op | | | | | | | | | | | | | | | | | |
| 9 | P or PS | IND | | | | la. | 0.8 | 0.18 | 0.02 | 6.25 | 6.25 | l+v+s; l>v; s=ot | | | | | | | | | | | | | | | | | |
| 10 | S or PS | IND | | | | lb. | 0.85 | 0.15 | | | | l+v; l>v | | | | | | | | | | | | | | | | | |
| 11 | PS or S | IND | | | | lb. | 0.95 | 0.05 | | | | l+v; l>v | | | | | | | | | | | | | | | | | |

| Sample | Facies | Inclusion | Th _{CO2} | Ts _{sytv} | Ts _{ot1} | Ts _{ot2} | Ts _{hi} | Tl-v | Final Th | Final Th by vbd, Id cb, hd, CO2d, d, otd | % NaCl | % KCl | % CaCl ₂ | eq. wt. % NaCl+/- KCl+/-CaCl ₂ | KCl/NaCl | NaCl/CaCl ₂ | comments | | | | | | | |
|--------|--------|-----------|-------------------|--------------------|-------------------|-------------------|------------------|-------|----------|---------------------------------------------|--------|-------|---------------------|----------------------------------------------|----------|------------------------|----------------------------------------------------|-------|--|-------|-------|--|--------------------------------------------|----------------------------------------------------|
| AR-131 | C | 7 | 29.2 | 75 | 108 | 432 | 288 | 288 | 288 | vbd | 17.25 | | | 17.25 | | | ot is most likely nahcolite (NaHCO ₃). | | | | | | | |
| | | 8 | | | | | 470 | 218 | 470 | hd | 55.79 | | | 55.79 | | | | | | | | | | |
| | | 9 | | | | | 390 | 288 | 390 | hd | 46.37 | | | 46.37 | | | | | | | | | | |
| | | 10 | | | | | 280 | 189 | 280 | hd | 36.68 | | | 36.68 | | | | | | | | | | |
| | | 11 | | | | | 201 | 201 | 201 | CO2d | 6.37 | | | 6.37 | | | | | | | | | | |
| | | 12 | | | | | 258 | 226 | 258 | hd | 26 | 19 | | 45 | 0.72 | | | | | | | | | |
| | | 14 | | | | | 380 | 162 | 380 | hd | 45.33 | | | 45.33 | | | | | | | | | | |
| | | 15 | | | | | 286 | 180 | 432 | otd | 27 | 21 | | 48 | 0.75 | | | | | | | | | |
| | | AR-6A | | | | | D | 1 | | | 414 | | 390 | 331 | 414 | otd | | 46.37 | | | 46.37 | | | ot is most likely nahcolite (NaHCO ₃). |
| | | | | | | | | 3 | | | | | 229 | 68 | 229 | hd | | 33.42 | | | 33.42 | | | |
| | | | | | | | | 6 | | | | | 250 | 280 | 280 | vbd | | 34.68 | | | 34.68 | | | |
| | | | | | | | | 7 | | | | | 186 | 186 | 186 | vbd | | 0.66 | | | 0.66 | | | |
| | | | | | | | | 8 | | | | | 224 | 386 | 386 | vbd | | 33.14 | | | 33.14 | | | |
| | | | | | | | | 9 | | | | | 300 | 365 | 364.5 | vbd | | | | | | | | |
| | | | | | | | | | | | | | | | | | | 38.16 | | | 38.16 | | | |
| 11 | 388 | | 388 | 388 | vbd | 8.65 | | | | | | | | 8.65 | | | | | | | | | | |
| 13 | 410 | | 410 | 410 | vbd | 9.19 | | | | | | | | 9.19 | | | | | | | | | | |
| 14 | 390 | | 390 | 390 | cb | 10.48 | | | | | | | | 10.48 | | | | | | | | | | |
| 15 | 299 | | 204 | 299 | hd | 38.09 | | | | | | | | 38.09 | | | | | | | | | | |
| 16 | 400 | | 201 | 298 | 400 | otd | | 31.92 | | | | | | | 31.92 | | | | | | | | | |
| 17 | 376 | | 376 | 376 | vbd | 8.38 | | | | | | | | 8.38 | | | | | | | | | | |
| AR-78 | D | | 1 | | | 290 | | | | | | | 385 | 371 | 385 | hd | 45.85 | | | 45.85 | | | No change when frozen, did not see Tm ice. | |
| | | | 2 | | | | | | | | | | 383 | 383 | 383 | vbd | | | | | | | | |
| | | | 3 | | | | | | | | | | 467 | 466.5 | 466.5 | vbd | 7.96 | | | 7.96 | | | | |
| | | | 4 | | | | | | | | | | 370 | 220 | 370 | hd | 44.32 | | | 44.32 | | | | |
| | | 5 | 373 | | | | 372.5 | | 372.5 | vbd | | | | | | | | | | | | | | |
| | | 6 | 342 | | | | 183 | | 342 | hd | 41.67 | | | 41.67 | | | | | | | | | | |
| | | 7 | 407 | | | | 183 | | 407 | hd | 48.21 | | | 48.21 | | | | | | | | | | |
| | | 8 | 384 | | | | 384 | | 384 | vbd | 0.5 | | | 0.5 | | | | | | | | | | |
| | | 11 | 338 | | | | 212 | | 338 | hd | 41.31 | | | 41.31 | | | | | | | | | | |
| | | 13 | 190 | | | | 300 | | 300 | vbd | 31.39 | | | 31.39 | | | | | | | | | | |
| | | AR-5 | E | | | | 2 | | | | | | 403 | 120 | 403 | hd | 47.77 | | | 47.77 | | | | |
| | | | | | | | 3 | | | | | | 176 | 176 | 176 | vbd | 11.1 | | | 11.1 | | | | |
| | | | | | | | 4 | | | | | | 415 | 157 | 415 | hd | 49.11 | | | 49.11 | | | | |
| 5 | 286 | | | 117 | 286 | hd | 37.11 | | | | | | | 37.11 | | | | | | | | | | |
| 6 | 259 | | | 320 | 320 | vbd | 35.25 | | | | | | | 35.25 | | | | | | | | | | |
| 6a | 485 | | | 485 | 485 | ld | | | | | | | | | | | | | | | | | | |
| 8 | 424 | | | 317 | 424 | hd | 50.14 | | | | | | | 50.14 | | | | | | | | | | |
| 9 | 488 | | | 488 | 488 | vbd | | | | | | | | | | | | | | | | | | |
| 10 | 290 | | | 290 | 290 | vbd | 0.83 | | | | | | | 0.83 | | | | | | | | | | |
| 11 | 220 | | | 220 | 220 | vbd | 12 | | | | | | 13 | 25 | 0.79 | | | | | | | | | |

| Sample Comments and Photographs | Sample | Facies | Inclusion | Paragenesis | Assigned Paragenesis | Type | %L CO ₂ | %V CO ₂ | %L | %V | %S | Length in um | Width in um | Phase | Tm _{CO2} | Te | Tm _{hh} | Tm _{ice} | Tm _{clath} |
|-------------------------------------------------------------------------------------------------------|--------|--------|-----------|-------------|----------------------|------|--------------------|--------------------|------|------|------|--------------|-------------|-------------------------------|-------------------|-----|------------------|-------------------|---------------------|
| | AR-5 | E | 12 | P or PS | IND | lb. | | | 0.6 | 0.4 | | 12.5 | 12.5 | l+v; l>v | | | | | |
| | | | 13 | P or PS | IND | llb. | | | 0.65 | 0.15 | 0.2 | 6.25 | 6.25 | l+v+s; l>v; s=hl, ops | | | | | -8 |
| | | | 14 | P | P | llc. | | | 0.75 | 0.15 | 0.1 | 9.375 | 6.25 | l+v+s; l>v; s=hl, rtl, hm, ot | | | | | |
| | | | 15 | P | P | llc. | | | 0.85 | 0.05 | 0.1 | | | l+v+s; l>v; s=hm, hl, op | | | | | |
| | | | 17 | S or PS | IND | lb. | | | 0.9 | 0.1 | | 6.25 | 6.25 | l+v; l>v | | | | | -0.5 |
|  AR-64 - Incl. 1 & 2 | AR-64 | E | 1 | P or PS | IND | llc. | | | 0.75 | 0.1 | 0.15 | 12.5 | 12.5 | l+v+s; l>v; s=hl, ot | | | | | |
|  AR-64 - Incl. 3 | | | 2 | P or PS | IND | lla. | | | 0.78 | 0.1 | 0.12 | 6.25 | 6.25 | l+v+s; l>v; s=hl | | | | | |
| | | | 3 | S or PS | IND | lb. | | | 0.85 | 0.15 | | 12.5 | 6.25 | l+v; l>v | | | | | 0 |
| | | | 5 | P or PS | IND | llc. | | | 0.5 | 0.15 | 0.35 | 6.25 | 4.688 | l+v+s; l>v; s=hl, op, ot | | | | | |
| | | | 6 | P or PS | IND | llc. | | | 0.7 | 0.1 | 0.2 | 12.5 | 12.5 | l+v+s; l>v; s=hm, hl, ots | | | | | |
| | | | 7 | PS or S | IND | lb. | | | 0.85 | 0.15 | | 12.5 | 4.688 | l+v; l>v | | -36 | | | 0 |
| | | | 8 | P or PS | IND | lb. | | | 0.7 | 0.3 | | 18.75 | 4.688 | l+v; l>v | | -23 | -22.9 | | -13 |
|  AR-64 - Incl. 10 | | | 9 | PS or S | IND | llc. | | | 0.73 | 0.15 | 0.12 | 12.5 | 12.5 | l+v+s; l>v; s=hl, op, ot | | | | | |
| | | | 10 | PS or P | IND | llc. | | | 0.78 | 0.1 | 0.12 | 12.5 | 12.5 | l+v+s; l>v; s=hm, hl, ot, op | | | | | |
| | | | 12 | P or PS | IND | llc. | | | 0.75 | 0.1 | 0.15 | 9.375 | 9.375 | l+v+s; l>v; s=hl, ots | | | | | |

| Sample | Facies | Inclusion | Th _{CO2} | Ts _{sytv} | Ts _{ot1} | Ts _{ot2} | Ts _{hl} | Tl-v | Final Th | Final Th by vbd, ld cb, hd, CO2d, d, otd | % NaCl | % KCl | % CaCl ₂ | eq. wt. % NaCl+/- KCl+/-CaCl ₂ | KCl/NaCl | NaCl/CaCl ₂ | comments | | |
|--------|--------|-----------|-------------------|--------------------|-------------------|-------------------|------------------|------|----------|---------------------------------------------|--------|-------|---------------------|----------------------------------------------|----------|------------------------|----------|--|--|
| AR-5 | E | 12 | | | | | 408 | 408 | 408 | cb | 11.7 | | | 11.7 | | | | | |
| | | 13 | | | | | 357 | 283 | 357 | hd | 43.06 | | | 43.06 | | | | | |
| | | 14 | | | | | 403 | 297 | 402.5 | hd | 47.77 | | | 47.77 | | | | | |
| | | 15 | | | | | 510 | 179 | 510 | hd | 61.12 | | | 61.12 | | | | | |
| | | 17 | | | | | | 252 | 252 | vbd | 0.83 | | | 0.83 | | | | | |
| AR-64 | E | 1 | | | | | 346 | 343 | 346 | hd | 42.03 | | | 42.03 | | | | | |
| | | 2 | | | | | 350 | 293 | 350 | hd | 42.4 | | | 42.4 | | | | | |
| | | 3 | | | | | | 240 | 240 | vbd | 0 | | | 0 | | | | | |
| | | 5 | | | | | 370 | 310 | 370 | hd | 44.32 | | | 44.32 | | | | | |
| | | 6 | | | | | 356 | 347 | 356 | hd | 42.96 | | | 42.96 | | | | | |
| | | 7 | | | | | | 239 | 239 | vbd | 0 | | | 0 | | | | | |
| | | 8 | | | | | | 490 | 490 | vbd | 16.89 | | | 16.89 | | | | | |
| | | 9 | | | 186 | | | 220 | 348 | 348 | vbd | 32.92 | | | 32.92 | | | | |
| | | 10 | | | | | | 365 | 340 | 365 | hd | 43.83 | | | 43.83 | | | | |
| | | 12 | | | | | | 360 | 330 | 360 | hd | 43.35 | | | 43.35 | | | | |

APPENDIX B – PETROGRAPHIC ANALYSIS

Legend for Petrographic Analyses

assoc – association
crs - coarse
d.z. – digital zoom
defm'n – deformation
dissem – disseminated
f.g. – fine grained
grn(ed) – grain(ed)
lg – large
med - medium
MHBX – magmatic-hydrothermal breccia
pln – plane light
reflect – reflected light
sm – small
trans – transmitted light
vnlt – veinlet
xcuts – cross-cuts
xpol – cross polars
+ occurring after bt, kspar, QSP, etc. – addition of these minerals in alteration
> - greater than

Rocks and Minerals

alt – alteration
anhy – anhydrite
ap - apatite
blch - bleached
bt – biotite (aka fluorophlogopite)
ca – calcite
chlor - chlorite
cp – chalcopyrite

fl – fluorite
grn – green
gyp - gypsum
kaol – kaolinite
kspar – potassium feldspar
mo – molybdenite
mt - magnetite
par – paragonite (green mica)
pheno(s) – phenocryst(s)
plag – plagioclase feldspar
py – pyrite
QSP – qtz-ser-py alteration
qtz – quartz
rtl – rutile
SABQ – source aplite barren quartz
ser – sericite
Tan – Tertiary andesite
Tlgp – Tertiary late granite porphyry
tpz – topaz
tr – trace
uTan – unbrecciated Tertiary andesite
uTana – unbrecciated Tertiary andesite above the breccia body
uTanb – unbrecciated Tertiary andesite below the breccia body

Paragenesis

+ included in time assemblage
+/- may or may not be included in time assemblage
→later assemblage

Sample: AR-105
Facies: A1
Phase: Matrix
Borehole: 23.4-11.8G
Elevation: 7343'

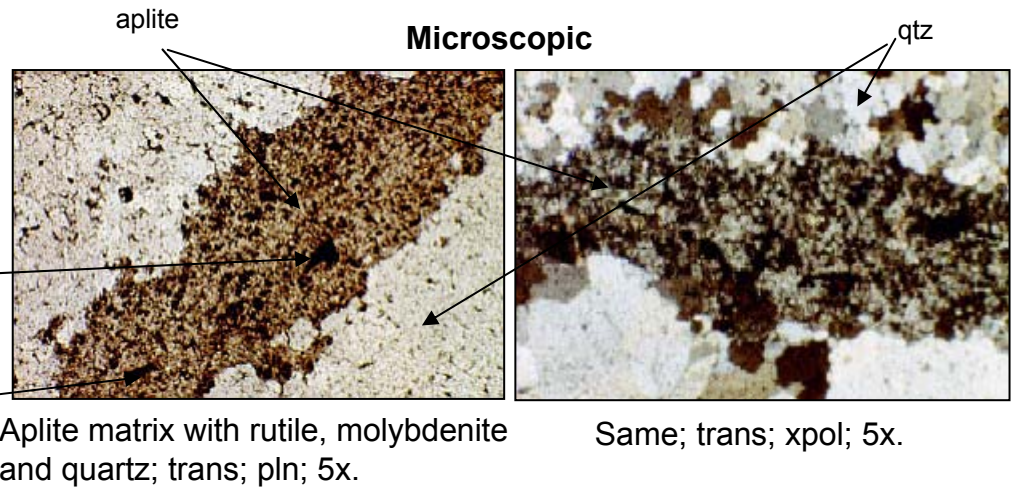
Macroscopic

Biotite altered Tan clasts with aplite-qtz-tr mo matrix.

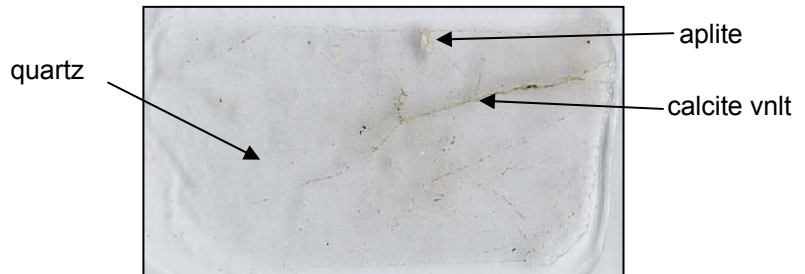


Microscopic

- **Matrix:**
 - mostly quartz; subhedral to anhedral, with few euhedral grains; 100-1750 microns; stress features
 - minor aplite; consists of qtz and kspar altering to ser and tr kaol
 - minor kspar; altered to sericite and trace kaolinite
 - fluorite disseminated throughout; fl pocket and vein
 - interstitial calcite between fine grained quartz grains
 - abundant rutile
 - trace moly within kspar grain; < 75 microns
 - trace pyrite; <75 microns
 - sericite stringers throughout



Petrographic Section



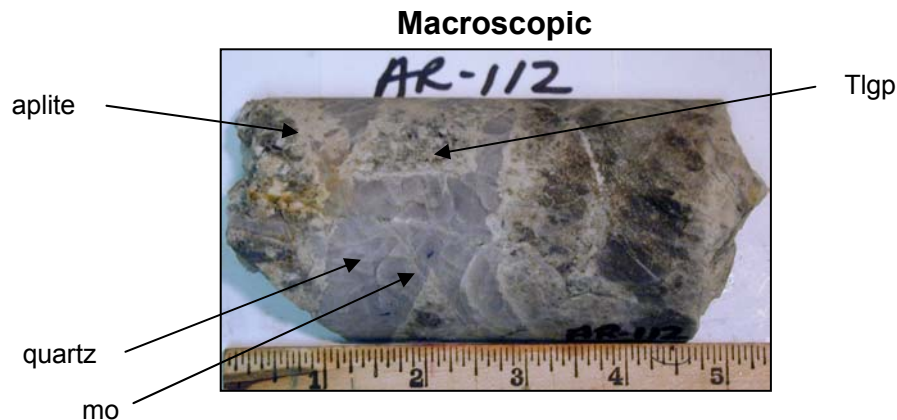
Paragenesis

Matrix:
 aplite → qtz+kspar+fl+mo+rtl+/-ca → qtz+rtl+tr tpz+fl+/-ca
 → qtz+ser+py+/-ca+/-rtl → kaol

Sample: AR-112
Facies: A1
Phase: Matrix
Borehole: 23.5-11.8G
Elevation: 7259.5'

Macroscopic

Predominantly source aplite and some Tlgp clasts; qtz-mo matrix.



Microscopic

• predominantly matrix with small piece of clast

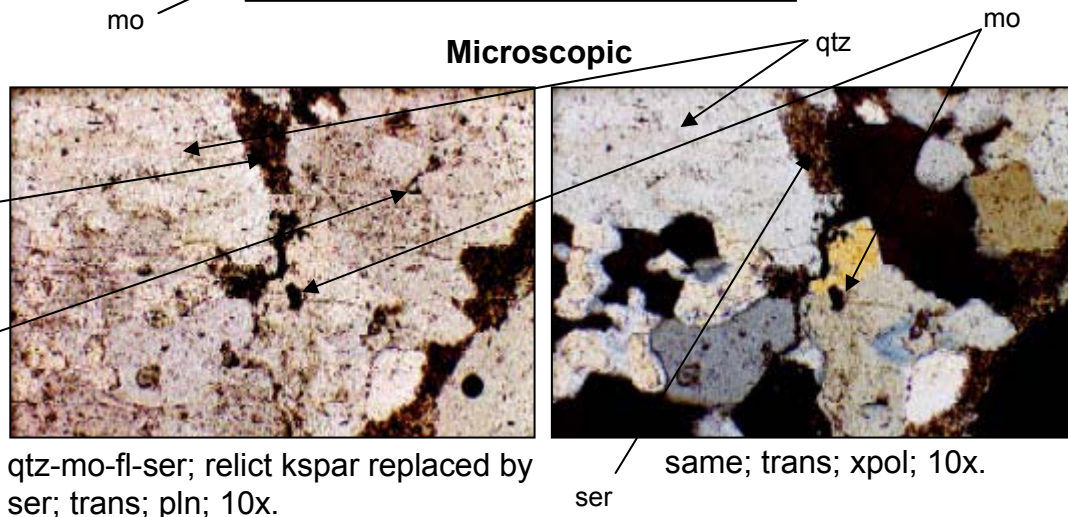
• Matrix:

- very large grains of qtz; med grains of qtz variable size; small grains of qtz associated with QSP
- very little rutile (tr)
- some mo; mo with sericite and some fluorite; ser most likely was originally kspar
- minor kspar
- tr pyrite
- ca-qtz and/or ser-qtz vnlt matrix qtz
- disseminated fl; fl vnlt xcuts matrix

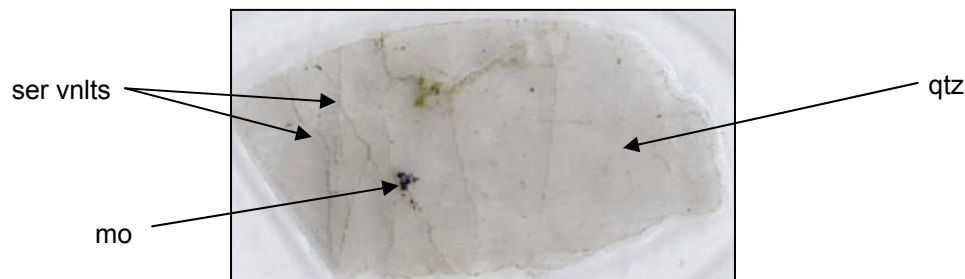
• Clast:

- ser-fl-qtz

Microscopic



Petrographic Section



Paragenesis

Matrix:

qtz+ksp+mo+fl+/-tr rti → qtz+ser+tr py+/-tr rti

Clast:

qtz+fl → qtz+fl+ser

112

Sample: AR-106

Facies: A2

Phase: Matrix

Borehole: 23.4-11.8G

Elevation: 7363'

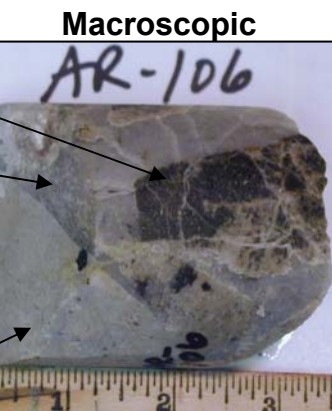
Macroscopic

Qtz-mo-kspar-aplite matrix; source aplite, bt alt Tan, and blch ovrprnt bt alt Tan clasts matrix.

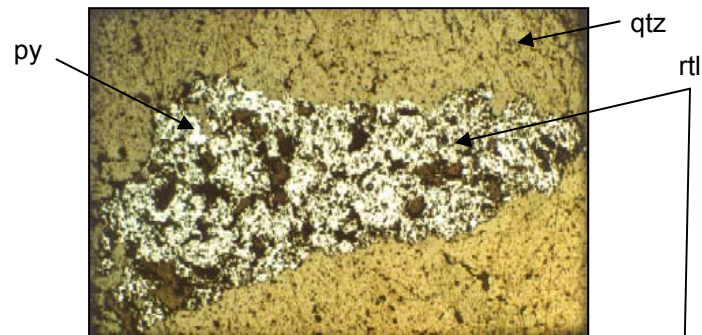
Microscopic

• Matrix:

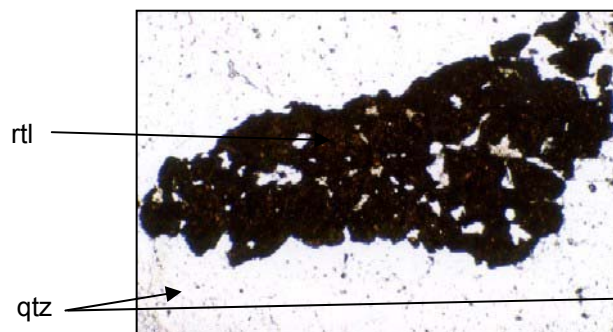
- minor aplite-qtz-kspar-mo-fl-rtl-bt-py-ser-ca-kaol
- qtz is subhedral to anhedral; finer grned generation and coarser grnd generation, 25 microns to 2200 microns; highly fractured
- relict subhedral kspar grains; kspar alt to ser and/or kaol; bt association; mo association
- euhedral-subhedral mo blades and hexagons; associated with finer grned qtz and kspar
- fl dissem throughout and as vnlts; fl-mo association
- tr bt occurring along clast/matrix interface and with kspar; anhedral to subhedral; 25 microns to 250 microns
- rtl occurring throughout; association with fluorite, py, and sericite
- py is euhedral to anhedral
- ca vn xcutting matrix and fl vnlts



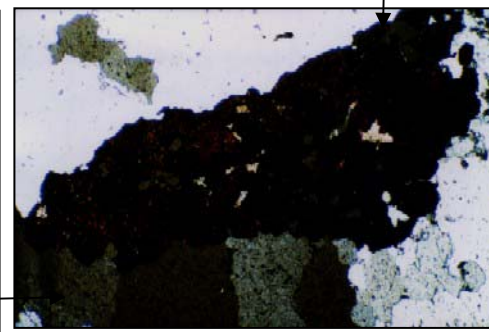
Microscopic



Rutile, ser, qtz, fl; reflect; pln; 5x.



Same; trans; pln; 5x.



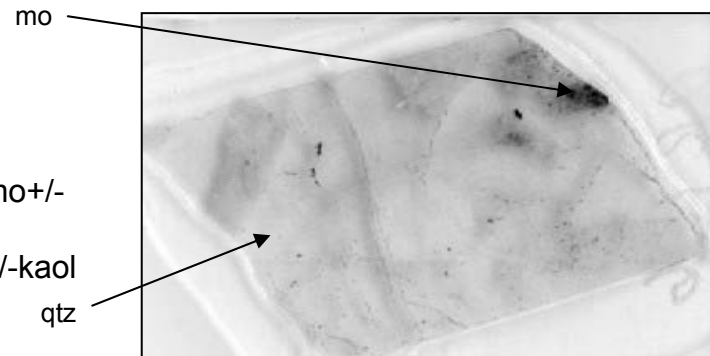
Same; trans; xpol; 5x.

Paragenesis:

Matrix:

aplite → qtz+kspar+fluorite+mo+/-
 bt → bt+fl+rtl+/-mo+/-qtz+/-
 kspar → qtz+ser+py+rtl → ca+/-kaol

Petrographic Section

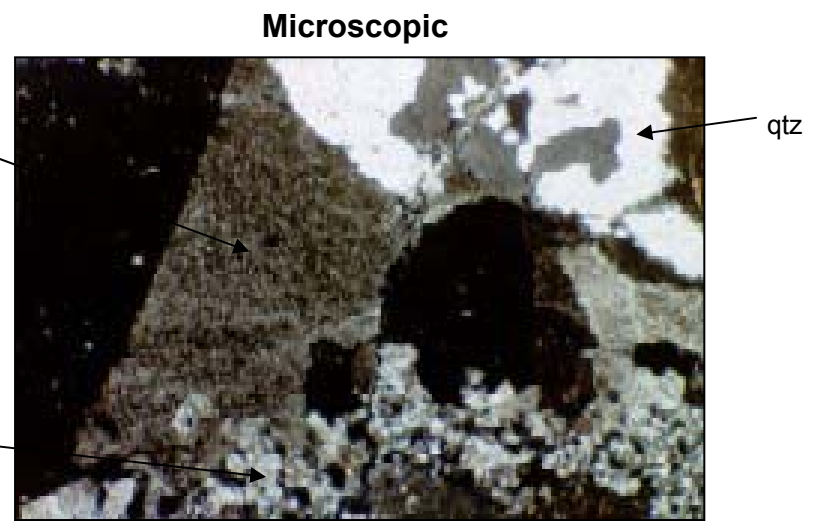
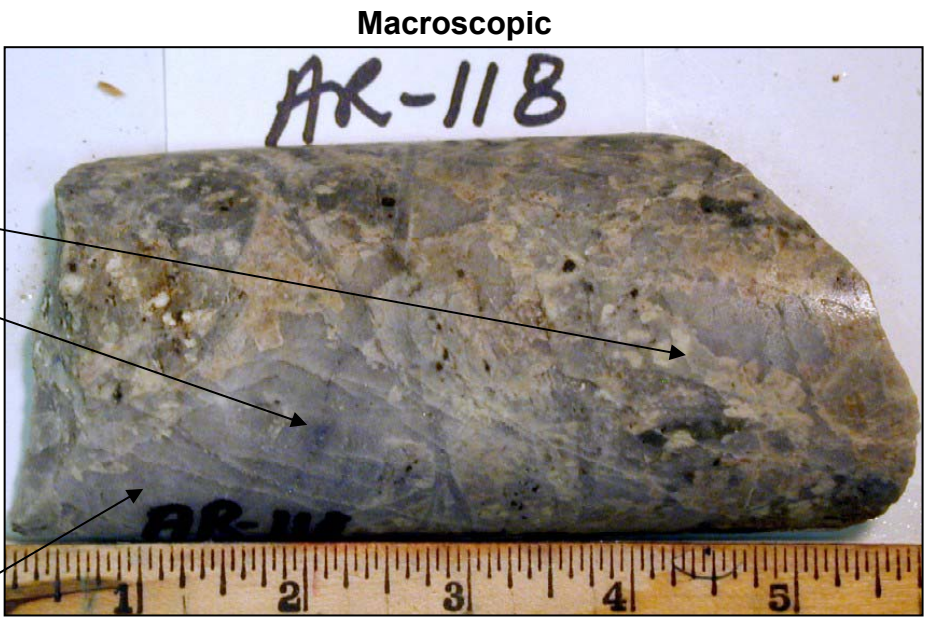
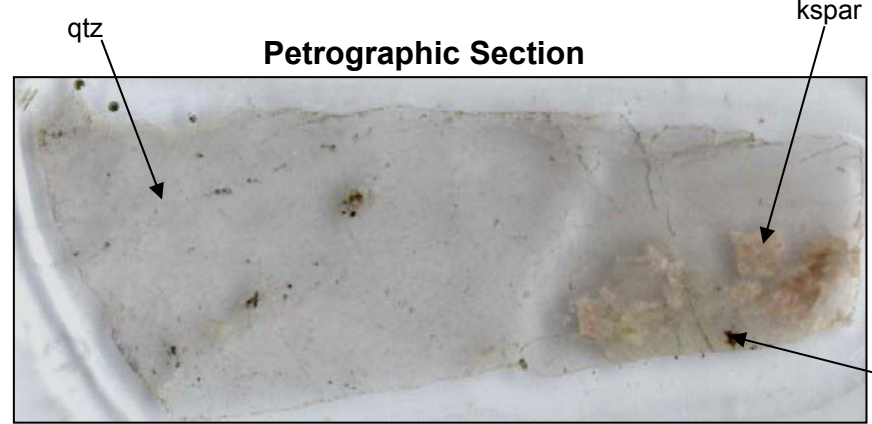


Sample: AR-118
Facies: A2
Phase: Matrix
Borehole: 23.5-11.8G
Elevation: 7397'

Macroscopic
 Aplite-kspars-qtz-mo-Tlgp matrix

- Microscopic**
- Matrix:
 - aplite-kspars-qtz-mo-rtl-py-ser-ca-tr bt-tr fl
 - aplite consists of qtz+kspars+rtl+py+ser+/-kaol
 - smaller qtz grains...associated with QSP?
 - xcut by minor ser or ca vnlt
 - lots of fluid inclusions

Paragenesis:
Matrix:
 aplite → qtz+kspars+/-tr mo+/-bt → bt+rtl+/-
 mo → rtl+qtz+ser+py → ca+/-kaol



Aplite-qtz-kspars matrix; trans; xpol; 5x.

114

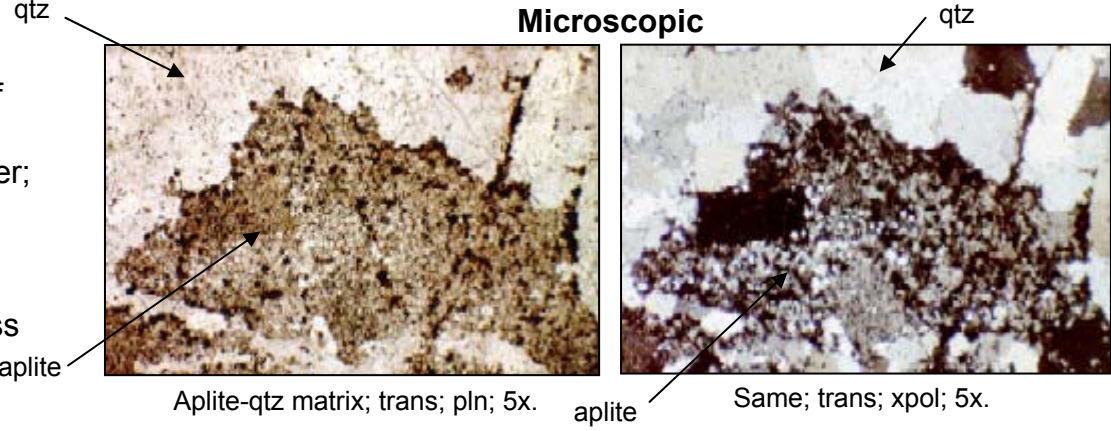
Sample: AR-93
Facies: A3
Phase: Matrix
Borehole: 22.0-14.0
Elevation: 7391.5'

Macroscopic

Bt alt Tan; qtz-kspar-tr mo matrix.

Microscopic

- Matrix:
 - qtz-aplite-kspar-tr bt-tr rtl-tr py
 - some very large qtz grns in matrix (> field of view), med and sm grns also
 - aplite – qtz+kspar and some minor bt and ser; “digested” into matrix;
 - bt alt Tan may also be slightly digested into matrix
 - minor bt within matrix; rtl-bt association; poss tpz-bt assoc
 - fl dissemin throughout; fl-bt assoc
 - ser and/or ca stringers
 - no visible mo; however very thin blades occur in qtz matrix, may be mo, rtl, or fluid inclusions
 - kspar alt to ser and kaol in some areas
- Clast:
 - bt altered clast; bt-qtz-kspar+fl+rtl+/-tpz
 - ser and/or ca stringers

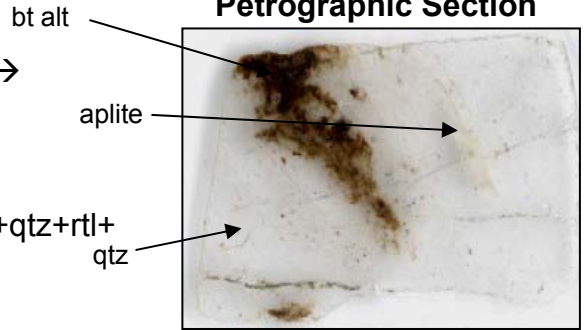


Paragenesis

Matrix:
 aplite → qtz+kspar+fl → qtz+rtl+bt+fl →
 qtz+ser+/-rtl+/-py → kaol → ser/ca

Clast:
 qtz+kspar → bt+qtz → bt+qt+tpz → bt+qtz+rtl+
 tpz → qtz+rtl+py → ser/ca

Petrographic Section



115

Sample: AR-91 (replaced AR-170 due to insufficient material)
Facies: A3
Phase: Matrix
Borehole: 22.0-14.0
Elevation: 7426.5'

Macroscopic

Bt alt Tan clasts; qtz-tr mo-kspar matrix.

Microscopic

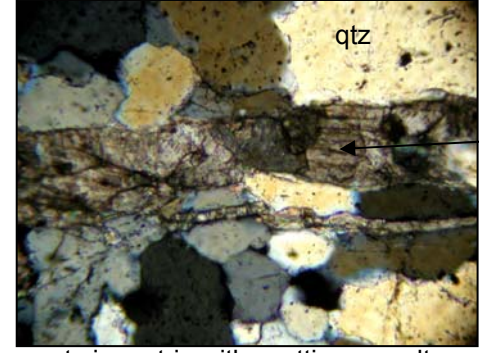
- **Matrix:**
 - kspar-aplite-qtz-mo-fl
 - qtz is fine to lg grned; 5 to 200 microns; anhedral; random grn distribution; qtz and kspar cogenetic
 - kspars fairly pristene, but altered slightly to ser and kaol; some kspars well altered to ser and/or kaol; kspars are anhedral; 5-50 microns
 - f.g. fl dissem in matrix
 - mo as anhedral to subhedral grns
 - some clast "digestion"
 - ser and/or ca vnlt xcutting matrix and clast

- **Clast:**
 - qtz-bt-rtl-tr tpz-fl-py-ser-kaol-mt?
 - typical bt alt clast
 - lots of kspar @ clast/matrix interface
 - leucoxene or clay replacing plag phenos; relict plag phenos are replaced by ruddy dk brown-black material and ser/clays
 - rtl-bt assoc

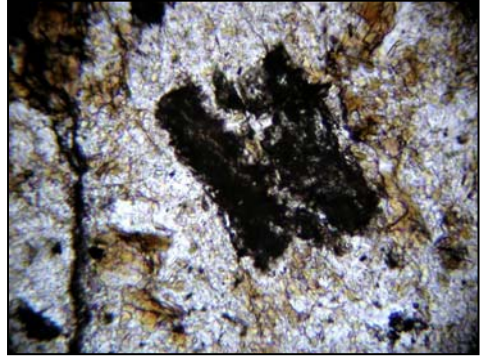
Macroscopic



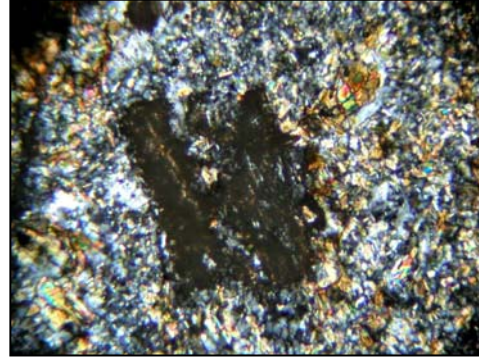
Microscopic



qtz in matrix with xcutting ca vnlt; trans; xpol; 10x and d.z.



Bt alt clast with altered plag pheno, bt, ser, qtz, and rtl; trans; pln; 10x and d.z.



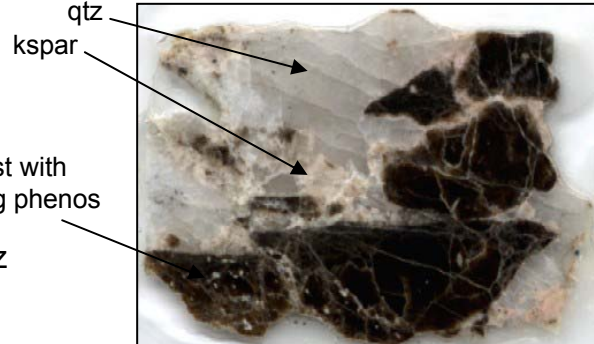
Same; trans; xpol; 10x and d.z.

Paragenesis

Matrix:
 aplite → qtz+kspar+/-fl → qtz+mo+fl → ser/ca

Clast:
 qtz+bt+/-rtl+/-tpz+/-fl → qtz+bt+rtl+tpz+/-fl → qtz+fl → qtz+ser+py → ser/ca → kaol

Petrographic Section



116

Sample: AR-169

Facies: B

Phase: Matrix

Borehole: 19.9-12.1

Elevation: 7459'

Macroscopic

Qtz-kspar-tr mo matrix and bt alt Tan; xcutting ca vnlts

Microscopic

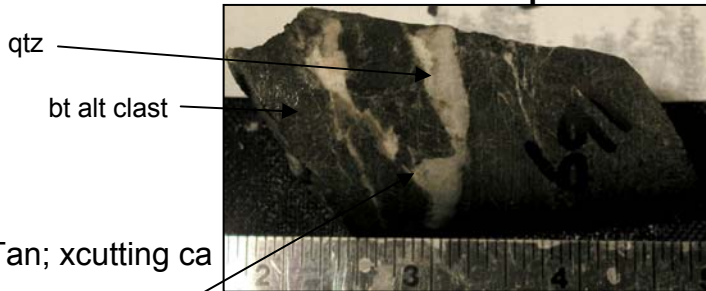
• Matrix:

- qtz-kspar-mo-py-fl-minor ca-tr bt-tr rtl
- some very lg qtz grns farthest from clast; finer grn qtz closest to clast
- kspar and mo mostly close to clast
- mo is euhedral hexagons and blades to anhedral; mostly assoc w/ fine-med grn qtz
- some ca matrix material
- fl dissem throughout
- kspar altered to ser and kaol in some areas
- partially “digested” clast contributing some bt and rtl; tr hydrothermal bt also
- xcutting ca-fl vnlts

• Clast:

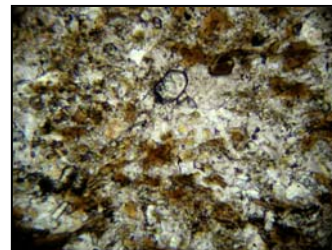
- bt-qtz-fl-rtl-py-mo-tpz-ap-some kspar-tr mt
- fine grned kspar along matrix-clast boundary
- bt-rtl-tpz-ap-qtz groundmass
- abundant crs grn topaz
- py dissem throughout clast

Macroscopic

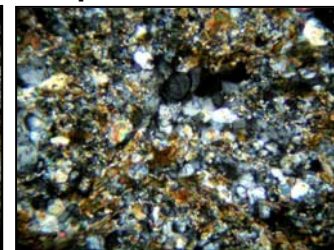


kspar at clast-matrix interface

Microscopic



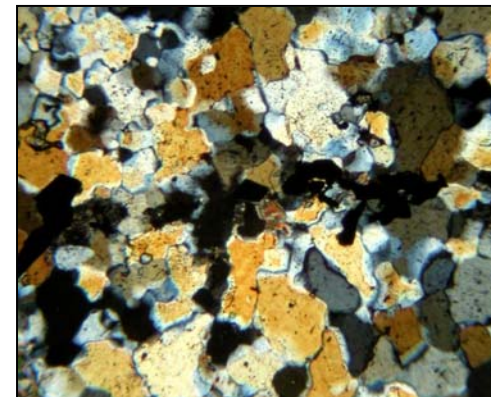
bt-tpz-rtl-apatite-qtz in bt alt clast; trans; pln; 10x



same; trans; xpol; 10x and digital zoom



qtz and mo in matrix; trans; pln; 5x and digital zoom



same; trans; xpol; 5x and digital zoom

Paragenesis

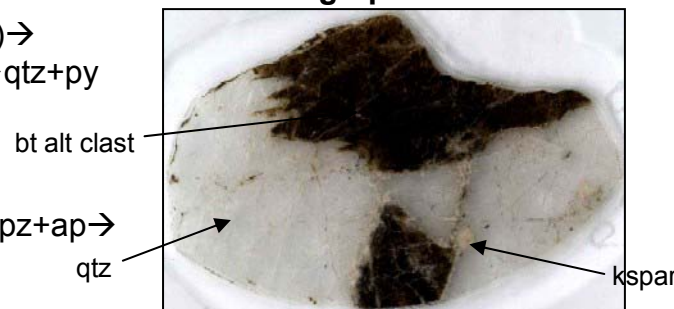
Matrix:

“digested” clast (bt+qtz+tpz+rtl)→
 qtz+kspar+mo+fl→qtz+mo+fl→qtz+py
 →ca+fl

Clast:

qtz+bt+/-tpz+/-ap→qtz+bt+rtl+tpz+ap→
 qtz+mo+fl→qtz+py→ca+fl

Petrographic Section



bt alt clast

qtz

kspar

Sample: AR-13

Facies: B

Phase: Matrix

Borehole: 21.7-15.5

Elevation: 7429'

Macroscopic

Bt alt clasts with py; qtz-mo matrix; minor ca present.

Microscopic

• Matrix:

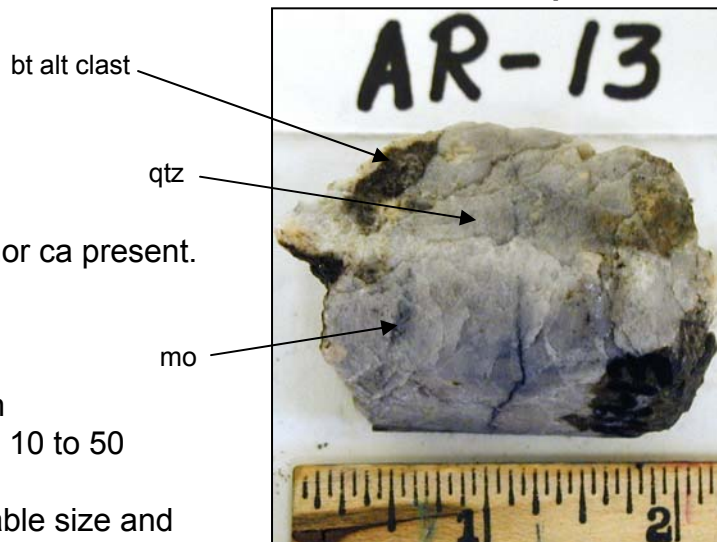
- no clast in thin or thick section
- few small grns of py in matrix; 10 to 50 microns
- mo occurring in matrix is variable size and shape; 20 to 500 microns; anhedral to euhedral (hexagons and blades); fl-mo assoc
- fl occurring along grn boundaries
- in general, mo assoc with finer grned qtz
- some very lg grns of qtz; > than field of view @ 5x (>2500 microns); no mo within these grns; some qtz grns have an "interlocking" texture (mostly smaller grns)
- fine-med grned bt with fl
- xcutting ca or ser vnlt

Paragenesis

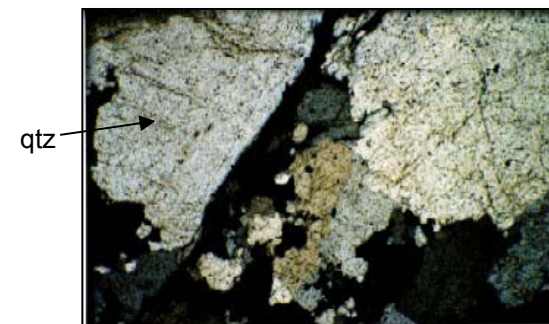
Matrix:

qtz → qtz+mo+fl+/-bt → qtz+bt+fl+/-mo → qtz+ ser+py
 → ca/ser

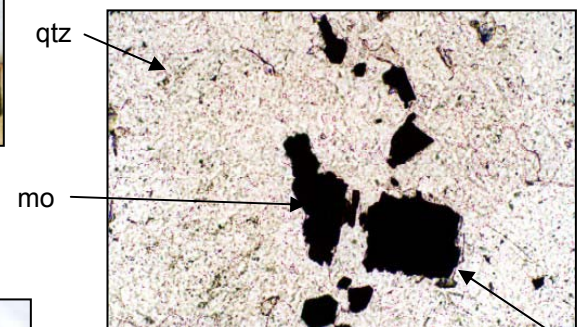
Macroscopic



Microscopic

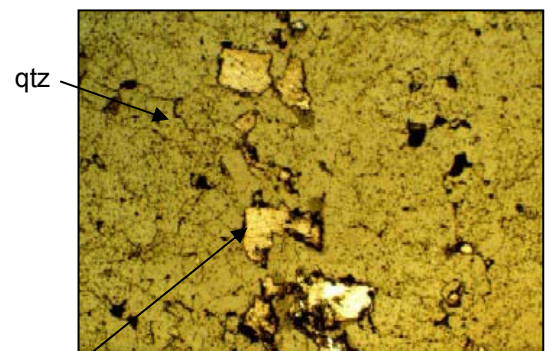
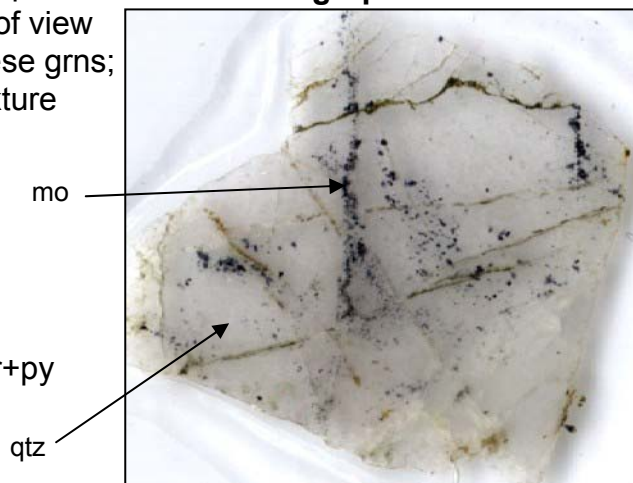


Qtz; trans; xpol; 10x.



Mo w/fl, qtz; trans; pln; 10x.

Petrographic Section



Mo and qtz; reflect; pln; 10x.

118

Sample: AR-131

Facies: C

Phase: Matrix

Borehole: 22.0-14.0

Elevation: 7505'

Macroscopic

Crs grn bt-kspars-mo-qtz-anhy-gypsum matrix; most anhy alt to gypsum.

Microscopic

• Matrix:

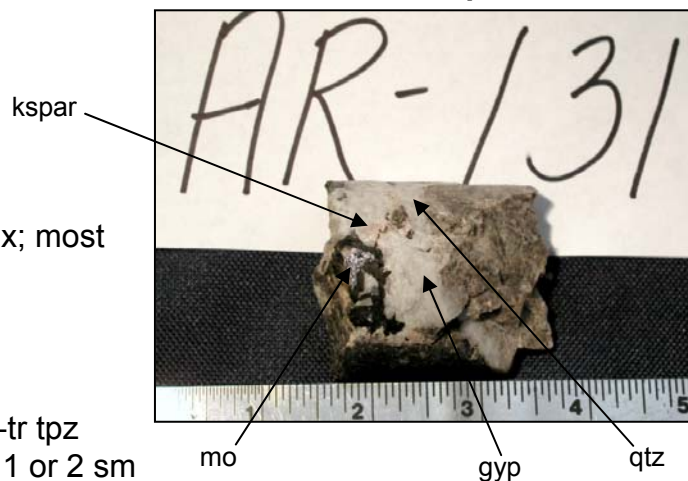
- qtz-mo-bt-kspars-rtl-gyp-py-fl-ap-ca-tr tpz
- qtz vn through large qtz grns, only 1 or 2 sm grns thick; lg matrix qtz grns are field of view at 5x; ca-gyp-fl with qtz vn lts xcutting lg qtz grns
- kspars alt to ser; rtl within kspars
- euhedral rtl in bt
- ap included in qtz
- rtl within bt within kspars with qtz vn adjacent; bt alt to rtl
- py grn within kspars; qtz and kspars within py
- fl slightly dissem throughout
- qtz and gyp grn within mo
- gyp occurring along grn boundaries; gyp in cleavage of bt; relict twinning of anhy in some gyp

Paragenesis

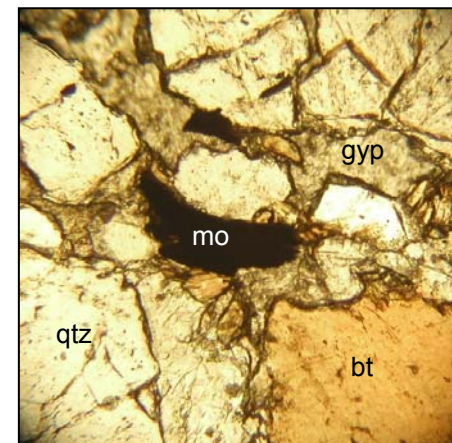
Matrix:

qtz+bt+/-kspars+/-mo+/-fl+/-rtl → qtz+kspars+mo+fl+/-bt+/-rtl → anhy+fl+mo → qtz+py+ser+/-rtl → qtz+ca+gyp+fl

Macroscopic

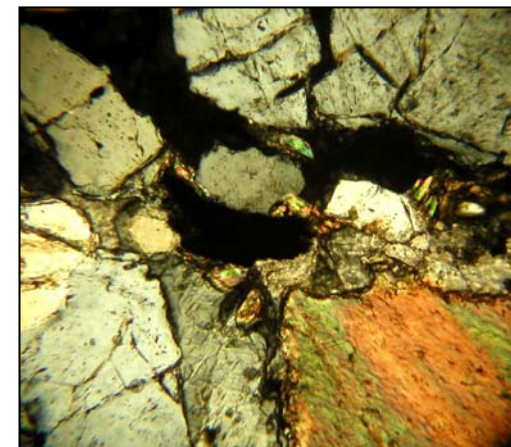
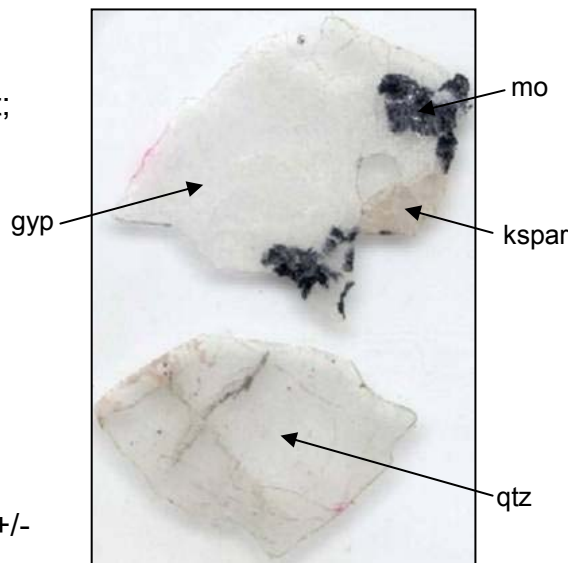


Microscopic



Qtz-mo-bt-gyp matrix; trans; pln; 10x and d.z.

Petrographic Section



Same; trans; xpol; 10x and d.z.

Sample: AR-8
Facies: C
Phase: Matrix
Borehole: 21.7-15.5
Elevation: 7479.5'

Macroscopic

Predominantly bt alt clast with some kspar flooding, qtz-bt-ca-mo matrix.

Microscopic

- Matrix:
 - qtz-mo-bt-ca-tr py-tr ser-tr hem-tr kaol
 - subhedral to anhedral qtz grns; solid inclusions in qtz; larger qtz grns occurring with bt
 - mo as euhedral to subhedral hexagons and blades
 - interstitial ca
 - fl disseminated throughout and as vnlts

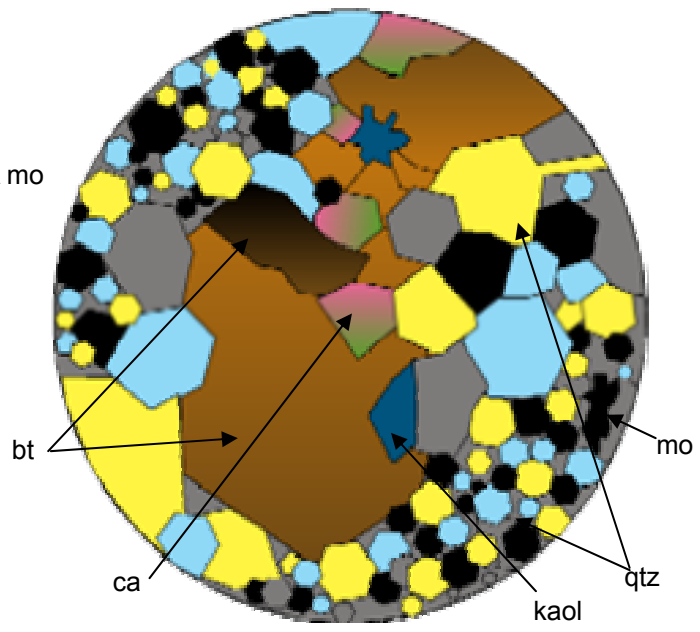
Paragenesis:

Matrix:
 qtz → qtz+bt+mo+fl → qtz+ca+/-fl → qtz+ser+py → kaol

Macroscopic



Microscopic



Field of view at 4x; qtz-mo-bt-ca matrix.

Petrographic Section



120

Sample: AR-78

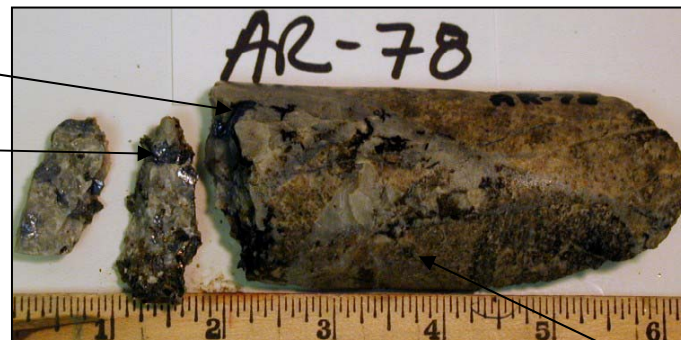
Facies: D

Phase: Matrix

Borehole: 22.0-14.0

Elevation: 7576.5'

Macroscopic

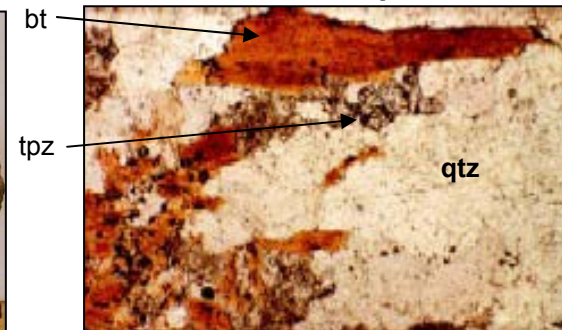


crs grned bt

crs grned mo

clast

Microscopic



tpz

qtz

Qtz-kspar-bt-tpz matrix; trans; pln; 10x.

Macroscopic

Blch and blch ovrprnt bt alt Tan, bt-qt-mo matrix; qtz-mo vnlt xcuts matrix.

Microscopic

• Matrix:

- qtz-mo-bt-fl-tpz-py-rtl-kspar-ser-ca
- moly is subhedral blades and hexagons to anhedral
- closest to clast, smaller qtz grns; outer matrix contains very lg qtz grns
- fl dissemin throughout; not as much fl in very lg qtz grn; subhedral fl along matrix/clast interface containing inclusions of bt and qtz
- tpz is euhedral to anhedral; some tpz alt to ser; tpz-bt assoc; fl inclusions in qtz
- ser in matrix
- kspar alt to ser
- ser border on lg bt grns in matrix
- ca vnlt xcuts matrix and vn

Clast Cont'd

- bt along clast/matrix interface; inclusions of rtl in bt; tpz also along substrate
- ca vnlt xcuts matrix and vn

Paragenesis

Matrix:

qtz+bt+kspar → qtz+bt+mo+fl+/-kspar → qtz+bt+fl+tpz+rt+/-mo → qtz+ser+py → ca

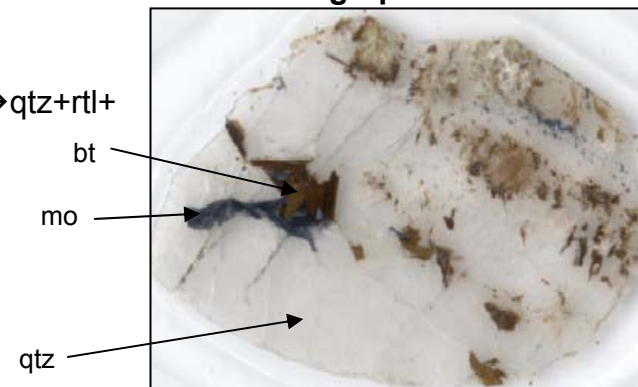
Clast:

bt+qtz → bt+qtz+tpz+rtl+fl+/-mo → qtz+rtl+ser+py → kaol → ca



Same; trans; xpol; 10x.

Petrographic Section



bt

mo

qtz

121

• Clast:

- qtz-ser-bt-rtl-py-fl-topaz-mo-kaol
- fl mostly w/mo; mo also assoc w/bt in clasts
- rtl everywhere
- fl w/tpz or included in tpz

Sample: AR-6A

Facies: D

Phase: Matrix

Borehole: 21.7-15.5

Elevation: 7535'

Macroscopic

Bt alt clasts, bt-qtz-anhy matrix, QSP, crs grned bt, grn and purple anhy.

Microscopic

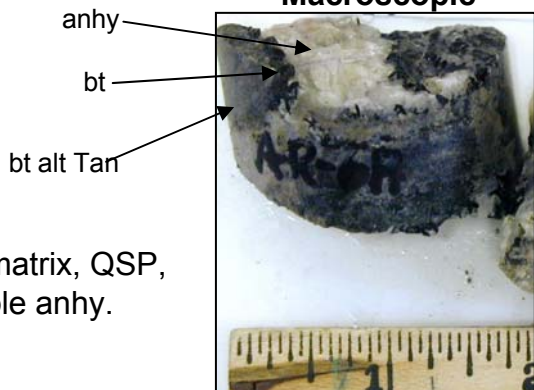
• Matrix:

- bt-anhy-mo-qtz-fl-gyp-ser-ca
- crs grn bt; some ser selvages on edges and/or going through bt crystal; 20-2400 microns; euhedral to subhedral; bt growth from substrate of clast; bt containing euhedral inclusions of rtl
- qtz, anhy, and fl growth from clast substrate also
- most mo growth along matrix/clast interface, with most of the mo on the clast side; mo is anhedral to subhedral
- anhy alt to gypsum
- bt grn contained within lg anhy grn which is being altered to gyp along anhy/bt boundary
- some py in matrix; occurs with fl or gyp or within lg anhy crystal
- ca or ser vnlxt xcutting matrix

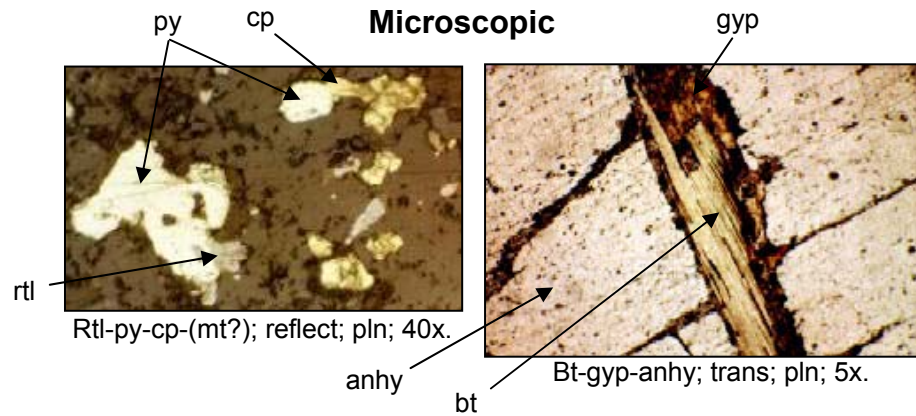
• Clast:

- bt-qtz-rtl-ser-py-cp-fl-anhy-tr tpz-tr ap-mt?
- fl disseminated throughout clast

Macroscopic

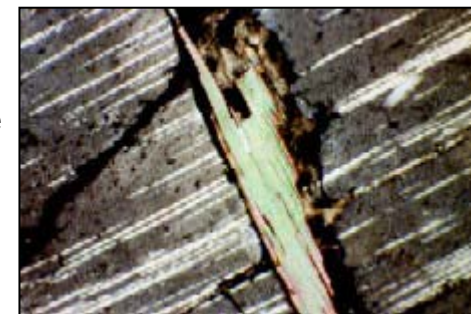


Microscopic



Clast Cont'd

- rtl disseminated throughout
- py-cp-rtl assoc; py is subhedral to euhedral; 20-100 microns; mt may be replacing py in some instances
- fl occurring in qtz pockets within clast
- fl vn xcuts clast
- bt alt to ser alt to kaol
- ser and/or ca stringers xcut clast and matrix



Same as above; trans; xpol; 5x.

Paragenesis

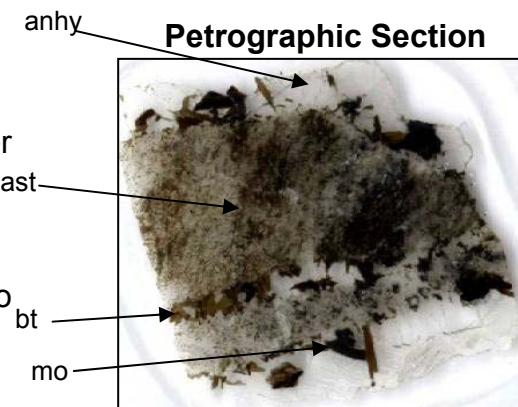
Matrix:

qtz → bt +/- rtl +/- fl → mo + fl → anhy(gyp) → ser + py +/- rtl +/- qtz +/- gyp → ca

Clast:

qtz + bt → qtz + bt + rtl +/- tpz +/- ap → qtz + fl + mo → ser + py + cp +/- mt → ca/kaol

Petrographic Section



Sample: AR-5

Facies: E

Phase: Matrix

Borehole: 21.7-15.5

Elevation: 7578'

Macroscopic

Qtz-bt-mo-ca matrix, bt and blch alt tan clasts, QSP, dissem mo in clasts, grn ser, crs grned bt.

Microscopic

• Matrix:

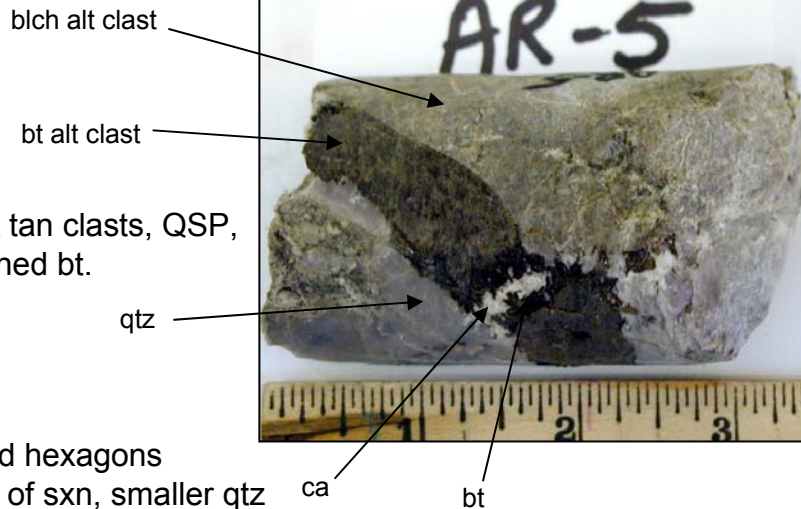
- qtz-mo-bt-rtl-ca-fl-ser
- mo as euhedral blades and hexagons
- larger qtz frn on perimeter of sxn, smaller qtz grns in various areas in center of sxn; in some areas smaller grns occur in "pockets" where grns are fairly uniform in size; in some areas, smaller grns occur intermixed with med to lg sized grns; smaller grns have dominant zoning within grns; smaller grns seem to be assoc with dissem f.g. ser and ser vns; lg qtz grns have some zoning but not as much as sm grns
- fl occurs with mo or as sm, high relief grns dissem within qtz; fl also occurs vnlt; anhedral to euhedral; 2 to 10 microns
- bt occurs as subhedral to euhedral grns; ser alt on bt rims and some centers; euhedral rtl inclusions in bt
- ca as matrix filling and as f.g. xcutting vnlt

Paragenesis

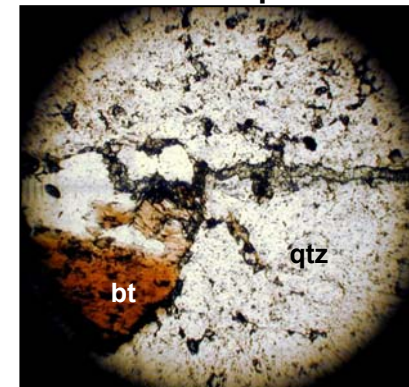
Matrix:

qtz → qtz+bt+rtl+/-fl → qtz+mo+fl → ser/ca

Macroscopic

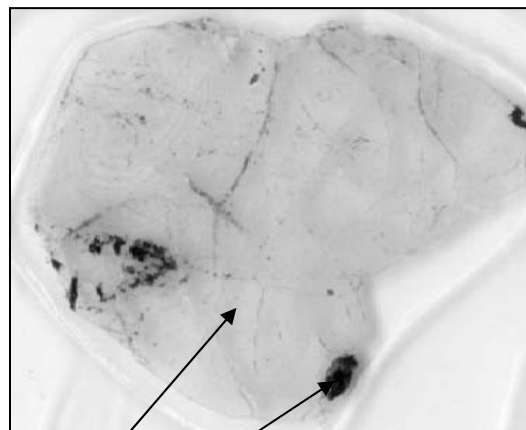


Microscopic

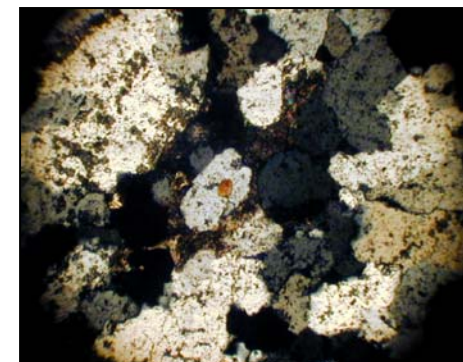


Ser or ca vn in bt-qtz-mo matrix; trans; pln; 10x and d.z.

Petrographic Section



qtz mo



Qtz-bt-mo matrix; trans; xpol; 10x and d.z.



rtl

Rtl inclusions in bt; trans; pln; 10x and d.z.

Sample: AR-64
Facies: E
Phase: Matrix
Borehole: 22.0-14.0
Elevation: 7621'

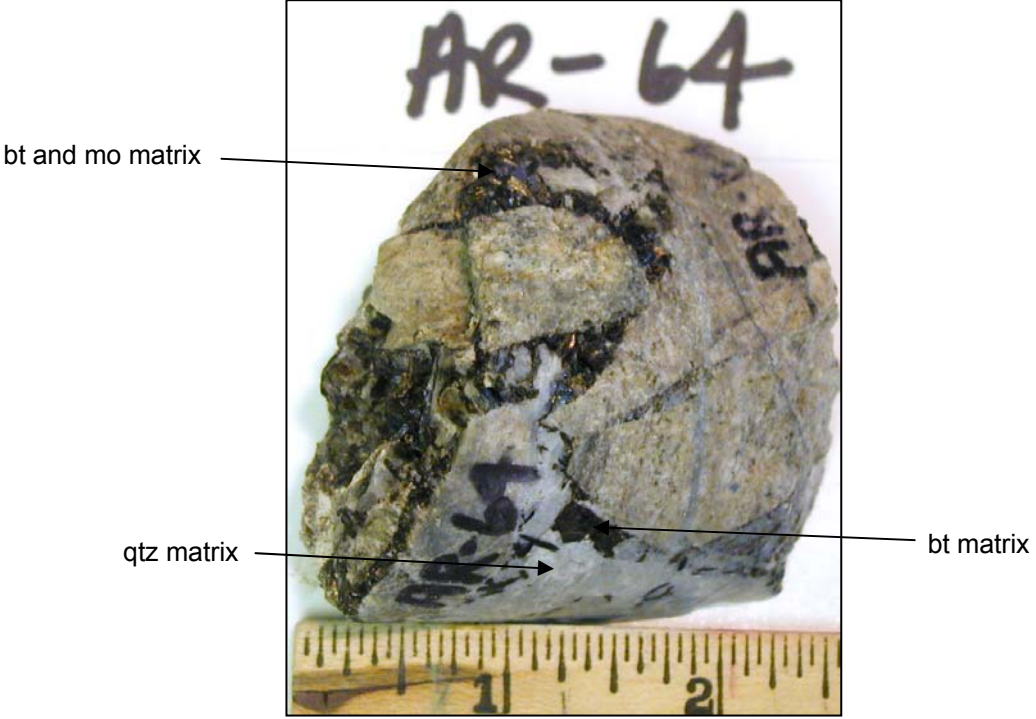
Macroscopic

Blich Tan clasts with some dissem mo; qtz-bt-mo matrix and small qtz-mo vnl; bt is crs grn; QSP.

Microscopic

- Matrix:
 - qtz-bt-mo-fl-py-rtl-tpz
 - very lg qtz grns 20 microns to 2000-2800 microns; some have serious zoning; subhedral to anhedral; inclusions of tpz in qtz
 - tpz is abundant throughout matrix; occurring mostly adjacent to and in proximity to bt crystals; anhedral to euhedral; high relief; low birefringence; some relict tpz in matrix altered to ser; fl inclusions in tpz; 10 to 1000 microns in size
 - anhedral to subhedral bt; 50 to 3000 microns in size; inclusion of euhedral qtz frn in bt; inclusions of rtl in bt (subhedral to euhedral); minor ser rims on bt
 - mo occurring with bt and along bt grn boundaries; 2400 microns
 - rtl and py dissem throughout; rtl-bt assoc; py in bt grn
 - fl dissem throughout matrix; also fracture filling in lg qtz grns; also occurs as coarser euhedral to subhedral matrix filling

Macroscopic



Microscopic



Mo filling bt grn boundaries in qtz-bt-mo matrix; trans and reflect; pln; 5x.

Sample: AR-64 cont'd

Matrix cont'd

- py is anhedral to euhedral; occurs with fl in some cases
- late stage ca vnlx cuts matrix and clast
- bt, qtz, tpz, and fl growth from clast/matrix substrate

• Clast:

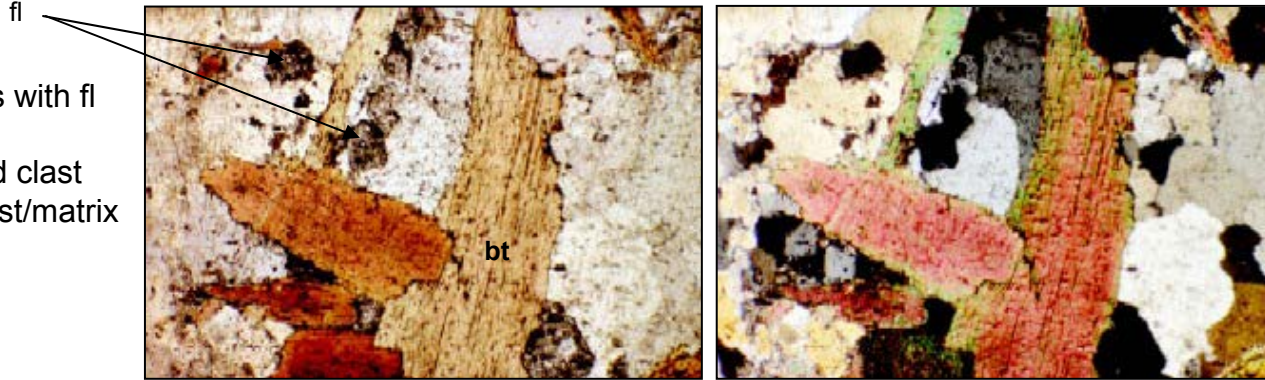
- qtz-bt-rtl-tpz-fl-ser-mo-py
- py as lg euhedral grns, 10-150 microns; some anhedral smaller grns
- fine grned qtz
- mo as subhedral blades; 550 microns; with tpz, rtl, and some bt
- rtl dissem throughout; 10-150 microns
- tpz-bt assoc
- bt mostly alt to ser, but some pristene bts remaining
- fl dissem throughout; some crser grns, but mostly f.g.
- lots of ser throughout; some tpz alt to ser
- no py-rtl assoc in this sample

Paragenesis

Matrix:
 qtz+tpz+bt+rtl+fl+/-py → qtz+mo+fl+/-py → ser/ca

Clast:
 qtz+bt+/-rtl+/-tpz → qtz+bt+fl+rtl+tpz → qtz+fl+mo+/-rtl+/-tpz → qtz+/-py+/-mo+/-fl → qtz+ser+py+/-fl → ca

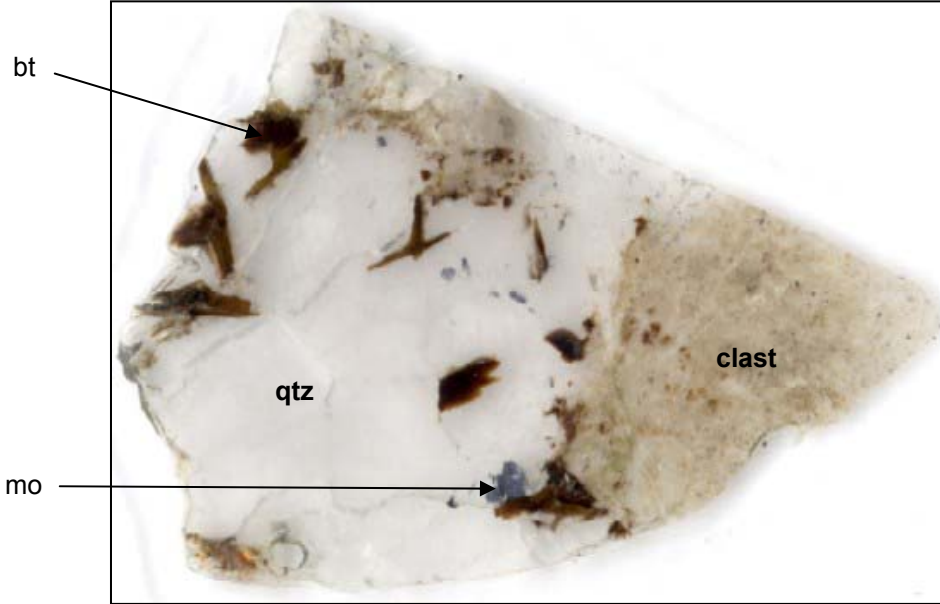
Microscopic cont'd



Bt-fl-tpz?-qtz matrix; trans; pln; 5x.

Same; pln; xpol; 5x.

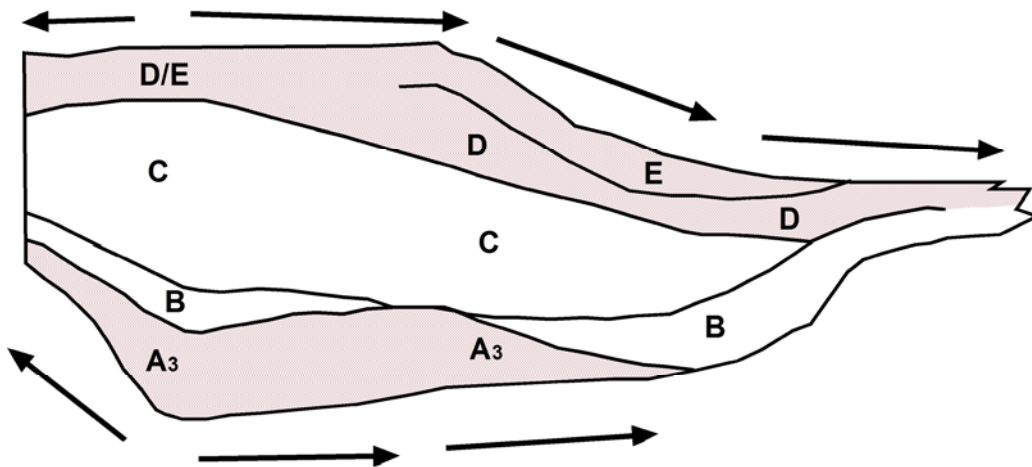
Petrographic Section



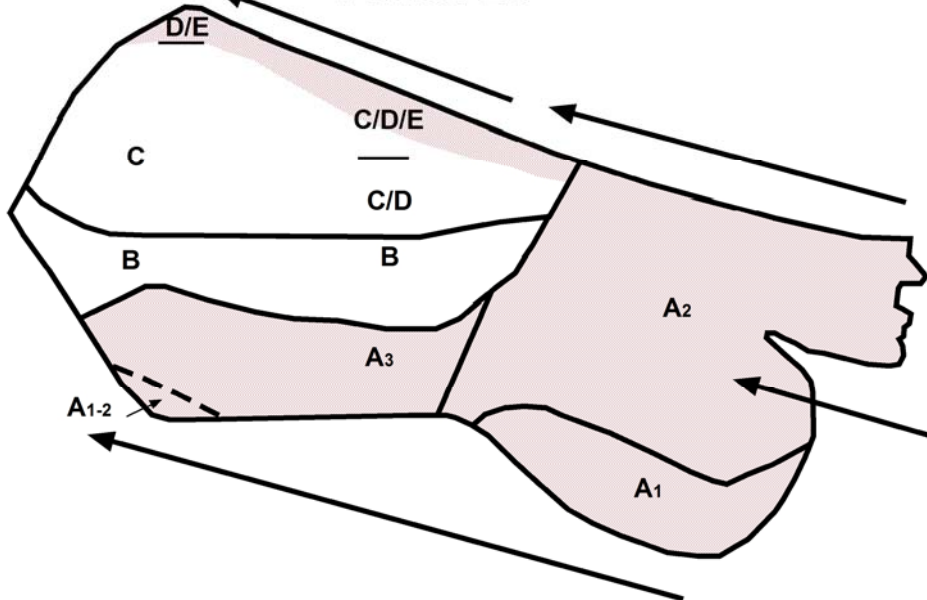
125

**APPENDIX C – SPATIAL DISTRIBUTION OF FLUID INCLUSION
POPULATIONS**

Line 8-9

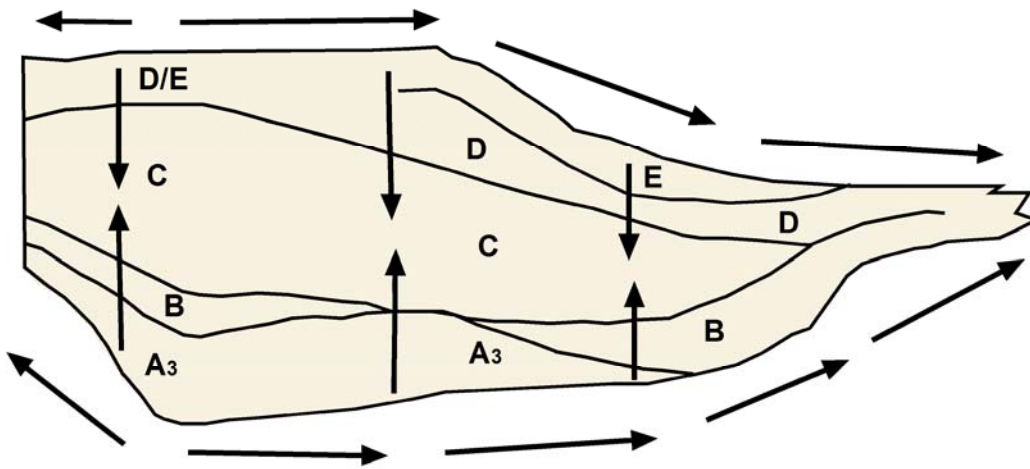


Panel 26

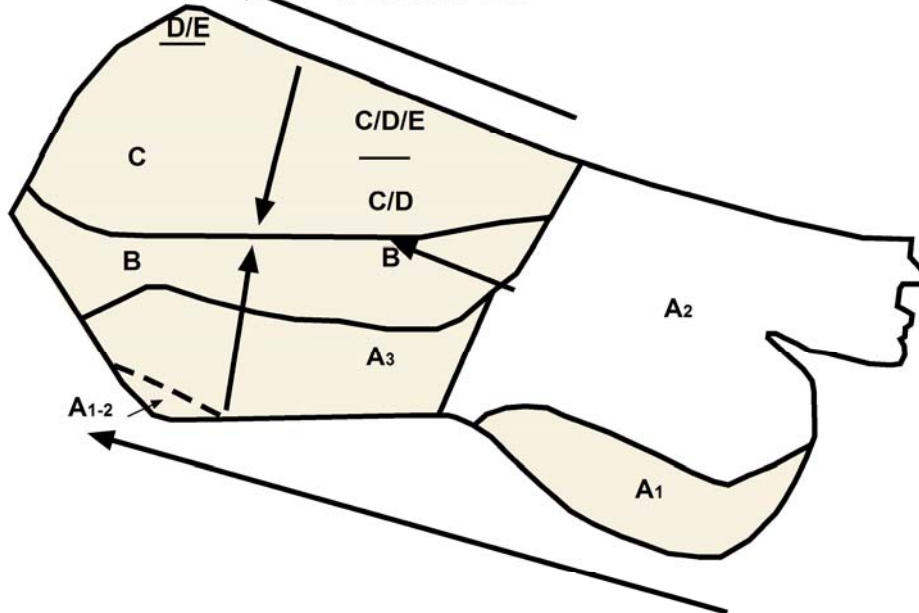


Spatial distributions for *populations 6 and 7* in line 8-9 and Panel 26 represented by shaded areas. Areas of Line 8-9 and Panel 26 taken from Figures 6 and 7 (modified from Ross, 2002). Possible schematic fluid paths indicated by arrows. Populations 6 and 7 occur in facies A, D, and E. Note that the fluid paths for populations 6 and 7 are along the boundaries of the breccia. Not to scale.

Line 8-9

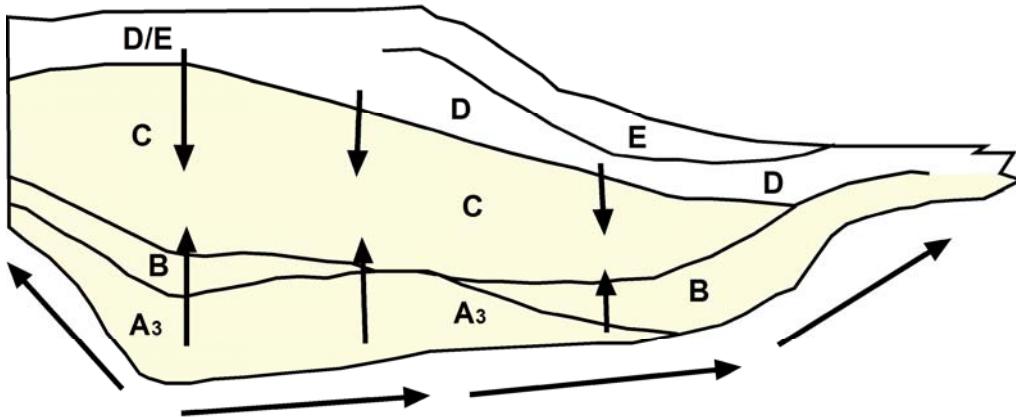


Panel 26

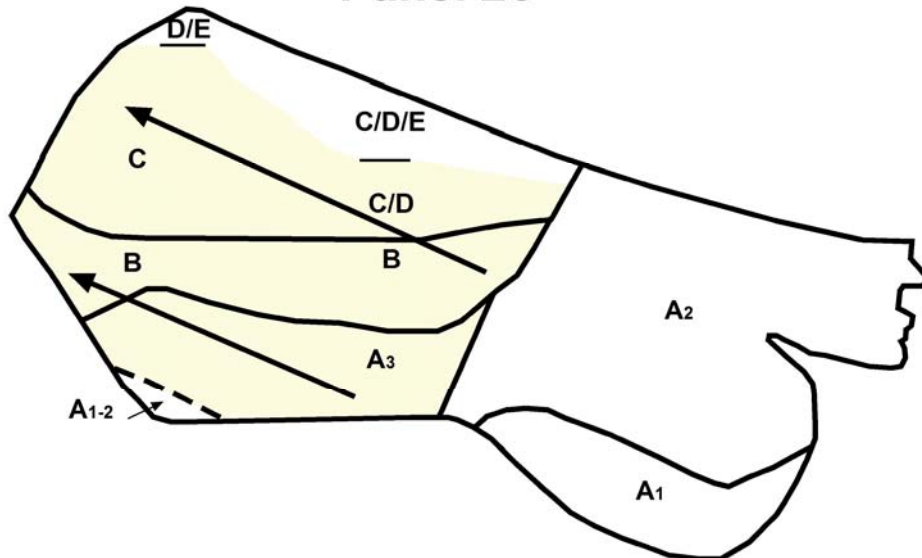


Spatial distributions for *population 4* in line 8-9 and Panel 26 represented by shaded areas. Areas of Line 8-9 and Panel 26 taken from Figures 6 and 7 (modified from Ross, 2002). Possible schematic fluid paths indicated by arrows. Population 4 occurs in all facies except A₂. Note that the fluid paths for population 4 move into the the breccia compared to populations 6 and 7 that are along the boundaries of the breccia. Not to scale.

Line 8-9

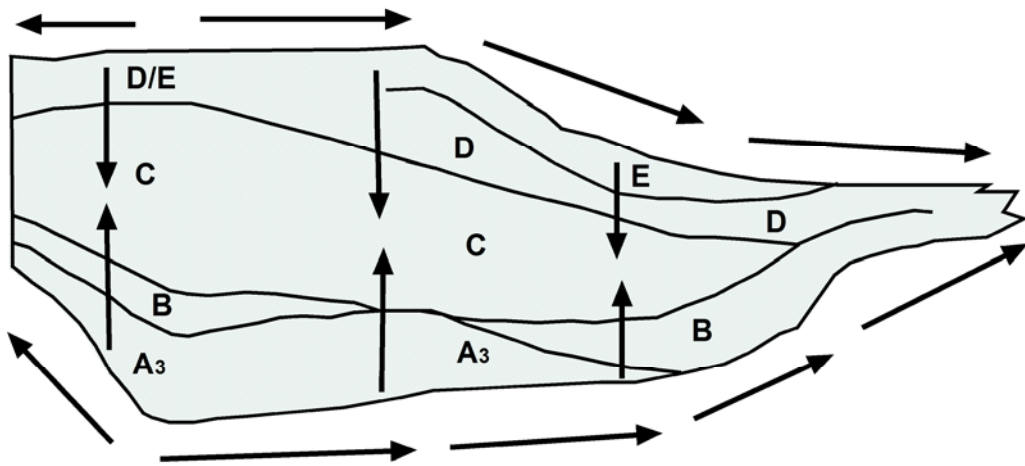


Panel 26

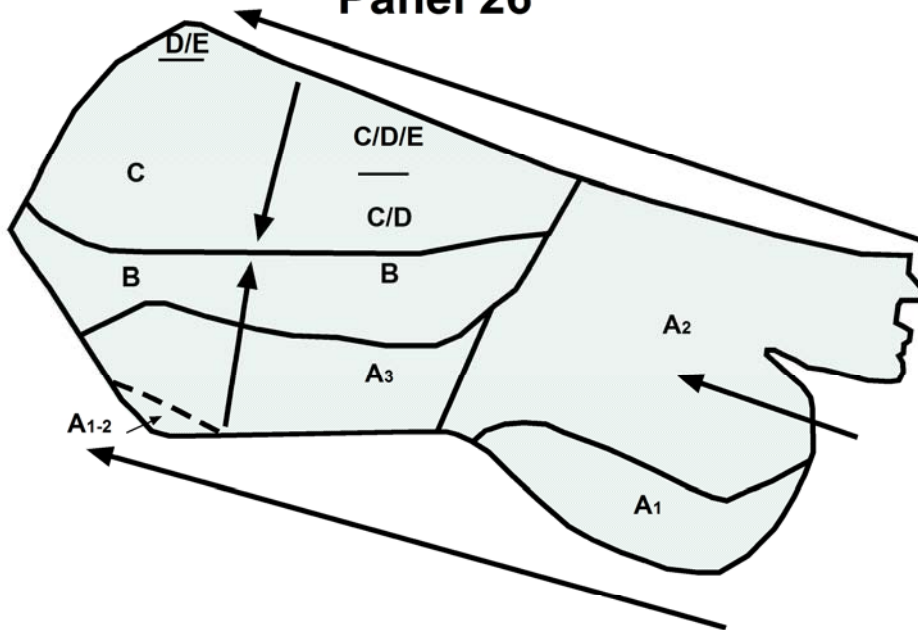


Spatial distributions for *population 5* in line 8-9 and Panel 26 represented by shaded areas. Areas of Line 8-9 and Panel 26 taken from Figures 6 and 7 (modified from Ross, 2002). Possible schematic fluid paths indicated by arrows. Population 5 occurs in facies A₃, B, and C. Not to scale.

Line 8-9

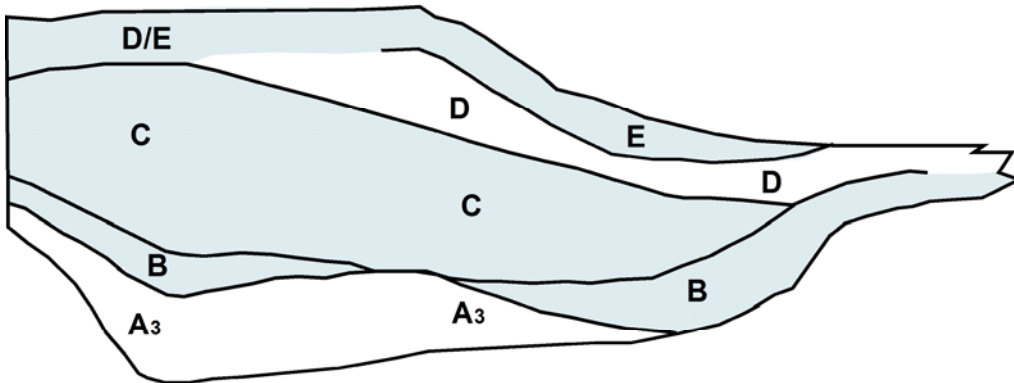


Panel 26

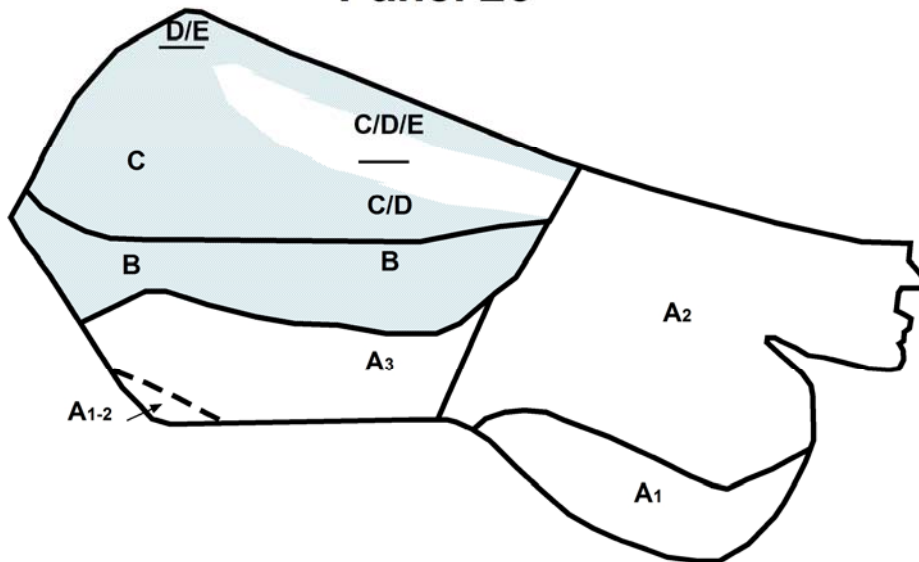


Spatial distributions for *population 2* in line 8-9 and Panel 26 represented by shaded areas. Areas of Line 8-9 and Panel 26 taken from Figures 6 and 7 (modified from Ross, 2002). Possible schematic fluid paths (indicated by arrows) for the portion of population 2 that is on or below the halite saturation curve (representative of a real fluid). Population 2 contains all facies. Not to scale.

Line 8-9

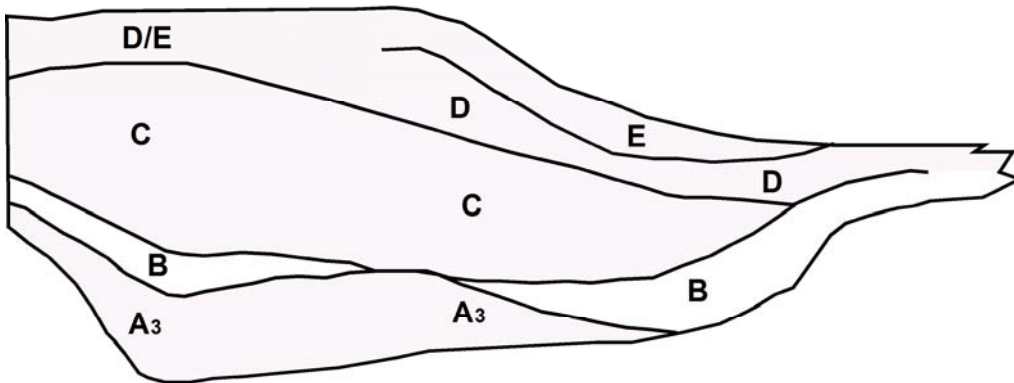


Panel 26

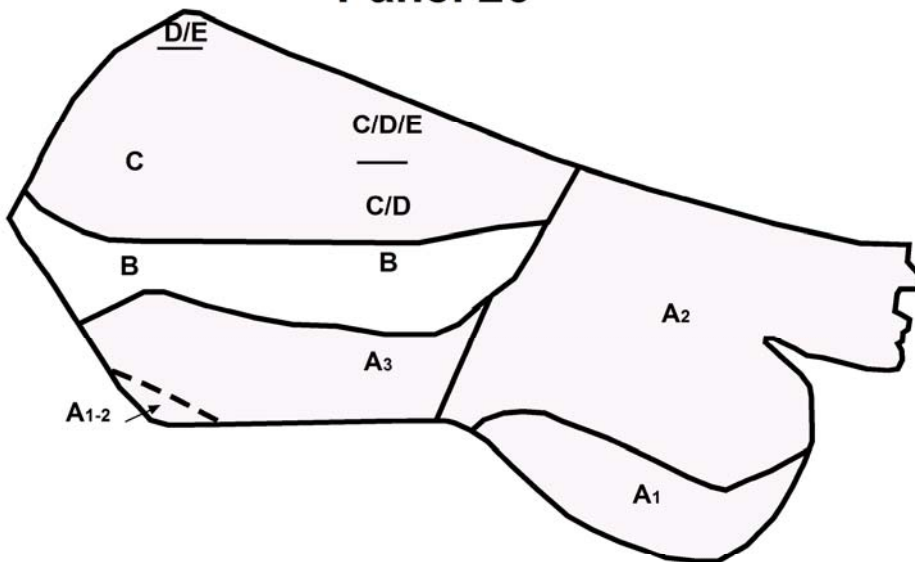


Spatial distributions for *population 9* in line 8-9 and Panel 26 represented by shaded areas. Areas of Line 8-9 and Panel 26 taken from Figures 6 and 7 (modified from Ross, 2002). Population 9 occurs in all facies except facies A and D. Not to scale.

Line 8-9

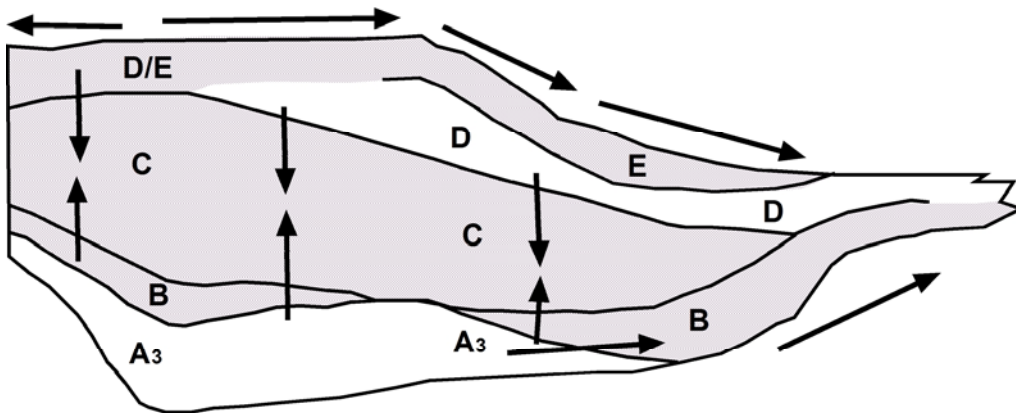


Panel 26

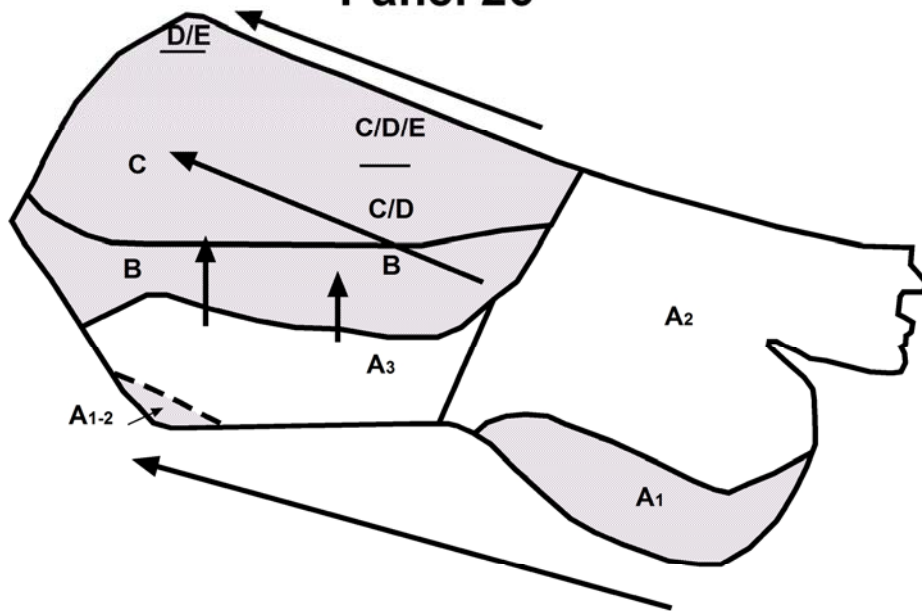


Spatial distributions for *population 3* in line 8-9 and Panel 26 represented by shaded areas. Areas of Line 8-9 and Panel 26 taken from Figures 6 and 7 (modified from Ross, 2002). Population 3 contains all facies except B. Not to scale.

Line 8-9

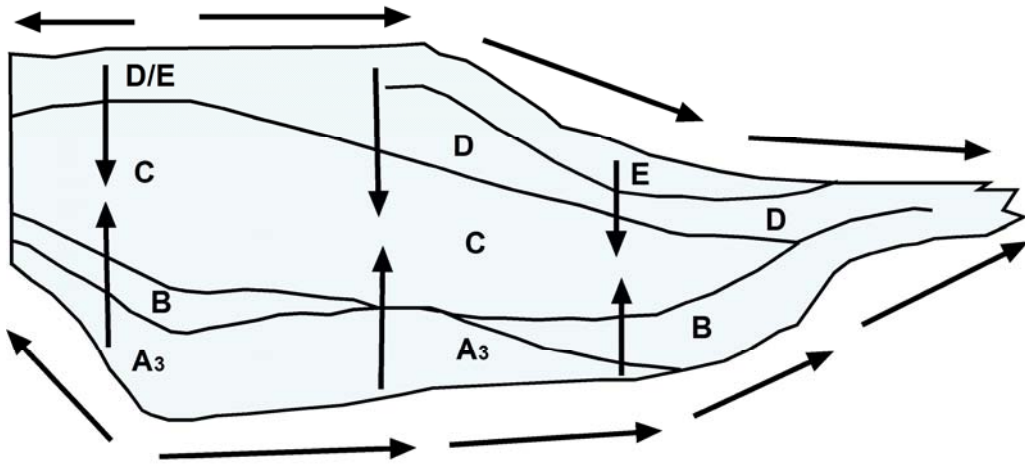


Panel 26

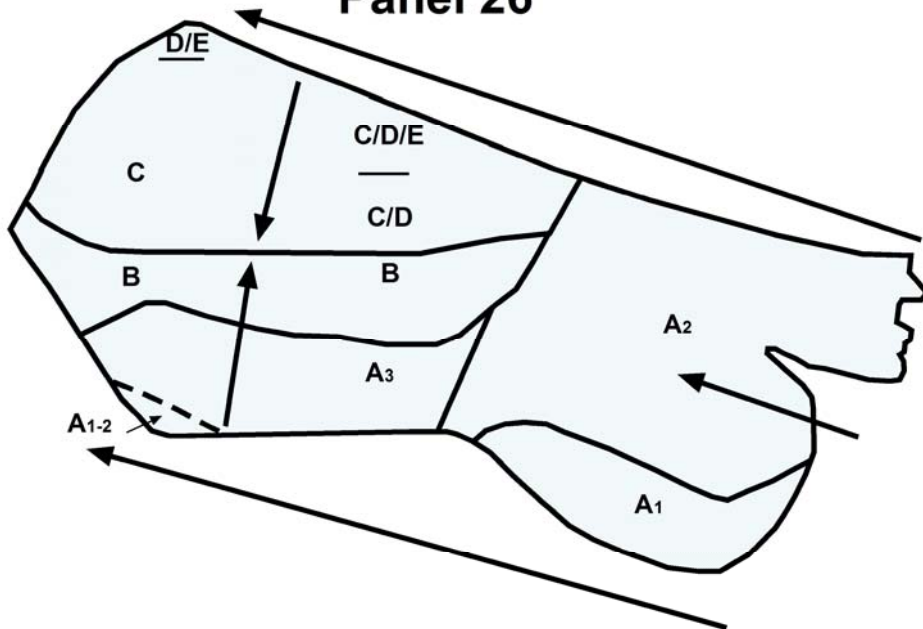


Spatial distributions for *population 8* in line 8-9 and Panel 26 represented by shaded areas. Areas of Line 8-9 and Panel 26 taken from Figures 6 and 7 (modified from Ross, 2002). Possible schematic fluid paths indicated by arrows. Population 9 contains A₁, B, C, and E facies. Not to scale.

Line 8-9



Panel 26



Spatial distributions for *population 1* in line 8-9 and Panel 26 represented by shaded areas. Areas of Line 8-9 and Panel 26 taken from Figures 6 and 7 (modified from Ross, 2002). Possible schematic fluid paths indicated by arrows. Population 1 contains all facies. Not to scale.